Utilization of Biorenewable Polymers for Functional Applications

by

Prachi Panchal

A thesis
presented to the University of Waterloo
in fulfilment of the
thesis requirement for the degree of
Master of Applied Science
in
Chemical Engineering

Waterloo, Ontario, Canada, 2020

Author's Declaration

This thesis consists of material all of which I authored or co-authored: see Statement of Contributions included in the thesis. This is a true copy of the thesis, including any required final revisions, as accepted by my examiners.

I understand that my thesis may be made electronically available to the public.

Statement of Contribution

Chapter 2 of this thesis consists of literature review on cellulose nanocrystals and lignin. A modified version of this chapter has been published as a literature review paper in Processes. The paper was co-authored by myself, a post-doctoral fellow, Dr. Ogunsona and my supervisor, Prof. Mekonnen. The paper was written by myself; where Dr. Ogunsona extended, organized, and edited by Dr. Ogunsona;the work written, while Dr. Mekonnen provided overall guidance and reviewed the paper.

Chapter 3 has been incorporated in a paper that has been published in Nanoscale Advances under the co-authorship of myself and my supervisor, Prof. Mekonnen. I designed and conducted the experiments, analyzed the data, and wrote the paper, while my Prof. Mekonnen provided overall guidance and reviewed the work.

Chapter 4 consists of research work that is conducted by myself under the guidance of my supervisor, Prof. Mekonnen. I carried out the lab experiments, analyzed the data, and wrote the manuscript under the guidance of Dr. Mekonnen.

Abstract

The need to transition to more sustainable and renewable technology has resulted in a focus on the two bio-renewable polymers, cellulose and lignin. Cellulose nanocrystals (CNCs) and lignin can be the materials of the future, with the potential of replacing currently used synthetic materials. CNCs are naturally hydrophilic due to the abundance of hydroxyl (-OH) groups on their surface, making them an excellent recipient for functional composite materials. However, their hydrophilicity is a deterrent to many industries, subsequently limiting their application scope. In either light, the increased rate of progress using CNCs in advanced material applications is well underway and is becoming applicable on an industrial scale. Lignin, a biopolymer found in biosphere, is a by-product of pulp industries. Due to its chemical structure, it can be used as a UV-stabilizer, antioxidant, antiradical, and antimicrobial biopolymer in material applications. However, because of its complexity in structure and inconsistencies in properties associated with differences in the source and extraction process, the use of lignin in specialty materials is limited. Nanoparticles of renewable polymers have gained an interest in academia due to the advantageous properties they offer. Thus, the synthesis of lignin nanoparticles can be of relevance.

Epoxy is an extensively used polymer in several applications such as coatings, adhesives, structural composites, etc. However, it is a poor ultraviolet (UV) absorber and suffers from UV- degradation, which usually leads to discolouration and loss of structural integrity. In this study, cellulose nanocrystals (CNCs) conjugated with UV absorber molecules were investigated as a functional nanomaterial to enhance the UV absorption of epoxy polymers. The grafting of a UV absorbing molecule, para-aminobenzoic acid (PABA), on the surface of CNC was confirmed using FTIR, proton NMR, and via elemental analysis. The modified CNC was then incorporated into an epoxy polymer and its efficacy in mitigating the photo-degradation of epoxy was evaluated. The

incorporation of native CNC displayed some UV absorption and reduction in the UV mediated discolouration of the epoxy, but the most pronounced effect was obtained in PABA decorated CNC based epoxy nanocomposites. The use of such tailored CNCs has great potential to mitigate the UV induced degradation of a range of polymers that are used especially in outdoor applications where direct exposure to UV is significant.

Lignin, an aromatic, renewable, and biodegradable material offers many unique properties. The potential of lignin can be valorized with the synthesis of nanoparticles. In this study, lignin (Dealkaline lignin) was used to produce lignin nanoparticles (LNP) through top-down and bottom-up processes. LNPs produced through a top-down process used ultrasonication as the source of energy to break down the larger molecule. A shift in pH was used inthe bottom-up approach, where LNPs were synthesized in three different solvents: water, glycerol, and ethylene glycol. LNPs produced were characterized, analyzed and compared through different methods. LNPs synthesized through different approaches maintained a similar structure. LNPs with functional attributes such as UV-absorbing and antioxidant properties can be used for functional material applications.

Acknowledgement

I would like to offer my gratitude to my supervisor, Prof. Tizazu Mekonnen for giving me the opportunity to enter the research world. I would like to thank him for providing constant support, guidance, and motivation to become successful throughout my master's program.

I would like to thank post-doctoral fellow, Dr. Ogunsona, for the support and guidance he provided. I appreciate the presence of my friends, Ewomazino Ojogbo, Malin Ly, and Joanna Jardin, at every moment providing me mental warmth along with technical support. I would like to thank the entire Mekonnen's research group for their help. I would also like to thank all my other friends for the inspiration and support they have provided throughout my academic career.

Most importantly I appreciate the care and silent support provided by my parents, my family and divine family that I received with the grace of God. Their unconditional love, unwavering faith and positive outlook have been the backbone of this journey. I cannot thank enough the love of my life, Parth Patel, for believing in me**.** You are my strength and inspiration who bring out the best in me.

Finally, I would like to express my utmost gratitude to God and Dadaji for giving a purpose to my life. This is because of you and for you.

Table of Contents

List of Figures

List of Tables

List of Abbreviations

AGU	Anhydro-D-glucose unit
CA	Contact angle
CNC	Cellulose nanocrystals
CNC@PR	Cellulose nanoparticles with polyrhodanine
CNP	Cellulose nanoparticles
DBTDL	Dibutylin dilaurate
DMSO	Dimethyl sulphoxide
EG	Ethylene glycol
EIS	Electrochemical impedance spectroscopy
EPA	Environmental Protection Agency
Fe^{3+}	Ferric
FTIR	Fourier Transfer Infrared Spectroscopy
GO	Graphene oxide
GPTMS	Glycidyloxypropyl trimethoxysilane
HALS	Hindered amine light stabilizers
HMFCA	superhydrophobic micro fibrillated cellulose aerogel
IPDI	Isophorone diisocyanate
KOH	Potassium hydroxide
LNP	Lignin nanoparticles
MTES	Methyltriethoxysilane
NFC	Nanofibrillated cellulose
NMR	Nuclear Magnetic Resonance
PABA	Para aminobenzoic acid
PFSC	Perfluorooctylated quaternary ammonium silane coupling agent
PLA	Polylactic acid
PU	Polyurethane
PVA	Poly vinyl alcohol
QAC	Quaternary ammonium compounds
RTA	Ricinoleic acid triglyceride
TCVS	Trichlorovinylsilane
TEMPO	(2,2,6,6-Tetramethylpiperidin-1-yl)oxyl
TEOS	Tetraethyl orthosilicate
TGA	Thermogravimetric Analysis
UV	Ultraviolet
WCA	Water contact angle
XPS	X-ray photoelectron Spectroscopy
ΔE	Total color change

CHAPTER 1: Introduction

1.1. Motivation

There is an increasing demand for polymeric functional materials as civilization is progressing towards technical advancement. Plastic production has been increasing since the latter half of the last century due to increasing demand for it [1]. By 2015, global production of polymer resins and fibers has increased to 380Mt from 2Mt in last 65 years [1]. From construction, automobile, industrial, medical, food packaging, to household items, polymeric items have made an irreplaceable place in one's life. A majority of these polymeric items originate from fossil fuels. There are two major concerns related to using fossil-based polymers. Depleting source of fossil fuels due to increasing demands is the first concern. Secondly, the use of it leaves a negative impact on environment, which is detrimental to global climate issues. Due to these arising concerns, there has been a focus on using natural polymers derived from biomass for material applications. Cellulose, lignin, starch, chitosan, protein, triglycerides, and natural gums are an interesting nature-derived and renewable feedstock for advanced functional material applications.

1.2. Components of Biomass

In the biosphere, widely distributed lignocellulose can be derived from wood, grass, agricultural residues, and forestry materials [2,3]. While there is variation in the composition depednding on the source, the primary components in lignocellulosic biomass are cellulose, hemicellulose, and lignin. In general, a comparison of the softwood versus with hardwood the composition of cellulose, hemicellulose and lignin are shown in Table 1. Figure 1 shows the alignment of cellulose chain encompassed in a hemicellulose and lignin matrix.

Table 1. Composition of Hardwood and Softwood [3,4]

COMPONENT	HARDWOOD	SOFTWOOD
Cellulose	40-55%	45-50%
Hemicellulose	24-40%	25-35%
Lignin	18-25%	25-35%

Cellulose is a major source for pulp and textile industries. Cellulose is a homopolymer with a linear chain consisting of six-carbon rings, which are anhydro-D-glucose unit (AGU) monomers linked with a $\beta\ (1 \rightarrow 4)$ glycosidic bonds [5,6]. Cellulose is a rigid and stiff polysaccharide known for its excellent tensile strength [7]. It contains amorphous and crystalline structures. The amorphous region can be easily broken through chemical treatment, but on the contrary the crystalline part is hard to break due to strong hydrogen bonding [8].

Cellulose nanocrystals (CNC) extracted from cellulose is in demand due to its renewability, biodegradability, high strength, low density, high crystallinity, high aspect ratio, and unique optical properties [9,10]. Due to its excellent reinforcing capabilities CNC is used in polymeric matrix such as polylactic acid, polyethylene oxide, polyvinyl alcohol, polyamide-6 to improve mechanical strength of the composite [11–14]. CNC has large number of hydroxyl groups, which allows for many chemical modifications including, but not limited to: sulfonation, esterification, etherification, amidation, silylation, carbonization, oxidation, urethane linkages via isocyanates [15,16]. As a result, some applications for which CNC can be used include CNC barrier coating, superhydrophobic CNC, antimicrobial CNC, and CNC micelles for drug delivery [17].

Hemicellulose is a branched polysaccharide. Hemicellulose has lower molecular weight than cellulose, and can be easily hydrolyzed into monosaccharides [3]. Hemicellulose is composed of different sugar units: D-xylose, D-mannose, D-galactose, D-glucose, L-arabinose, 4-O-methyl

glucuronic, and D-galacturonic, connected through $\beta-1,4-$ glycosidic and $\beta-1,3-$ glycosidic bonds [3].

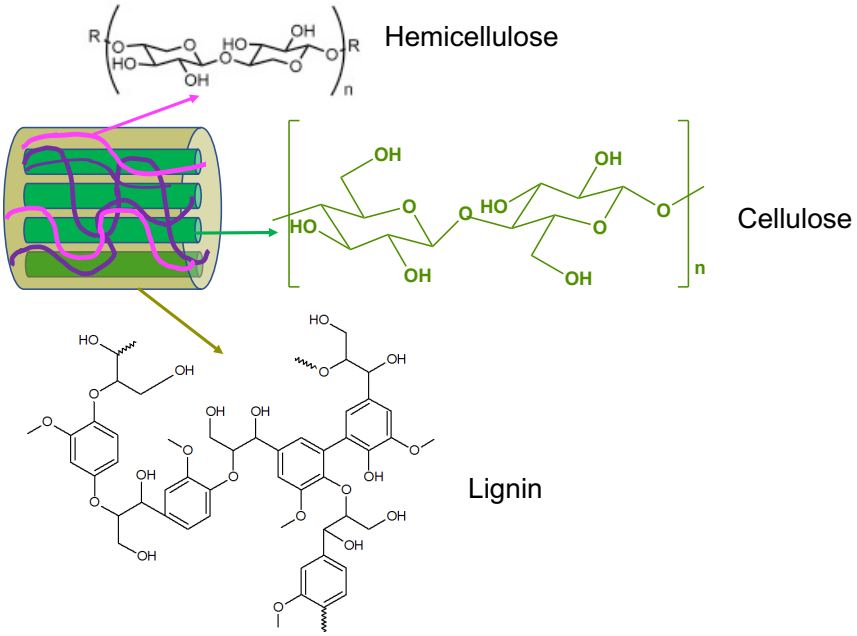

Figure 1. Structure of lignocellulose including cellulose, hemicellulose and lignin[18].

Lignin has a 3-D amorphous phenolic structure. It consists of three phenylpropane monolignols. Polymerization of guaiacyl, syringyl and p-hydroxyphenyl units forms complex lignin [19]. In industry, lignin is produced as a by-product of pulping processes. Since various industries employ different types of pulping and extraction processes, it typically leads to heterogeneity and diversity in technical lignin. Lignin has UV-absorber, antioxidant, antiradical, and antimicrobial properties [20,21]. These advantageous properties can be enhanced with the use of lignin nanoparticles. Recently, efforts have been made on producing lignin nanoparticles through various methods [21–23].

1.3. Research Objective

The main goal of this research was to utilize renewable biopolymers for advanced applications. Cellulose nanocrystals have many beneficial properties, which have attracted many researchers for using it in advanced functional materials. Chemical modification of CNC with functional groups can be useful for tailored applications. Lignin is another biopolymer with aromatic structure. Valorization of lignin for value-added application is in demand. Thus, this research focused on the utilization of these two biopolymers for material applications. The specific research objectives were:

1. Decoration of CNC with UV absorbing agent and incorporation in polymers to reduce or avoid UV-mediated degradation of the polymers.
2. Synthesize lignin nanoparticles through the bottom-up and top-down method and evaluate their properties for material applications.

1.4. Hypothesis

The main hypothesis of this work are:

1. CNC can be sucessfuly modified with absorbing molecule. The modified CNC would be compatible with epoxy matrix.
2. Epoxy-CNC can mitigate disocolarion due to UV-irradiation.
3. Lignin nanorparicles can be synthesised through different methods without compromising the main structure and its properties.

1.5. Thesis Outline

This thesis is comprised of five chapters: introduction, literature review, two experimental research projects, and finally conclusion and recommendations. The literature review describes in detail the

background information on cellulose, cellulose nanocrystals and lignin. Next, two chapters discuss the experimental research work. The third chapter discusses the decoration of CNCs with UV absorber molecule, para-aminobenzoic acid using a coupling agent. The modified CNC was further characterized to confirm the chemical reaction and change in properties. Addition of modified CNC in epoxy composite is discussed, along with composite characterization after UV-irradiation. To the best of our knowledge, the use of decorated CNCs to inhibit UV-mediated degradation of epoxies has not been reported before, and this study showed promising results. Chapter four presents the fabrication of lignin nanoparticles from dealkaline lignin. The use of ultrasonication to produce lignin nanoparticles was investigated in detail. The next approach employed to produce nanoparticles was the pH-shift method in three different solvents: water, glycerol and ethylene glycol. The nanoparticles produced via the various approaches were characterized form material application perspective. While few studies have reported either high shear (e.g. ultrasonication) or pH-shift process to produce lignin nanoparticles, no study has provided comparison of the methods in terms of the particle size, surface charge, or their dispersibility.

CHAPTER 2: Literature Review: Trends in Advanced Functional Material Applications of Cellulose Nanocrystals (CNCs) and Lignin Properties and Use

2.1. Functional Material Applications of Cellulose Nanocrystals

2.1.1. Introduction

Cellulose, lignin, starch, chitosan, protein, triglycerides, natural gums, and polyphenols constitute an interesting nature-derived feedstock for advanced material applications. Cellulose, reneable feedstock, has an approximate annual production of 10^{10} tons [24,25]. As such, it has been an immense source for the paper and textile industries for thousands of years. Cellulose is a homopolymer with a linear chain of six-carbon ring, anhydro-D-glucose unit (AGU) monomers. Each AGU monomer in a chair conformation is linked with a $\beta\ (1 \rightarrow 4)$ glycosidic bonds [5,6].

Overall, cellulose is a rigid and stiff polysaccharide that has tensile strength comparable to other commercial fibers such as carbon fiber [7]. Reinforcement of high melting temperature polymers with modified biomass has extensively been reported [26–31]. Likewise, it has also been extensively reported that the addition of cellulose fibrils in various forms to produce polymeric composites can greatly enhance the mechanical properties of the base polymeric materials at significantly lower loadings compared to other biomasses [11,12,14,32–34]. Forms of cellulose fibrils can range from cellulose powders to microcrystalline cellulose and nanocrystalline cellulose. In the last two decades, a substantial and continuing interest in the utilization of cellulose nanoparticles in material applications has been observed. This is accrued from a breakthrough in the largescale production of nanocellulose, as well as their multifaceted benefits in traditional polymer composites and functional materials. Nanocellulose is a material extracted from cellulose which has one or more dimensions in the nanometer range of 100 or less [25,35], and considered as the next

generation of renewable reinforcing agents for the production of biocomposites, and especially for advanced functional materials applications.

2.1.1.1.Nanocellulose

Nanocellulose is a generic name referring to different cellulose nanoparticles (CNPs) such as bacterial cellulose, microbial cellulose, cellulose nanocrystals, cellulose nanofibrils, cellulose nanofibers, and cellulose nanowhiskers [36]. Amongst the variety of CNPs, the two major structures are cellulose nanocrystals (CNC) and cellulose nanofibers (CNF) [10,25]. The extraction process of these two structures from the feedstock and their morphology are the two main differences between these CNPs [10,37]. Cellulose nanocrystals are extracted through chemical processes such as hydrolysis and they have a rod -like structure. Contrarily, cellulose nanofibers contain web-like network and are mainly extracted through mechanical and chemo-mechanical processes [7,10,37].

Similar to other bio-based materials used for advanced materials applications [38,39], the renewability and biodegradability, high strength, low density, high crystallinity, high aspect ratio, and unique optical properties make CNCs highly desirable materials in several advanced and functional material applications [9,10]. CNCs can be isolated from bioresources such as wood, cotton, hemp, linen, flax, tunicate (aquatic invertebrate) [7,9,10,34,35,37]. It can also be generated by a bottom-up methods or biosynthesis from simple molecules. Bacterial nanocellulose produced by bacteria and algae via fermentation of sugar is a typical example of such bottom-up approach [40]. The properties of CNCs can vary depending on bio-sources and the extraction process used. Some of the extensively researched material applications of CNCs include plastic composites, paints and coatings, packaging films, cement, rubber products, biomedical applications (e.g. pharmaceuticals, diagnostic imaging, drug delivery, tissue engineering materials), sensors, and many more [16,36,41].

CNC aggregation, surface energy and incompatibility with large number of matrices are some of the challenges associated with CNC for these applications.

2.1.1.2. CNC Characteristics

Cellulose exists in seven allomorphs: Cellulose I_α, I_β, II, III_I, III_{II}, IV_I and IV_{II}, where cellulose I is the most crystalline structure with the highest axial elastic modulus [6,35]. The two polymorph of cellulose I, cellulose I_α and I_β, coexists where I_β is more thermally stable than I_α due to weaker hydrogen bond in I_α [35]. CNC contains 64-98% I_β depending on the source [35]. CNCs are found in rod shapes. Typically, they can be 3-5 nm wide and 50-500 nm long [35]. However, CNC from tunicate can be as wide as 20 nm [35]. The larger dimensions for CNCs derived from tunicate is a result of highly crystalline tunicate cellulose, which contains less amorphous regions that leave behind larger crystalline region [42]. One of the most attractive properties of CNC is its high aspect ratio. This is because the functional application of CNC is dependent on the aspect ratio in several cases. For instance, the use of CNC as a reinforcing agent relies on its higher aspect ratio. On the other hand, CNCs with uniform crystallinity and lower aspect ratio are beneficial in renewable liquid crystals applications [43,44]. Table 2 shows that the variation in aspect ratio of nanocrystals depending on the source of CNC. Overall, nanocrystals derived from sea plants and animals have significantly higher aspect ratio as compared to those extracted from wood and cotton.

Table 2. Aspect ratio of CNC derived from different sources

Source	Length (nm)	Width (nm)	Aspect Ratio*	Reference
Bacterial	640-1070	12-22	50	45
Cotton	100-300	4-10	29	25
Flax	100-500	10-30	15	46
Ramie	150-250	6-8	29	47
Sisal	150-350	3-5	62	48
Valonia (Sea plant)	1000-2000	20	75	25
Tunicate (Sea animal)	500-2000	10-20	83	25
Wood	100-200	3-15	17	25

Aspect Ratio*= Aspect ratio calculated using average length and width

It is important to highlight that cellulose nanocrystals are a highly crystalline fraction of cellulose. CNCs have degree of crystallinity of 54-88% depending on the amorphous content present in the feedstock, and the production process [35]. Nanocrystals derived from tunicate have been reported to have the highest crystallinity, which ranges from 85-100% [35]. As a result of the higher crystallinity caused by hydrogen bonding, cellulose nanocrystals are rigid and stiff. CNCs are also rich in hydroxyl groups (-OH) since each AGU unit offers one primary and two secondary -OH groups leaving it open to endless modification and functionalization possibilities [35]. Moreover, the high surface area to volume ratio of CNCs further facilitates surface functionalization or other -OH chemistry efforts making it suitable for various advanced functional material applications [49].

Due to the sheer numbers of published review articles on CNCs with focus on their modifications and applications towards polymer composites and nanocomposites, extraction and purification processes and determinations of their properties and characteristics just to mention a few, these subjects will only be highlighted. To the best of our knowledge, only few review articles were published on advances in applications of CNC covering several topics. However, due to growing interest, research being conducted and achieved on CNC continually and especially in niche areas such as wettable surfaces, coatings, several applications of biotechnology and electronics, there is need to produce updates and disseminate the new developments achieved and knowledge gained. Therefore, this review focuses on the current advanced material functionalization of CNCs geared towards these areas.

2.1.2. Cellulose Nanocrystals in Wettable Applications

Wettability of a substrate or surface is the ability of that surface to create intermolecular interactions such as cohesive and adhesive forces when typically in contact with a liquid. The degree of wettability is determined by the aforementioned forces which also govern the contact angle (CA) between the substrate and liquid. The CA subsequently determines if a material or substrate is hydrophobic, hydrophilic or in those extremes. In recent years, many researchers have been drawn towards the development of hydrophobic nanomaterials due to the increasing demand in both academic and industrial sectors. Hydrophobicity is an important property to determine the application of nanocomposites. Hydrophobic materials with self-cleaning, antifouling, water repellency, and reduced friction properties are highly desirable for industrial applications. CNCs are known for their strength and commonly used as reinforcing agents. However, the application of CNC is currently limited because it cannot be readily incorporated into many polymer matrices that are typically hydrophobic due to its high hydrophilicity. Thus, hydrophobic modification of CNC can lead to better dispersion in non-polar and hydrophobic matrices. Furthermore, hydrophobic CNC surfaces can also be used as a coating agent for marine vehicles, biomedical devices, windows, textiles, paints, and many other applications. The advancement of hydrophobic CNC surfaces can open doors to many commercial applications of this rich biopolymer found in nature.

In nature, butterfly wings, lotus, and other plant leaves are greatly studied for their superhydrophobicity [50,51]. Lotus leaves are known for their self-cleaning properties and have hierarchical rough structure containing two levels of roughness [50]. Superhydrophobic properties of lotus, known as lotus-effect, have inspired the synthesis of many artificial hydrophobic materials. An important aspect to study while investigating hydrophobicity is the water contact angle (WCA).

A hydrophilic material has a WCA of less than 90°, a hydrophobic material has a WCA higher than 90° while materials displaying WCA greater than 150° are superhydrophobic [51,52]. Various relations including Young's equation, Wenzel equation and Cassie equation have been developed to determine WCA [51]. Along with water contact angle, another important characterization property of hydrophobicity is sliding angle. Sliding angle is a measure of tilt angle between the surface and substrate droplet at which droplet starts to roll off of the surface. Superhydrophobic material has sliding angle less than 10°, which is often used to describe the anti-water repellency property [51,53].

Hydrophobicity can be controlled through chemical modification or surface roughness. Reduction of surface energy through chemical modifications and enhanced roughness are both the factors that must be simultaneously controlled to achieve superhydrophobicity [54]. Preparation of superhydrophobic materials involves harsh chemical and physical treatments. Chemical modifications to obtain hydrophobicity include attachments of low surface energy molecules such as fluorinated agents [55], silanes [54], organic hydrophobic chains [56] and etc. Table 3 lists various chemical treatments and attachments to cellulose -based materials such as cotton, paper, and cellulose nanocrystals.

Table 3. Hydrophobic treatment of Cellulose-based materials.

Surface	Modification	WCA	Reference
CNC	Pentafluorobenzoyl chloride	112°	55
CNC	Castor Oil	97°	56
CNC	Stearyltrimethylammonium chloride	71°	57
Cotton	Silica sol treated with PFSC	145°	58
Paper	TEOS and tridecafluorooctyl triethoxysilane	170°	53

Although chemical modification has been the traditional approach to functionalize the surface of a material for a number of applications, a recent trend in enhancing the surface roughness provides some interesting hydrophobic characteristics in several materials. Increasing surface roughness

plays a key role in enhancing water repellency [58]. In this, air, which is very hydrophobic (water contact angle 180°) gets trapped between the grooves of the roughness [59]. When a water droplet rests on the surface it comes in contact with the entrapped hydrophobic air leading to hydrophobicity enhancement [59]. Surface roughness strategies such as etching, laser, electrospinning, etc. are commonly used [51,60].

Salajkova *et al*.[57] employed quaternary ammonium salts modification to bring about hydrophobic modification of CNCs. In this study, four different quaternary ammonium salts were used for the CNC modification. Figure 2 shows the attachment of (1) stearyltrimethylammonium chloride as well as the structure of other three quaternary ammonium salts (2) phenyltrimethyl-ammonium chloride, (3) glycidyl trimethylammonium chloride, (4) diallyldimethylammonium chloride [57]. The highest WCA for stearyltrimethylammonium chloride modified CNC was 71°. Although great improvement was observed in WCA of the CNC surface, a higher WCA (> 90°) is typically desirable for employing the hydrophobicity of CNC for advanced material applications.

Silica nanoparticles are widely used for hydrophobic modification of cellulosic materials. Tetraethyl orthosilicate (TEOS) prepared through sol-gel process was used for the hydrophobic treatment of cotton fabric [61]. Silica is not hydrophobic, therefore fluorinated silane and alkylanated silane, or other alternative water repellent agents are commonly used to achieve water repellency [61]. Silica, TEOS, sol-treated with perfluorooctylated quaternary ammonium silane coupling agent (PFSC) showed water contact angle of 145° proving PFSC to be very effective [58].

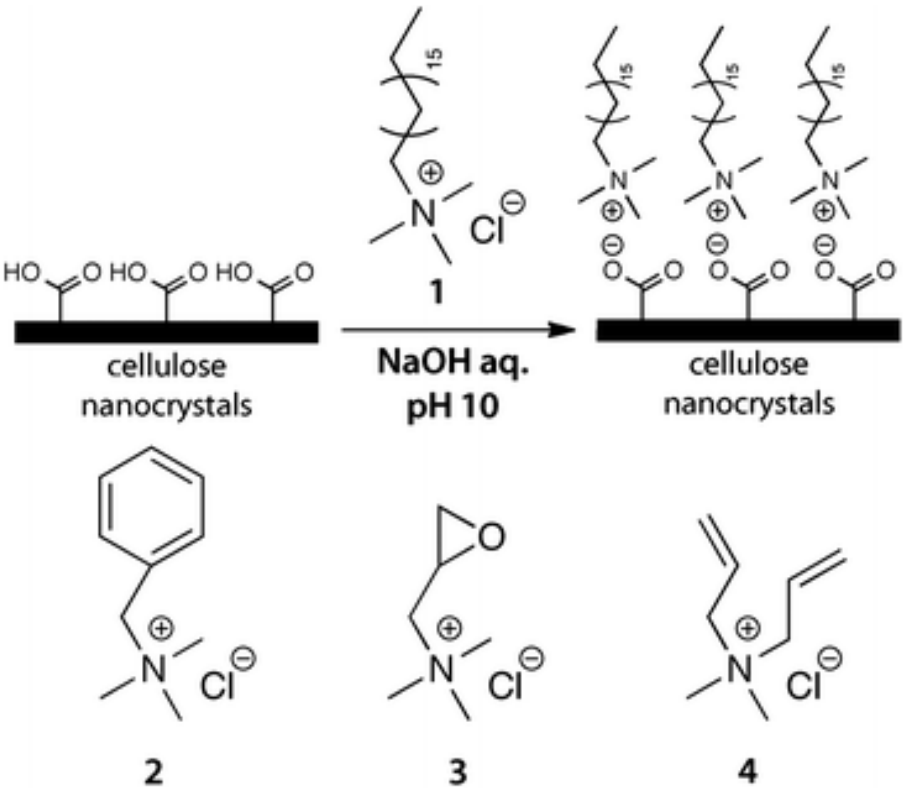

Figure 2. CNC modified by Quaternary Ammonium Salts. Adapted from Salajkova et al.[57,] RSC copyright © 2012.

Paper, a major product from cellulose, was coated with TEOS sol and tridecafluorooctyl triethoxysilane to produce a hydrophobic surface 53. The modified paper had a WCA greater than 170o and sliding angle less than 7o displaying superhydrophobic properties 53. Instead of only using silica nanoparticles, the treatment of silica with fluorinated compounds often offers better water repellency. Salam et al.55 reported fluorine-based modification of nanocellulose to obtain hydrophobic and oleophobic properties. Figure 3 shows the modification of CNC surface through fluorinating agents. The modified CNC displayed a water contact angle of 112o and maintained 80o even after 1,200 seconds 55. However, due to the surface modification, the crystallinity of cellulose nanocrystals was slightly modified. The modified CNC had a crystallinity index of 82% while the unmodified CNC displayed a higher crystallinity index, 91% 55.

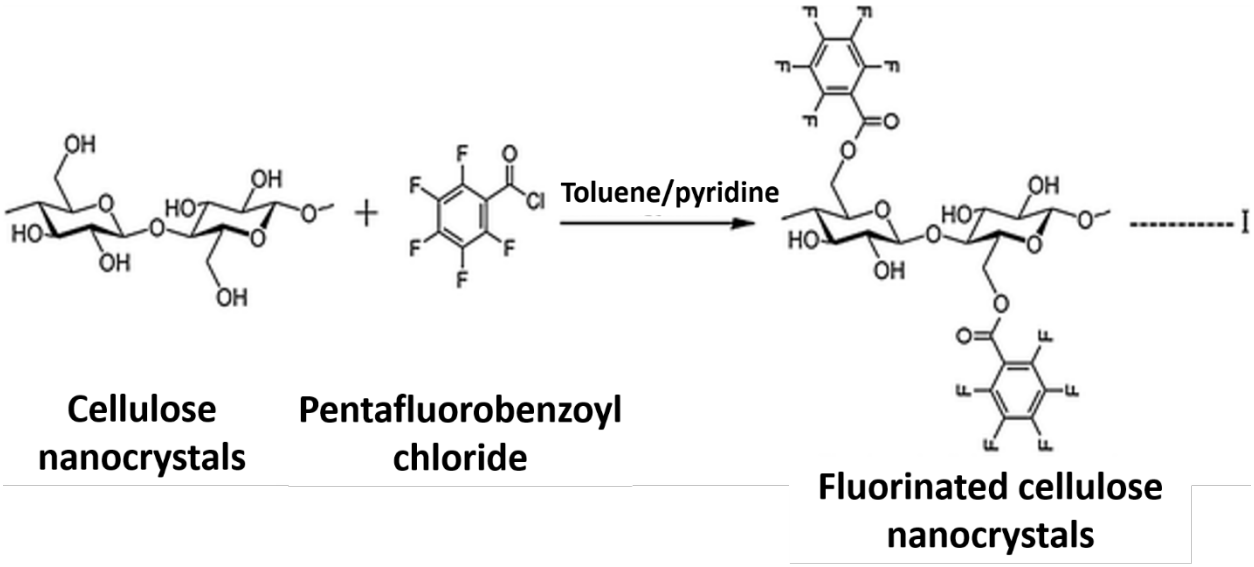

Figure 3. Hydrophobic modification of CNC via fluorine-based agents. Adapted from Salam et al. [55]. Springer copyright © 2015.

Shang et al.56 has reported another approach of producing hydrophobic CNC, by attaching castor oil on the surface of the CNC. Castor oil containing hydroxylated fatty ricinoleic acid triglyceride (RTA), was attached to CNC surface via grafting-onto modification approach while using diisocyanate as a coupling agent 56. Only one hydroxyl group was maintained active while other two were terminated in order to link one end of diisocyanate with castor oil and another with the CNC. Successful grafting led to a reduction in the surface energy. The increase in water contact angle of grafted material to 97o also suggested hydrophobicity of the nanocellulose 56. The resulting material was dispersible in non-polar solvents such as toluene and ethyl ether 56.

Hydrophobic surfaces provide the advantage of efficient and enhanced performance of materials when used in targeted applications. Hydrophobic and superhydrophobic surfaces are highly desirable for marine equipment coating. Watercrafts, marine platforms, offshore rigs, and jetties are highly vulnerable to fouling. As a result, operational and maintenance cost for sustaining water-

based structure is relatively high. Thus, hydrophobic surfaces with the correct combination of surface roughness and chemical modification can reduce the wetting behavior that result in minimizing attacks from marine organisms and corrosions. CNCs with great reinforcing ability can be modified to achieve both superhydrophobicity and antimicrobial properties. Dual function CNC can greatly enhance the performance of underwater objects and marine equipment.

Surface containing hydrophobic coatings is desirable for self-cleaning windows, satellite dishes, solar energy panels, photovoltaics, exterior architectural glass 51. Furthermore, water repellent paper can have practical applications for valuable printable paper, filter paper, packaging and photographs 59. Recently, textiles with water repellency, anti-stain and self-cleaning properties are of interest in outdoor sporting textile applications 61. Due to the increasing demand of hydrophobic materials, researchers are developing various approaches for hydrophobic modification of CNCs. Despite numerous research being conducted in this field, commercial applications of hydrophobic and superhydrophobic materials is limited due to susceptibility of CNCs to environmental degradation over time 53,62.

Zhou et al. recently developed a superhydrophobic micro-fibrillated cellulose aerogel (HMFCA) to efficiently separate oil from water 63. In this study, silanization in an ethanol solution containing methyltriethoxysilane (MTES) was used to modify the aerogel by introducing polysiloxane groups on the surface of the HMFCAs. Prior to silanization, the HMFCA was oxidized to introduce hydroxyl groups, which was used as anchor points for the silanization process. The polysiloxane groups are highly water repulsive (hydrophobic) while allowing the absorption of oil (lipophilic) into the porous structure of the aerogel. The resulting modified aerogel when immersed in oil-contaminated water exhibited oil selective capability of up to 159 g/g. Experimental runs after 30 cycles revealed a reusability capacity of up to 92 g/g which was approximately 58%. Figure 4(a)

shows the contact angle of the unmodified HMFCA and modified HMFCAs with different MTES concentrations of 1, 2 and 3 mL which correspond to HMFCA-1, HMFCA-2 and HMFCA-3, respectively. It was observed that the contact angle increased with increasing MTES concentration up to 151.8o, indicating its superhydrophobic nature. Figure 4(b), (c) and (d) show the before and after modification of the aerogels and flotation of the modified aerogel in water due to the reduced surface energy created by the modification process. Figure 4(e) shows the possible reaction scheme for the modification of the hydrophilic aerogel into lipophilic aerogels. This study shows the great potential of micro-fibrillated cellulose and possibly nanocellulose to be used on a large scale for oil spill clean ups from offshore rigs and leaking underwater pipelines.

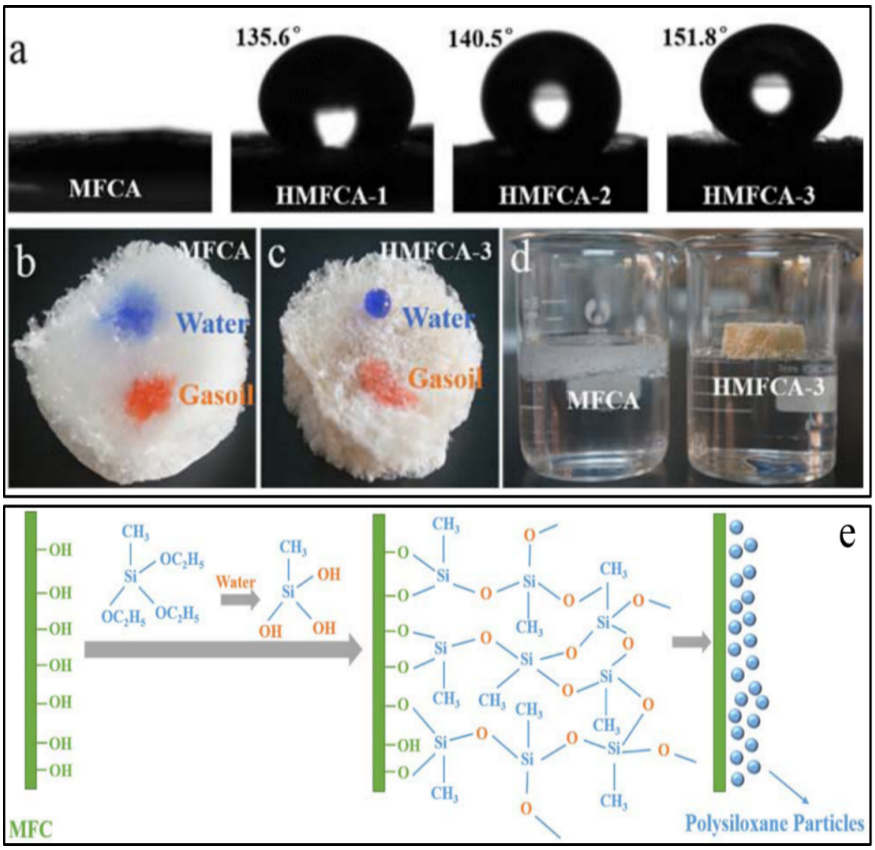

Figure 4. (a) Contact angle measurement of unmodified and modified MFCAs with 1, 2 and 3mL MTES concentrations. (b, c) Water/oil selectivity of unmodified MFCA and modified MFCA with 3 mL of MTES with both water and oil absorbed in the unmodified MFCA while only oil is absorbed in the modified MFCA. (d) Modified MFCA floating on water while

unmodified MFCA sinking into water. Adapted from Zhou et al.[63]. ACS publications copyright © 2016.

Water/oil selectivity of unmodified MFCA and modified MFCA with 3 mL of MTES with both water and oil absorbed in the unmodified MFCA was observed, while only oil is absorbed in the modified MFCA. Oil-water separation tests were also performed using a stainless-steel mesh treated with the superhydrophobic CNCs. Different oils such as toluene, N-haxane, xylene and cyclohexane were used to determine the efficiency of the treated mesh in separating the oil from the water while reusing the mesh for 40 cycles. The result from this test revealed that the mesh was able to efficiently remove all types of oils with a separation rate of at least 97.37%. Analogous to the above work, oil/water separation using superhydrophobic cotton fabric coated with CNC has been published and shown to have excellent results with a 98% separation efficiency with the coated cotton fabric capable of being reused without detriment to the separation efficiency [64]. The reusability, durability, and efficiency of oil-water separation most likely stems from the strong covalent bonds on the cellulose surface, as well as the excellent mechanical properties of the cellulose nanocrystals such as the strength, stiffness and wear resistance. Similar to the study by Zhou *et al.* [63], these works demonstrate the capability of superhydrophobic CNCs when geared towards applications such as water contaminant separation.

In a similar study by Huang *et al.*, CNCs were treated with 1H,1H,2H,2H-perfluorodecyltrichlorosilane in the liquid phase through water-ethanol-toluene exchanges to produce superhydrophobic CNCs [65]. In this reaction, the trichlorosilane groups react with the hydroxyl groups of the CNCs to form a covalent bond, while leaving the highly fluorinated tail dangling. The group reduces the surface energy and therefore makes it superhydrophobic. The superhydrophobic CNCs were then applied to different substrates such as wood, glass and stainless-steel mesh. Each substrate was first sprayed with a quick-drying adhesive before being

sprayed with the superhydrophobic CNCs and allowed to dry. Self-cleaning and water contact angle tests were performed on the treated substrates and are shown in Figure 5. It can be observed from Figure 5(a) and (b) that the coated wood and glass substrates exhibited superior hydrophobic characteristics with high contact angles of 158 and 156 degrees, respectively. The self-cleaning efficiency of the uncoated and coated substrates with the superhydrophobic CNCs can be observed in Figure 5 (c) and (d), respectively. The high degree of self-cleaning can be applied to marine equipment and vessel surfaces, thereby allowing for increased buoyancye and reduced need for expensive and frequent maintenance. Though, the substrate used by Huang *et al.*[65] might pose a challenge when it comes to large scale application due to the weight and possible high cost, it is highly durable and can withstand impacts and bumps over several cycles. Those used by Zhou *et al.* [63] and Cheng *et al.* [64] are light-weight, readily available and can be mass produced. However, it might not be as durable as the stainless-steel material in the long run. Regardless of the choice of material, the application of modified CNCs for superhydrophobic material applications is promising and on track for industrial scale use.

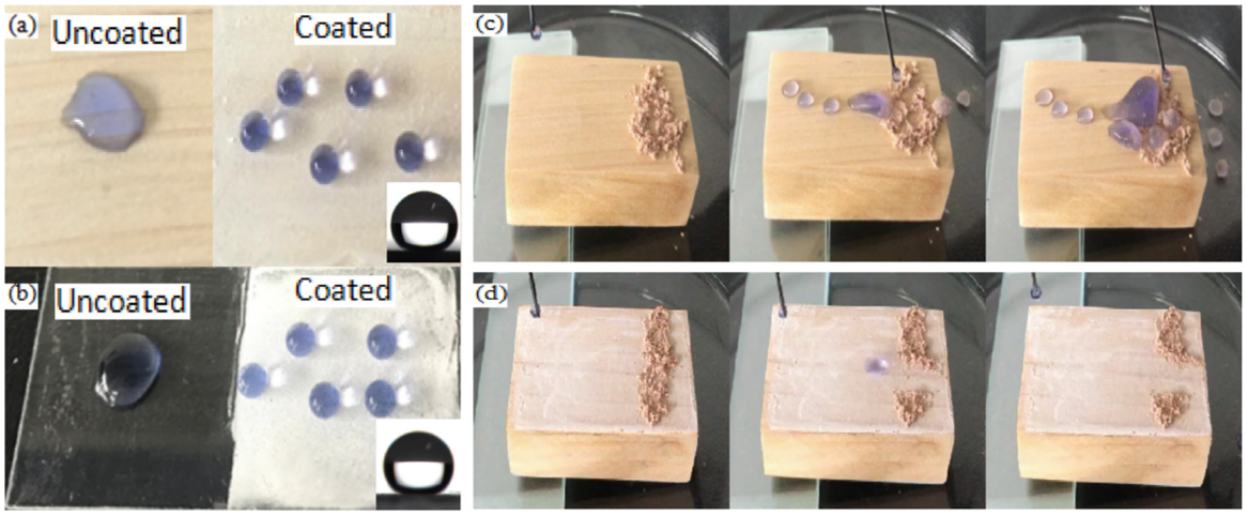

Figure 5. Demonstration of superhydrophobic coating from modified CNC with high contact angle on wood (a) and glass (b). Self-cleaning capability of uncoated (c) and coated (d) wood. Adapted from Huang et al.[65]. Elsevier copyright © 2018.

Recently, Gou *et al.* [66] developed a process to modify the surface of nanofibrillated cellulose (NFC) films to render portions of the films either superhydrophobic or superhydrophilic. In this process, the NFC film was immersed in trichlorovinylsilane (TCVS)-toluene solution to allow for the growth of TCVS silicone nanofilaments on its surface. Through hydrolysis and polycondensation, to form crosslinked porous polymeric silicone nanofilaments on the surface (TCVS-SNFs) were formed. This film was further modified to form superhydrophobic surfaces by exposure to ultraviolet light in the presence of hydrophobic thiol compounds such as 20% (v/v) 1H, 1H, 2H, 2H-perfluorodecanethiol solution in ethyl acetate or 20% (v/v) 1-butanthiol in ethanol. In order to selectively form superhydrophilic surfaces on the superhydrophobized film, it was further exposed to ultraviolent light in the presence of cysteamine or 2-mercaptoethanol as hydrophobic moieties, leaving only areas which was intended to be exposed to a UV light. The use of ultraviolent light was to catalyze the reaction between the TCVS-SNFs on the surface of the film and the hydrophobic moieties and between the hydrophobic moieties and the hydrophilic moieties through photo-induced thiol-ene reaction. Likewise, a slippery NFC surface was created by incorporating lubricant fluid into an already superhydrophobic NFC films until complete saturation of the fibrils was acheived. Figure 6 (a) demonstrates the process of superhydrophilic-superhydrophic dual surface modification of an NFC film using photo-induced thiol-ene reaction by UV light exposure. Figure 6 (b) shows the mapping of dual superhydrophobic-hydrophilic surfaces using secondary ion mass spectrometry coupled with time-of-flight mass analysis which was used to determine the elemental and molecular identities of the dual surface. Further geometric designs were made and are shown in Figure 6 (c), with different patterns of the hydrophobic-hydrophilic surfaces using dyed water solutions to clearly identify each region. The mechanism of reaction, stepwise functionalization, and modification of the NFC films to form both super - hydrophobic and

hydrophilic surfaces and slippery NFC films are shown in Figure 6 (d). Such findings can lead to an extensive utilization in biotechnology and biomedical applications such as specifically designed films, which can be used to repel or attract specific biological moieties in the body due to their polar or nonpolar characteristics.

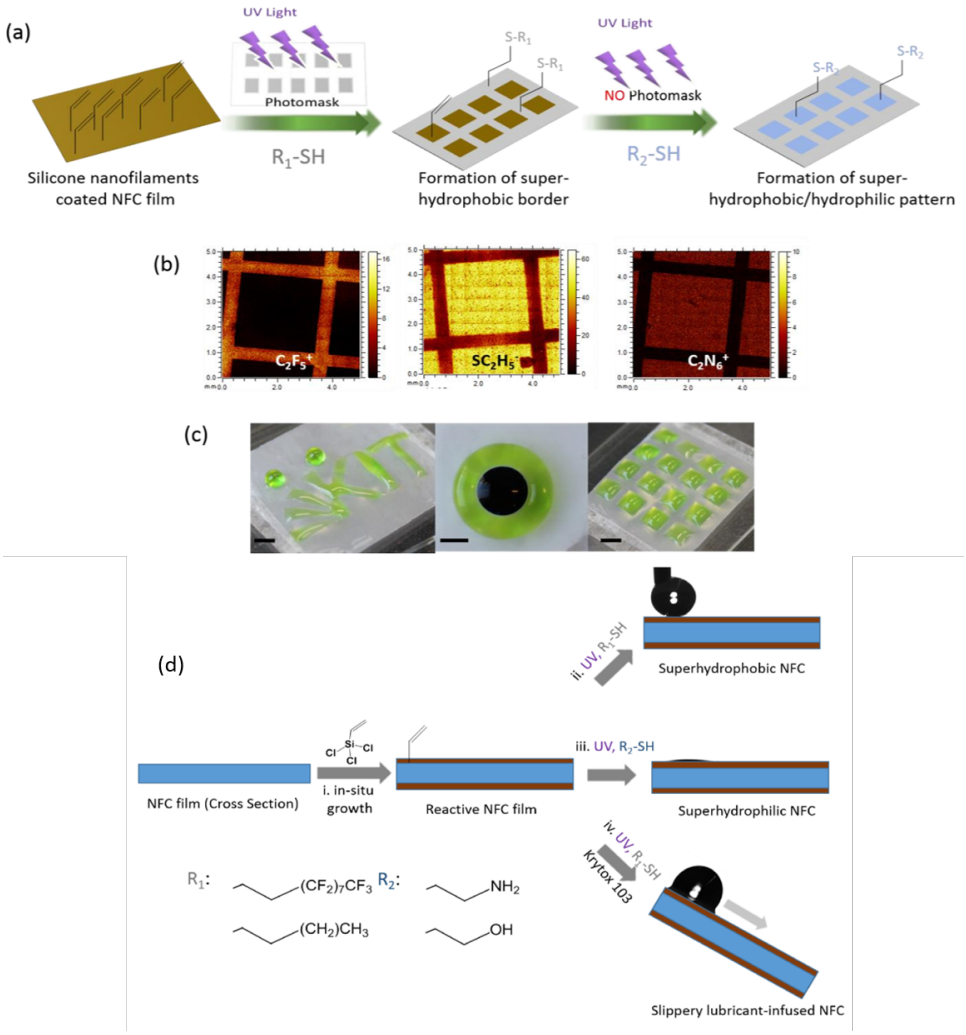

Figure 6. (a) Modification of NFC films to produce superhydrophobic/superhydrophilic patterns. (R1 and R2 – superhydrophobic and superhydrophilic moieties grafted on NFC film surfaces, (b) secondary ion mass spectroscopy with time of flight 2D mapping of superhydrophobic/superhydrophilic modified films with both positive (left and right) and negative (middle), (c) films designed with different patterns of superhydrophobic/superhydrophilic surfaces and highlighted with dyed water solutions. Adapted from *Gou et al.*[66]. ACS publications copyright © 2016 and (d) schematic of plausible chemical reactions to achieve superhydrophobic/superhydrophilic surfaces. Adapted from *Fan et al.*[67]. Elsevier copyright © 2018.

In the studies above, irreversible superhydrophobic surfaces were developed and shown to be extremely efficient. However, in a very recent study, a reversible superhydrophobic/superoleophilic-superhydrophilic /superoleophobic transition of modified cellulose fabric was developed and designed by Fan *et al.* [67]. Smart or transition-reversible superhydrophobic-superhydrophilic cellulose fabric was formed by introducing the fabric into an aqueous solution of sodium hydroxide, distilled water, and urea for a specific period of time after which it was treated in a zinc chloride aqueous solution to allow zinc cations and chlorine anions be absorbed onto the surface of the cellulose fibers. The fibers are swollen and allowed for the ions to penetrate into the pores. The loaded fabric was steamed to imprint the ions on the fabric fibers. The treated fabric was then washed repeatedly with deionized water and baked thereafter. The baking process was done to shrink the fibers, thereby physically locking the imprinted ions in the pores of the fibers as water is removed and shrinkage occurs. This fabric, now loaded with zinc oxide (ZnO-CFs), was further modified to give it a superhydrophobic-superhydrophilic reversible-transition surface by dipping it into a solution of lauric acid and ethanol. Thereafter, it was soaked in another solution of sodium hydroxide, ethyl alcohol and water. Figure 7 (a), (b), (c) and (d), displays the micrographs of the cellulose fibers before and after modification with ZnO, ZnO and lauric acid and ZnO, lauric acid, sodium hydroxide, and ethyl alcohol aqueous solution, respectively. It can be observed that there is the presence of ZnO attached to the fiber surface after modification which created a micro-nano rough surface structure which was partially ascribed as a factor in the formation of hydrophobic and hydrophilic surfaces thereafter. Likewise, in Figure 7 (e), the schematic demonstrates the steps taken in achieving this process. Readers should refer to the published work for a well-detailed experimental procedure and for more information as needed [67]. It was found that the reversable wettability of the modified cellulose fabric maintained

its properties such as separation efficiency and wettability phases even after 20 reversal cycles between hydrophobicity and hydrophilicity. The mechanism behind the hydrophobic to hydrophilic transition of the fabric was ascribed to the formation of sodium carboxylate after the scissioning of chelation between ZnO and carboxylate anion formed during the modification process. The newly formed sodium carboxylate would move to the liquid phase from the solid-liquid interface, thereby increasing the solid-surface free energy resulting in the local reduction of water surface tension from the loss of low free energy alkyl chains. This subsequently results to wettability reversal or transition. This study not only advanced the science of oil/water separation, but also took it a step further by broadening the application scope to include the removal of water from oil and not just oil from water. In cases where the contaminant is water, it can be removed by using the smart cellulose fabric in its superhydrophilic/superoleophobic form. On the contrary, while it is in its reversed form of superhydrophobicity/superoleophilicity, it can remove oil from water simply by immersing it in a solution to stimulate the transition back to the former as described above. These applications can be geared towards the oil industry where purity of oil is critical to its final use, or in industries where oil spill cleanup into large bodies of water is required.

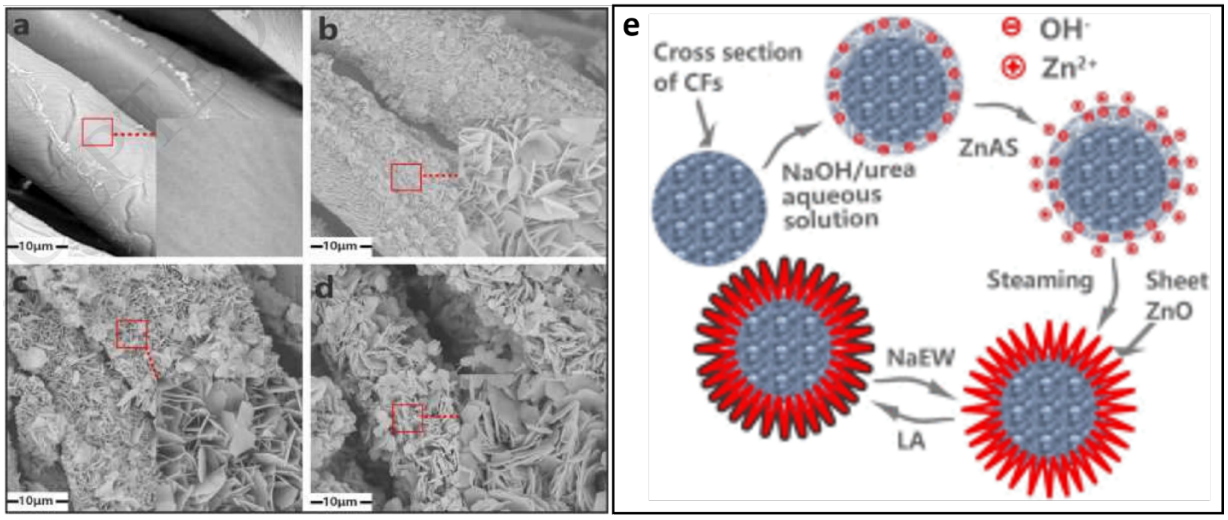

Figure 7. (a) Unmodified, (b) ZnO modified, (c) ZnO-lauric acid modified, (d) ZnO-lauric acid-sodium hydroxide and ethyl alcohol aqueous solution modified cellulose fabric fibers and (e) diagrammatic representation of functionalization of reversible superhydrophobic/superhydrophilic cellulose fabric fiber. (NaEW – sodium hydroxide ethyl alcohol aqueous solution, LA – lauric acid). Adapted from *Fan et al.*[67]. Elsevier copyright © 2016.

The development of superhydrophobic surfaces has resulted in potential applications in water purification, medicine, biotechnology, and materials interfaces. Modification of cellulose and its derivatives such as MCCs and CNCs have classically been modified using fluorinated moieties which typically exhibit hydrophobic characteristics especially to moisture. Though the technology of CNC is mostly at its infancy stage, the advancement in the use of CNCs in functional materials is a positive step towards moving away from dependence on petroleum-based materials. However, more research is needed in the modification techniques of CNCs to develop the use of fewer chemicals and steps. Reduction in modification steps will result in a lower cost of the end product, in addition to environmental benefits by cutting down on man hours and material cost of the added modification step(s).

2.1.3. CNCs as Antimicrobial Agent Carriers

The majority of the antimicrobial agents used are small in size, thus there is always a probability for these active agents to leach out from the material (e.g. fabric, plastics etc.) containing it [68]. Loss of antimicrobial agents to the fabric, skin, and the environment contaminates the material and poses threat to health and environment [68]. The direct addition of antimicrobial agent also reduces the activity and efficiency as a result of leaching out and side reaction with food contents such as proteins and lipids [69]. Some antimicrobial chemical agents pose risk to human health and safety that led to the ban of a number of such agents (e.g. triclosan, iodine complex, phenol, triclocarban, etc.) that were commonly found in over-the-counter consumer products such as soap [70]. In other cases, the prevalence of antibiotic resistance as a result of microbial mutation and a decreasing effectiveness of antibiotics in treating common microbial infections resulted in another motivation for innovative ways of antimicrobial carrier development [71]. Thus, interest has grown in attaching or incorporating active antimicrobial agents to long chain polysaccharides and polymers especially CNCs.

Commonly used antimicrobial agents are halogens, phenols, silver nanoparticles and quaternary ammonium salts [72]. Transition metal oxides such as Au, Ag, Ti, Mg, NO, ZnO, CuO and Fe_3O_4 have antimicrobial properties as well [73]. Antimicrobial enzymes such as lactoperoxidase and lactoferrin and antimicrobial peptides magainins, cecropins, defensins are also often used [74].

Quaternary ammonium compounds (QACs) are positively charged, thus they absorb onto negatively charged microorganisms. They attack the surface cytoplasmic membrane once diffused through the cell wall. Due to the loss of essential constituents of the cell cytoplasm, it becomes difficult for the microorganisms to survive and they eventually die [72,75]. Thus, QACs are one of

the most effective antimicrobial agents used. However, they are toxic to bacteria, pathogens (fungi and protozoa) as well as mammals which limit their applications.

Silver nanoparticles are preferred as antimicrobial agents due to the high activity against a wide range of microorganisms. Silver nanoparticles are active against yeast, fungi, viruses as well as both gram negative and gram positive viruses [76]. As the silver particles permeate through microorganisms, they disrupt and restrict the respiratory function of the microorganisms, thereby resulting in death [77]. As the size of the silver particles decreases, their efficacy increases due to increase in surface area thus nanosized silver particles are preferred [78]. Silver particles inhibits the growth of Escherichia coli (E. coli) and Staphylococcus aureus (S. aureus) [15,77]. Due to various uncertain health effects of silver nanoparticles, their use for food packaging in certain countries has not been accepted [76]. This has resulted in limited application and research especially in specific industries such as the food industry.

Triclosan is a synthetic biophenol (2,4,4'-trichloro-2'-hydroxydiphenyl ether) with excellent biocide activity. It is effective against both gram-positive and -negative bacteria, yeast, and mould [79]. Hence, triclosan has a wide range of applications such as in soap, mouthwash, toys, packaging, textiles and kitchen utensils [68,74,80]. Use of triclosan is regulated by the Environmental Protection Agency (EPA) due to its perceived toxicity and environmental risks, and as a result its use in consumer products is limited 79.

Amongst naturally occurring antimicrobial agents, chitosan is derived from chitin and has gained a lot of popularity in commercial applications. Chitin is extracted from the exoskeleton of insects, as well as algae and fungi 68. Chitosan is a polycationic polysaccharide with antimicrobial and antifungal activity 81,82. Chitosan alters or forms a polymeric membrane on the surface of the cell restricting any nutrients from being absorbed, thus resulting in reduced growth and ultimate death

of the cells 82,83. Chitosan has been investigated for many applications such as packaging, drug delivery and other biomedical applications 16,81,82. However, it is a slow acting antimicrobial agent due to its mechanism as stated previously, therefore, making it not as potent as other antimicrobial agents.

One of the main applications of antibacterial material is in the food packaging industry. Rather than just physical or moisture protection, successful packaging is one that inhibits the growth of microorganisms in food. Thus, active packaging is becoming popular in order to inhibit, reduce, and kill microorganisms from the food surface or the surroundings adjacent to the packaging. Recently, consumer demand for low preservative food has increased. Thus, to maintain food quality under low preservation, active packaging can be very attractive. Active food packaging films can increase the product shelf life, maintain the nutritional value of food, and provide microbial safety while restricting pathogenic growth. As a result, the need for active antimicrobial agents for food packaging has increased to maintain safe food quality 84.

As the demand for biodegradable and bioactive packaging gains popularity, research has been conducted to make active packaging film with nisin, showed in Figure 8, as an antimicrobial agent. Nisin, 34-amino acid long bacteriocin, is active against many foodborne gram-positive bacterium such as *Listeria monocytogens*, *Stephylococcus aureus* and many more [85,86].

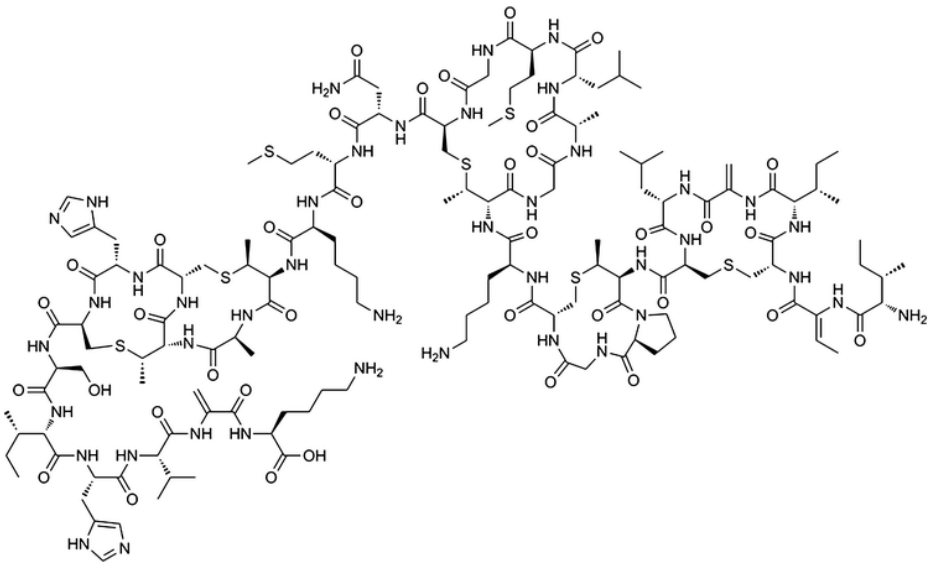

Figure 8. Chemical structure of Nisin[85].

Nisin has been used to activate chitin to make an active packaging for pasteurized milk [87]. Additionally, it was reported that microbial growth on oyster and ground beef was delayed when nisin-activated film was used for packaging [87]. Since nisin has demonstrated good antimicrobial activity, it was incorporated into PLA-CNC composite [85]. Overall the nisin active PLA-CNC film contained all three essential packaging properties: antimicrobial activity, strength and biodegradability. Weishaupt *et al*.[86] reported the self-assembly of nanofibrilled cellulose-nisin biocomposite. TEMPO-oxidized nano-fibrillated cellulose containing carboxylic groups provided a negative surface for nisin to be adsorbed onto the surface [86]. The binding of nisin to nanocellulose was greatly affected by electrostatic interactions. However at high salt concentration, the binding capacity between nisin and nanocellulose was compromised [86]. Nisin bound nanocellulose was investigated against S. aureus and a reduction in growth was observed [86]. Due to the beneficial properties observed, this biocomposite can be further enhanced to develop a promising application in biomedical industries.

Silver nanoparticles are another commonly investigated antimicrobial agents incorporated with cellulose nanocrystals. Drogat at al.[77] reported the activity of silver nanoparticles-CNC composite against *S. aureus* (Gram positive) and *E. coli* (Gram negative). Oxidation of CNC was conducted via periodate ($NaIO_4$) to produce aldehyde, which was then used to reduce silver ions to Ag^0 to inhibit the growth of both the gram positive and negative bacteria [77]. Figure 9 shows the schematic of reaction of CNC with periodate to produce aldehyde followed by reduction of silver ion.

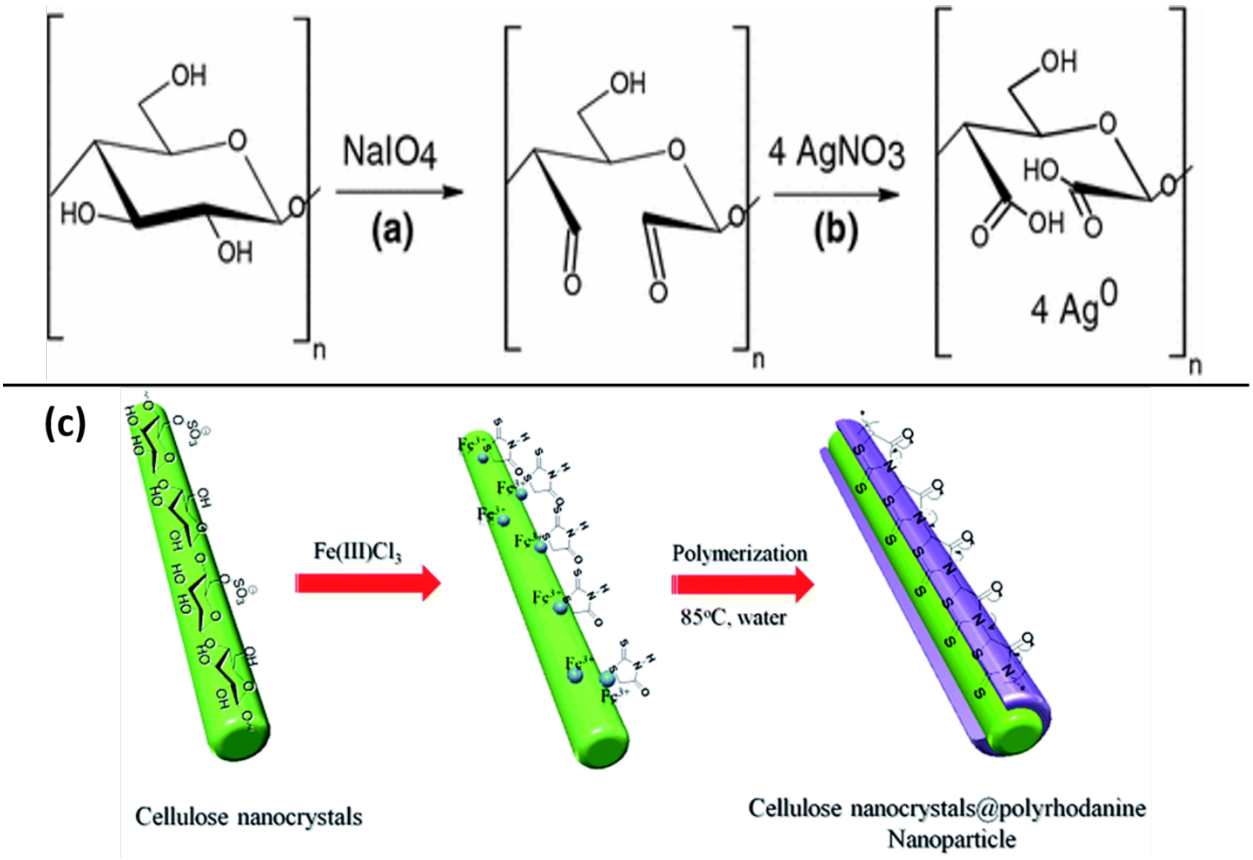

Figure 9. (a) Oxidation of CNC (b) Reduction of Ag^+ to Ag^o. Adapted from Drogat et al.[77]. Springer copyright © 2011 and (c) CNC@PR Fabrication. Adapted from Tang et al. [88]. RSC copyright © 2014.

Inhibited growth of bacteria suggests the potential application of silver-CNC matrix for wound healing gels, antiseptic solution, as well as other biomedical applications. Fortunati *et al*. also reports antimicrobial activity of PLA-CNC biocomposites containing 1 wt.% Ag nanoparticles

against *S. aureus* and *E. coli* [76]. Higher activity was observed against *E. coli* than *S. aureus* due to greater toxicity of silver ions towards *E. coli* while significant amount of activity was also achieved for *S. aureus*[76,89]. PLA biocomposites with excellent antimicrobial activity against both gram-positive and gram-negative bacteria offer more opportunities for the development of active packaging for food, sanitary, and biomedical industries.

Amongst different structures for antimicrobial compounds, core-sheath structure of cellulose nanoparticles with polyrhodanine was reported by Tang *et al.* [90]. Cellulose nanoparticles with polyrhodanine (CNC@PR) showed antimicrobial activity against *E.coli* and *B. Subtilis* [90]. CNC@PR was synthesized with Fe (III) complex and ferric chloride to negatively charge the CNC surface. Fe (III) was used as an initiator and oxidant for the *in situ* polymerization of rhodanine on CNC[88,90]. Figure 9 (c) shows the schematic of core-shell nanoparticles of CNC coated with polyrhodanine.

In academia and industry, antimicrobial materials are gaining a lot of interest due to the need to improve on the shelf life of food products. The application of antimicrobial materials is not only limited to food packaging but also a variety of other applications such as textile, coating, military, and household equipment as shown in Figure 10. High surface area and shorter diffusion path of nanofibers makes them an excellent choice for attaching antimicrobial molecules while also used as a reinforcing material for polymers as well [91]. Biomedical devices possessing antimicrobial-functionalized polymers can be proven very hygienic and efficient for health care purposes. Similarly, antimicrobial coatings can be used in hospital walls, kitchen counter tops, and other pharmaceutical laboratories to maintain a microbes-free environment. Household items, sanitary items for bathroom, kitchen utensils such as chopping board, kitchen towels, dish rack, and toys for kids made from antimicrobial materials can promote a healthy environment.

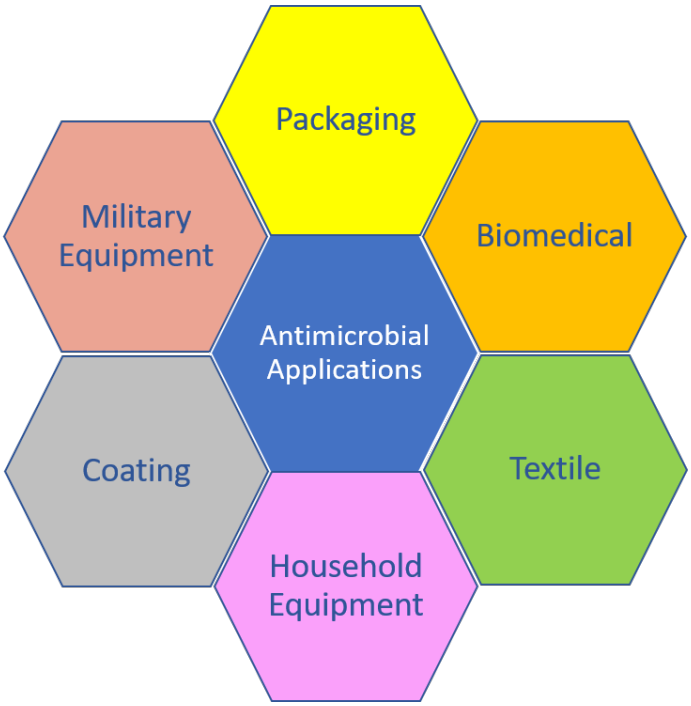

Figure 10. Applications of antimicrobial CNC composites.

However, unlike other antimicrobial agent carriers, nanofibers can also provide mechanical strength which is desirable for most of the applications mentioned. This is currently an active research area with a focus on acquiring enhanced antimicrobial properties, cost optimization, and scale-up studies to commercialize these products.

2.1.4. CNCs in Barrier Applications

Limiting the effects of the environment on materials has long been a major concern in numerous industries. In the oil and gas industry where a network of pipping systems is a major vessel for transporting oil and chemicals, corrosion is a major problem and concern. In the marine industry, the exposure of vessels to sea water is constantly corroding and eroding the bottom of the vessels. Ultraviolet light exposure over time can alter the micromolecular properties of materials such as polymers, therefore changing the bulk properties. The use of CNCs in barrier applications are limited except for a few explorations in academia.

2.1.4.1. UV Protection

It is well known that over time when exposed to UV, the physical appearance of polyurethane (PU) starts to change; thisat results in yellowing of the material from the photochemical degradation of the surface molecules. In order to prevent or slow this process, research was carried out using CNCs as a UV stabilizer by Zhang *et al.*[92]. 3-Glycidyloxypropyl) trimethoxysilane (GPTMS) was used to modify CNC at different concentrations. The GPTMS was hydrolyzed thereafter and the CNC was added and allowed to react over time. Figure 11 (a) shows the proposed reaction scheme during salinization and the interaction between the modified CNC and PU. The modified CNC was then incorporated into the PU formulation and homogenized to disperse the modified CNC in the PU as shown in Figure 11 (b) to create the PU/CNC composite. This composite was then exposed to a controlled UV radiation over time. The results from this study showed that the presence of a modified CNC in the PU drastically reduced the yellowing effect of the UV radiation, with further reduction observed with increase in the concentration of the modified CNC. With the addition of 1.5% modified CNC, the anti-yellowing effect was increased by approximately 58% which demonstrated the effectiveness of CNC as an antiyellowing agent or a UV barrier agent. It was postulated that the addition of the modified CNC inhibited the photo degradation of the CH2 group while preventing the scissioning of the urethane group.

In another study, CNC was used as a bifunctional filler that provides reinforcement and UV barrier for poly vinyl alcohol polymer 92. CNC pulp was oxidized using sodium metaperiodate and then reacted with sodium 4-amino-benzoate in an HCl solution to produce modified CNC with photo-active groups attached to it, which was further mechanically disintegrated to form *p*-aminobenzoic acid grafted CNC (PABA-CNC). This modified CNC was added to an aqueous PVA solution at different concentrations. This solution was further degassed and cast to form thin films which were

then used for further tests. The results from the addition of PABA-CNC to PVA on the UV transmittance revealed that the presence of PABA-CNC in the PVA in comparison to neat PVA was significantly reduced and was also a function of the concentration of PABA-CNC within the PVA. Increasing the concentrations of PABA-CNC showed further reduction in UV transmittance with PVA films containing 0.5 and 10% PABA-CNC, reducing the transmittance to 54 and 12%, respectively in comparison to that of neat PVA film that exhibited 70% transmittance. Likewise, enhancement in the mechanical properties such as the tensile strength and modulus of the film was observed with PABA-CNC incorporation. This increase was also a function of the concentration of PABA-CNC. Similarly, ethyl cellulose nanoparticles (ECNPs) have been studied as a means to confine or protect UV filters which tend to create reactive oxygen species when exposed to UV due to photodegradation[92]. Typically, these filters are used for applications in cosmetics such as sunscreens, and can scavenge carcinogenic reactive oxygen species which can be harmful when they come in contact with the skin.

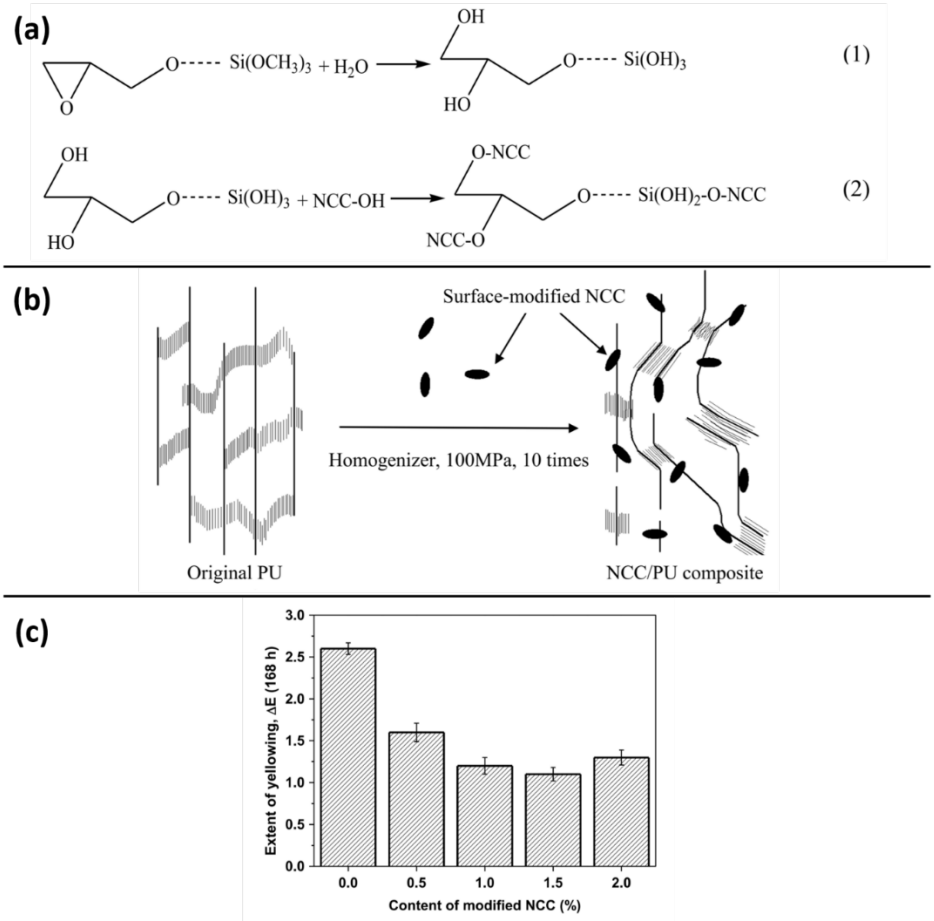

Figure 11. (a) Reaction scheme for the modification of CNC using GPTMS (reaction scheme 1) and interaction between modified CNC and PU (reaction scheme 2), (b) diagrammatic representation of the dispersion of modified CNC within the PU and (c) bar graph showing the effect of concentration of the modified CNC on the yellowing of PU upon exposure to UV radiation over a control period of time.

2.1.4.2. Solvent and Chemical Protection

Application of surface coatings to help protect surfaces from the surrounding environment is a common practice in industry in many products today. Some of the applications include the use of paint on metals to prevent rust, application of clear coat epoxies on plastics and wood to prevent scratching, and UV degradation and biodegradation, respectively. However, clear coat epoxies or paints for rust prevention do not always have good strength and chemical resistance. The characteristic properties of CNCs such as excellent strength and reinforcing capabilities at very

low loadings due to its crystallinity and nano-size have lent its service in the application as a functional material in epoxy surface coatings of metals in a study by Ma *et al.*[93]. In this study, epoxy containing 1, 1.5 and 2 wt.% of CNC was thoroughly mixed using a glass rod and then sonicated to ensure proper dispersion and then brush coated onto mild steel in thin layers. The coated steel was allowed to dry and tested for its corrosive resistance using electrochemical impedance spectroscopy (EIS) by immersion in 3.5% sodium chloride over a 30-day period. Similarly, the optical clarity or transmittance was tested using UV-vis analysis to determine the effect of CNC in the epoxy coating. The results from the optical transmittance showed that with increasing CNC loading, the transmittance dropped to 20% for the coating containing 2 wt.%. of CNC. However, the coating containing 1 wt.% CNC was observed to be very clear with a transmittance of 74%. It was further observed that for all composites, the light drop-off transmittance was at approximately 300 to 350 nm, which indicates high light absorption with no light reflections occurring in the UV range of 300 to 400 nm. This indicates that when used in clear coat applications, this coating (especially at 1 wt.% CNC) can act to prevent UV degradation while still having high clarity. The corrosion test on the other hand, revealed that the presence of CNCs in the epoxy significantly increased the corrosion resistance of the epoxy coating. This could be because the CNC acted as a barrier to the ions from sodium hydroxide solution by creating a tortuous path. This resulted in preventing complete penetration of the coating, thereby protecting the mild steel surface. Only the unreinforced epoxy suffered penetration after 1 day of exposure. It was suggested that this was due to the CNC creating a longer path through which the solution had to travel in order to come in contact with the mild steel. Electrochemical analysis of the coatings through bode plots revealed that only the neat epoxy coating showed two-time constants. At day 30, only the unmodified epoxy continued to reveal two-time constants revealing the

remarkable ability of the CNC to act as an anticorrosion agent. However, for the 2 wt.% CNC loaded epoxy coating, as the test continued over the 30-day period, the appearance of a two-time constant slowly developed. This was attributed to the possible agglomeration of the CNCs within the epoxy which did not homogeneously disperse like those in the 1 and 1.5 wt. % loaded samples. Therefore, exposing unprotected regions within the epoxy to the solution allowed diffusion of the ions (Na^+ and Cl^-) towards the mild steel that resulted in corrosion.

2.1.5. Electrical Applications of CNCs

Research into the development of functional applications of CNCs in electroactive materials such as electrical conductive materials, dielectric materials, microelectronics components, etc. is an upcoming research area with some current materials such as starch [39], proteins and peptides [94] already being researched for similar applications. The interest for using CNCs in electrical applications is accrued mainly from its ease of modification, piezoelectric and dielectric properties, and sustainability attributes similar to other bio-derived materials. . Csoka *et al.*[95] asked the question of whether ultrathin films containing well-aligned cellulose nanocrystals could exhibit piezoelectric effects stemming from the collective yield of the individual CNCs. Ultrathin films containing different degrees of CNC alignment were produced according to a process well described by the authors in a different publication [96]. The displacement of the film was measured using atomic force microscopy in tapping mode while an electric field was applied to them. It was observed that the higher the degree of alignment, the greater the piezoelectric effect. Therefore, the piezoelectricity of the film was dependent on the orientation of the CNCs. This observation was deduced not only to the alignment of the CNCs, but also due to dipolar orientation and the crystallinity of CNCs in the films. Figure 12 (a) shows the schematic of AFM in tapping mode with a diamond tip over ultrathin films containing aligned CNCs with an electric field applied

across it. Mean while, Figure 12 (b) graphically demonstrates the effect of applied voltage to the thin films in response to the displacement of the CNCs. Given the result from this study, ultrathin films with various degrees of CNC alignment can result into different levels of electro-mechanical actuation, which could potentially be used in applications such as ultra-sensitive micro balances. For examples, having a high degree of CNC alignment and concentration can potentially result in ultra-sensitivity of applied forces.

CNCs are able to change polarization densities due to the high level of crystallinity. Likewise, its dielectric property allows it to be applied as a functional insulating material in different applications. However, moisture plays a huge role in determining the final dielectric property as it acts as a conductor of electricity when present in the CNC. For use in dielectric applications, the moisture levels should typically be ~ 0.5% [97]. However, due to its hygroscopicity, it usually has a moisture level typically between 4–8%. This range of moisture content stems from the source of the CNCs and highly dependent on the cellulose crystallinity as determined from studies on water sorption of cellulose [98,99]. Overall, the higher the crystallinity of the cellulose, the lower the moisture content will be and vice versa. Bras *et al*. [97] studied the dielectric property of two nanocelluloses from wood (nanofibrillated cellulose, NFC) and algae (*Cladophora* cellulose). They found that the moisture sorption capability at low and high humidity was higher for NFC due to its lower crystallinity. However, contrary to the expectations that dielectric properties are highly related to crystallinity, a higher dielectric property was observed for NFC when compared to that of *Cladophora* cellulose. This was due to the high porosity of *Cladophora* cellulose which allowed for air entrapment, subsequently increasing its dielectric loss. It is apparent that CNCs do have excellent dielectric properties which can be harnessed for electrical insulation purpose such as in

cable insulation, but the effectiveness of this property not only depends on the source but also on the morphological features [97,100].

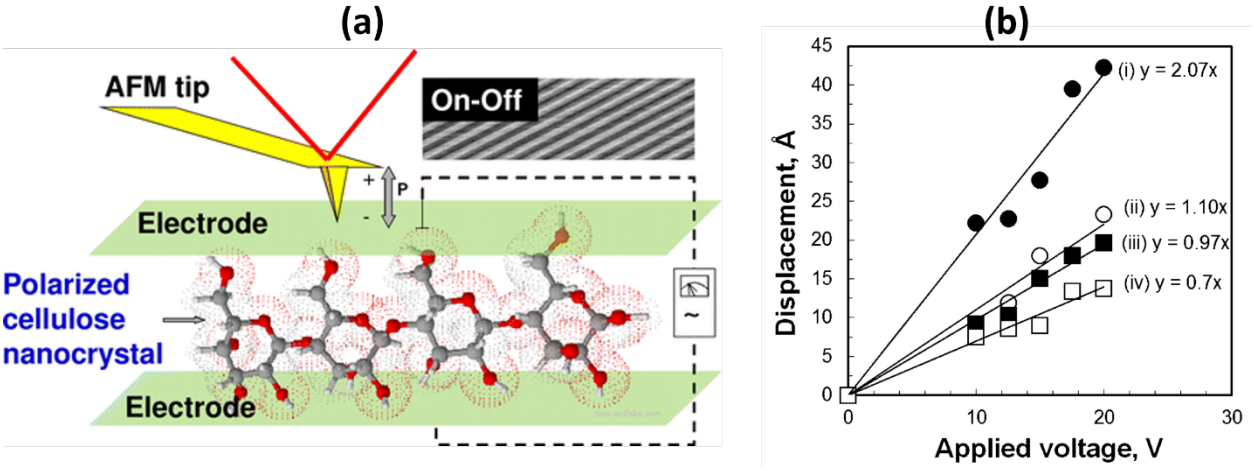

Figure 12. (a) Characterization of well aligned CNC ultrathin film for its dielectric property using AFM in tapping mode and (b) effect of voltage on CNC displace (piezoelectric effect).

2.1.6. Other Applications of CNCs in Advanced Functional Materials

Cellulose nanocrystals have gained a lot of interest as a renewable reinforcing filler due to its biodegradability, low density, higher aspect ratio and excellent mechanical properties. CNCs are considered for a wide variety of applications since the surface hydroxyl groups of CNC can be functionalized as per requirement. CNCs obtained through sulfuric acid hydrolysis contain negative charge on the surface providing electrostatic repulsion between the CNCs. As a result, CNC can easily be dispersed in polar polymer matrices such as PVA. In the last two decades, the many applications of CNC have attracted academia and industrial researchers. Other than its use as a reinforcing agent, CNCs demonstrated interesting potential for biomedical, antimicrobial, personal care and energy applications as shown in Figure 13.

2.1.6.1.Polymeric Reinforcement

Cellulose nanocrystals are commonly used as a reinforcing filler in polymer matrices to enhance their strength. Traditional polymers alone lack strength required for most structural applications, thus requiring fillers to reinforce them. CNC as a bio-based material provides excellent reinforcement for polymers. Several studies have shown enhancement in both thermal and physical properties of polymers at very low concentrations of CNC incorporation due to its nano-size and ability to efficiently absorb stress from the matrix [37,101]. Bras et al. reported the reinforcing effect of CNC in rubber [102]. They found that CNCs were able to enhance the thermomechanical and mechanical properties of rubber. However, due to the hydrophilicity of the CNCs, the water absorption was increased. This study shows that CNCs can be used as polymer property enhancement when specific applications are targeted that do not expose the composites to moisture. Furthermore, reinforcing capabilities of CNC is also evident in cement as investigated by Cao *et al.* [103]. The water absorbing property of hydrophilic CNCs was an advantage in improving the flexural properties of cement paste. It was postulated that the hydration of the paste was improved when up to 0.2 vol.% of CNC was added, subsequently leading to flexural strength increase of up to 30%. These examples suggest that CNC can be the future of nano-polymer composite materials used for construction, automobile parts, furniture, and other industrial high-strength materials when targeted appropriately for specific materials.

A variety of polymers have been successfully grafted on CNC to modify its surface and obtain modified CNC with desirable properties. For instance, the use of hydrophobic polymer grafted CNC in non-polar polymers usually results in improved dispersion and interaction of the CNC with the polymer and enhances the strength of polymer composites made thereof. In other cases,

the grafted polymer provides functionality attribute to the CNC that expands the application range of CNC.

2.1.6.2. Biomedical Applications

Biomedical applications of CNC include the use of CNC for medical devices, bioimaging, wound healing, scaffolds for tissue engineering, and controlled drug delivery[104]. High interest in biomedical application of CNC based materials stems from its biodegradability, biocompatibility, lower toxicity and excellent mechanical properties. Dong et Roman [105] investigated fluorescently labeled CNC for bioimaging applications. In this study, CNC was conjugated with fluorescein-5'-isothiocyanate using epichlorohydrin to study its biodistribution and in vivo interaction using the fluorescence labelling, which can be beneficial in many biomedical applications105.

CNC is extensively studied for tissue engineering where a scaffold device is used for self-healing and regeneration. In order to obtain enhanced performance, appropriate material selection for scaffold is very crucial. Mechanical, physical and biological properties play a vital role in elevated performance and suitable mechanical integration [106]. Thus, properties such as surface roughness, topology, porosity, pore size, and surface area to volume ratio must be considered [107]. Moreover, degradation rate of biodegradable material is very important so that the healthy tissue can be restored while scaffold material gets absorbed. In order to achieve both the mechanical and biological properties unfilled polymer materials cannot be used in most cases. Thus, nanofillers are incorporated to form a nanocomposite that provides functional benefits such as mechanical strength, electrical conductivity, adhesiveness, and ability to self-assemble [106,107]. A review on CNC-based biomaterial for tissue engineering by Domingues *et al.*[107] extensively describes the use of CNC-PLA composite material for tissue engineering to fulfill aforementioned requirements

for biomedical scaffolding applications. Along with other biomedical, and pharmaceutical products, CNC can open new doors to new personal care products [108,109].

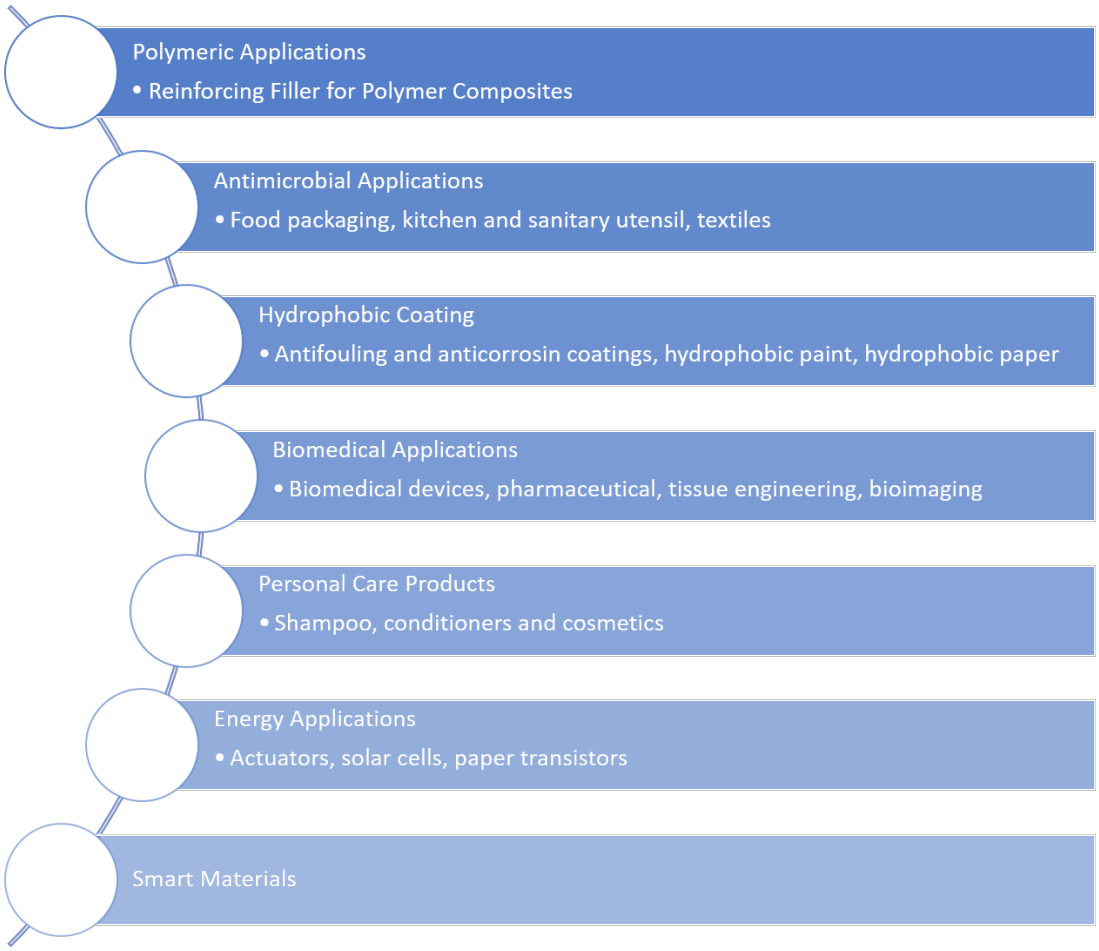

Figure 13. Various applications of CNC

2.1.6.3. Energy Applications

Energy application of CNC includes the use of cellulose-based composites for energy storage. With growing environmental concerns, interest has grown in making renewable energy source more efficient and feasible. An attempt to produce recyclable solar cell from cellulose nanocrystal by Zhou *et al.*[110] is a contribution towards the same initiative. While taking the advantage of the excellent mechanical properties of CNC and silver, a semitransparent electrode recyclable solar

cell was fabricated [110]. However, further improvements were needed to obtain efficient and desirable performance. Kim *et al*.[8] has reported other energy applications of cellulose based materials such as uses in energy harvesters, display devices, actuators and paper transistors. Excellent mechanical and biocompatible properties of CNC has the potential to provide environmentally friendly, sustainable technologies.

2.1.6.4. Smart and Responsive Materials

The application of smart responsive materials has increased in recent times. Smart responsive materials adapt to external environment and provide response. Changes in stimuli such as exposure to light, heat, chemicals, or magnetic fields can be used to generate mechanically adaptive, stimuli-responsive materials. Nanocomposite can respond to exposure to external stimuli in various ways such as swell or shrink, assemble or dissemble, or prompts for separation[111]. These changes generated as a response to stimuli variations can be used to develop a smart material. CNC can be used as a stimuli-responsive material for sensors and other applications. CNC displays responsiveness towards pH, light, moisture, heat, chemical and magnetic fields, which adds the stimuli-responsiveness functionality along with reinforcing capabilities. Changes in pH correspond with changes in rheological properties of CNC composites [112]. Way *et al*.[112] synthesized carboxylated and amine functionalized CNC to investigate pH responsiveness. By altering the surface chemistry of CNC, the nanocomposites can be reprogrammed to develop various mechanically adaptable materials.

Since modified CNC has the ability to generate a response to changes in external stimuli, they can be readily used in sensing applications. Smart CNC-based sensors can be designed for moisture, ions, organic vapors, and biological species sensing applications. Humidity sensor designed by Kafy *et al*.[113] is made from CNC-graphene oxide (GO) composite. CNC and graphene both are

hydrophilic with higher water uptake capacity. CNC-GO films displayed even increased water uptake capacity which is desirable for moisture sensitivity[113]. The sensing film did not compromise its performance with temperature change, demonstrating practical use of humidity sensor[113]. Similarly, CNC can be functionalized to make gas sensing material which can detect other organic and toxic vapors. Moreover, CNC based sensing material can also be used to detect ionic species. CNC containing pyrene was synthesized to detect ferric (Fe^{3+}) ions [114]. This concept can be further explored to design a sensing material for different ions, chemical and biological molecules. Other smart sensors made from CNC include proximity sensors and strain sensors by Sadasivuni *et al*.[115] and Wang *et al*.[116] respectively.

Hydrophilicity of CNC can be used to generate water-responsive mechanically adaptive polymer matrices. For instance, Pratheep *et al*.[117] designed a water sensitive styrene-butadiene-rubber (SBR) and CNC nanocomposite. First of all, the reinforcing capabilities was proven since the modulus of pure SBR (3 MPa) was improved significantly (to 740 MPa) [117]. CNC aids as a hydrophilic channel in a hydrophobic matrix for water uptake. CNC is used to generate water-responsive mechanically adaptive materials because upon water swelling, CNC networks are disrupted to cause a reduction in modulus [117,118]. Thus physiological variation can lead to changes in mechanical properties to design a mechanically adaptive materials[117]. Mendez *et al*. [118] also used the water-responsive ability of CNC to design a smart polyurethane-CNC nanocomposite, which displayed water activated shape memory effect.

Similar to pH and moisture response adaptive materials, thermal and photonic responsive materials were also generated. Cellulose nanocrystals grafted with thermoresponsive brushes of poly(N-isopropylacrylamide) have also been investigated [119–121]. Figure 14 shows the external stimuli that

can be altered to generate responses which can be used to develop smart CNC applications such as controlled drug delivery material, energy applications and chemo- and biosensors.

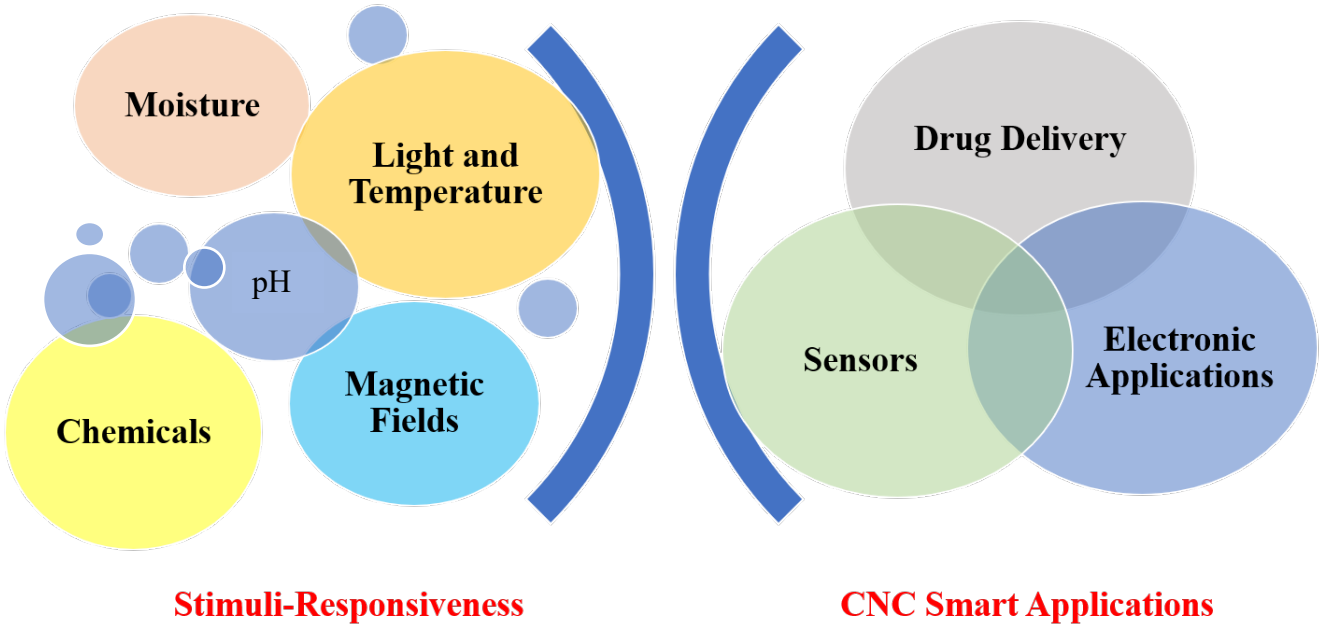

Figure 14. Cellulose based smart materials[8,104,110,111,122].

Novel and effective drug therapies have also been investigated to develop a controlled drug delivery method. Controlled drug release provides advantages such as maintaining required therapeutic concentration, localized drug delivery and improve patient compliance, however these novel techniques are yet to be explored to develop drug delivery materials sensitive to physiological changes [123]. Thus, stimuli-responsive polymeric drug delivery processes are typically used for controlled drug delivery. CNCs, being biocompatible and biodegradable materials, can be functionalized to develop smart material that offers a great potential in targeted, controlled drug delivery systems [8,123].

The study of CNC for smart electronic application has also gained enormous interest. In the Review of Nanocellulose for Sustainable Future Material, Kim *et al.*[8] has reported various use of

CNC based material in energy and electronics applications. Electroactive paper (EAPap), which functions based on two principles (*i.e.* ion migration and piezoelectric effect) has application in sensors, actuators, biomimetic robots, and other haptic technology [8,111].

2.2. Lignin Structure and Applications

Lignin, aromatic biopolymer, found on earth represents 30% of the total biomass produced in the biosphere [20]. Lignin, a by-product of paper and pulp industries, has an annual production of over 70 million tons [124,125]. It has an amorphous, complex structure found in the cell walls of the plants, between the secondary cell wall and lamella, distributed along with cellulose and hemicellulose providing rigidity to the cell structure [124,126]. Key functions of lignin include providing strength to the plant, controlling fluid flow, and protecting it from biochemical attacks [1].

2.2.1. Lignin Structure, Extraction and Properties

Native lignin can be extracted from hardwood, softwood and grass. It is a heteropolymer synthesized by radical coupling of three typical monolignols coniferyl alcohol, sinapyl alcohol, and p-coumaryl alcohol [127,128]. Three phenylpropane units are derived from these monolignols. In lignin, the phenylpropane units are known as guaiacyl, syringyl and p-hydroxyphenyl derived from coniferyl alcohol, sinapyl alcohol and p-coumaryl precursors respectively[19,127,128]. The monomers form different carbon-carbon and carbon-oxygen bonds developing a complex, amorphous, and phenolic structure. These units are bonded together mainly with $\beta - O - 4$ linkage along with $\alpha - O - 4$, $\beta - 5$, $\beta - 1$, $5 - 5$, $\beta - \beta$ and $4 - O - 5$ linkages [125,126,129].

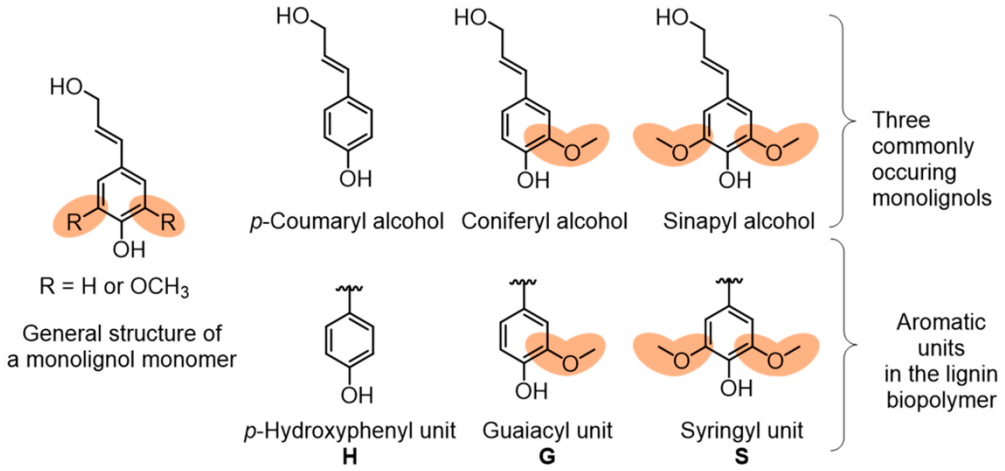

Figure 15. Monolignols and aromatic phenylpropane units in lignin-derived from monolignols[1]

Lignin extracted from pulping industries through different processes is referred to as technical lignin. There are mainly two types of technical lignin, classified based on the process of extraction: sulfur or sulfur-free technical lignin. Kraft and lignosulfonate are extracted through the sulfur-based process, whereas soda and organosolv lignin use sulfur-free processes [125]. Approximately 85% of the world's technical lignin produced is through kraft process [130]. Soda lignin, produced from a sulfur-free process, maintains structure similar to native lignin [125,130]. As a result soda lignin is often a preferable choice of technical lignin for chemical modification and used without any further purification [125,130].

Lignin has many valuable properties. The aromatic structure of lignin gives it UV-absorbing properties [125,131]. Therefore, lignin can find applications in UV-protective coatings and films, sunscreen cosmetics. Qian *et al.*[132] investigated the UV-absorbing capacity of lignin in commercial sunscreen lotion. It was observed that lignin absorbs light in a broad range. With 10 wt.% lignin added to commercial lotion, a drastic increase in performance was observed. Lignin also possesses free radical scavenging and antioxidant activity [21,126,127]. Lu *et al.*[128] reports this dominant property of lignin, which is dependent on its solubility. Antioxidant lignin can find applications in food

packaging as a functional filler. Yang *et al.*[133] also tested the antimicrobial properties of lignin nanoparticles. Antimicrobial activity was tested against Escherichia coli, Saccharomyces cerevisiae, Bacillus licheniformis, and Aspergillus niger showing bacterial inhibition [133]. However, lignin with such beneficial attributes is currently underutilized.

2.2.2. Utilization of Lignin and Challenges

Lignin is an extremely abundant source of raw material providing renewable carbon and many other functional groups such as aldehydes, aromatic, and hydroxyl compounds. Therefore, fragmentation of lignin through thermochemical decomposition processes such as pyrolysis has gained a lot of interest [134–136]. At elevated temperature, the C-C linkages are broken, producing a gaseous mixture of CO, CO_2 and CH_4 and pyrolysis oil [135]. Although thermal decomposition of lignin can produce valuable products, challenges associated with actually separating the end-products make this process less economical [137].

Lignin also has many hydroxyl groups that can be modified with different moieties. The phenolic hydroxyls are readily reactive allowing for many chemical reactions. Esterification, etherification, phenolation, sylilation, oxidation, reduction, and urethation of lignin are a few of the chemical modifications studied earlier [135]. Due to the recalcitrant nature of lignin, modification of lignin for functional applications has been a challenge. Only a small amount of lignin produced is used for value-added applications. Heterogeneity in the intrinsic structure of lignin, as well as diversity in source and extraction process makes the prediction of properties difficult.

Lignin has attracted many researchers on developing a value-added application from this complex yet environmentally friendly structure. Studies have been conducted to replace the phenol fraction of phenol-formaldehyde adhesives by lignin to form wood adhesive [19]. Lignin hydrogels are another area of interest. Renewable hydrogels with antioxidant, antimicrobial, and stimuli-

responsive properties can find application in biomedical, biotechnology, and tissue engineering [4]. Grossman *et* Vermerris [138] lists other uses of lignin such as lignin 3D printing resins, lignin nanocomposite, and lignin-based nanoparticles for biomedical applications.

Due to the advantageous properties of lignin biopolymer, obtaining and using lignin nanoparticles for a functional application can be of interest. Nanoparticles have gained popularity because nanostructure displays enhanced properties compared to the base material. Producing nanoparticles from macromolecules increases surface area, which in turn improves the surface properties [131]. Research has been conducted on synthesizing lignin nanoparticles through various methods [22,131]. Lu *et al*. [128] reported superior antioxidant activity of nanolignin compared to macro-size lignin.

2.3. Future Trends, Challenges and Conclusions

Although CNCs have many desirable properties, their high hydrophilicity and tendency to aggregate in polymer matrices, can drastically restrict their applications [5]. These characteristics lead to the formation of flake-like agglomerates in polymer composites due to surface area and volume effects and the strong intermolecular hydrogen bonding between CNC particles [76]. Recent studies were conducted to investigate the correlation between CNC dispersion and the resulting strength [139]. Results indicated that as the dispersity of CNCs was improved, the strength of cement plaster also increased [139]. This suggests that the issue with the agglomeration of CNCs must be resolved to achieve their touted reinforcing performance when used as a filler in polymeric and other applications. During CNC modification, it is important to limit the modification only to its surface so that the structural and morphological integrity of the CNC is preserved [49]. However, the reality is that most CNC modifications involve aggressive oxidization to increase the concentration of hydroxyl groups on its surface to be used as anchor points for further modifications. This usually

affects its structural integrity and crystallinity, which could subsequently alter its mechanical properties. Therefore, new and less aggressive modification processed and/or chemicals need to be developed to achieve the same level of modification as currently used.

Though CNCs have excellent thermal stability in comparison to other bio-based fibers, long term durability of products is of concern when it is incorporated or used as a functional material. Moreover, commercial products intending to apply CNCs in functional applications need multiple and abundant sources. Currently, the majority of CNC production is limited to North America and some Scandinavian countries (e.g. Sweden, Finland) [122]. The expected rise in CNC production in the future will give rise to the application on an industrial scale [35].

The versatility of CNC functionalization can be the future of sustainable, biocompatible, and biodegradable material for a variety of applications, especially with the current environmental concerns such as climate change from greenhouse gases due to the production and use of petroleum-derived materials. Due to its abundance across the globe, bio-renewability and the fast-growing technologies on its production, CNCs are becoming the focus of product development and research as observed from the numerous researches published on CNCs in recent years. Therefore, it is foreseeable that in the near future, CNCs will be widely and extensively found in the medical, electronics, oil and gas, biotechnology and food industries just to mention a few. CNCs have also been shown to be a viable option to potentially replace synthetic materials for functional applications in various industries. As CNCs continue to gain great attention from researchers all over the world, more understanding and applications with improved technology towards production will rapidly be developed thereby taking CNCs from lab to industrial scale.

Production of pulp and paper industries produces technical lignin in large quantity. Lignin with many beneficial properties, renewability, biodegradability, and availability can be a great source

in material industries. Currently, lignin is used as an energy source, but it can be further utilized for value-added applications. However, the heterogeneity and complexity of lignin structure has limited its use at the commercial level. Modification of hydroxyl groups with different moieties can open the door to many applications. Lignin nanoparticles can also offer advantageous properties finding applications in advanced nanocomposite for coating, biomedical, tissue engineering, and drug delivery applications.

CHAPTER 3: Tailored Cellulose Nanocrystals as a Functional Ultraviolet Absorbing Nanofiller of Epoxy Polymers

3.1. Introduction

Epoxy, a low molecular weight, thermosetting polymer resin, is extensively used in adhesives, paint and coatings, structural composites, electronics, construction, and biomedical applications [140]. The majority of these applications are found outdoors, involving continuous exposure of the epoxy surface to sunlight. Along with a number of other radiations, the sun emits ultraviolet (UV) rays, which are harmful not only to animals and plants but also damage materials such as plastics [141,142]. While UV radiations with longer wavelength such as UVA (315-400 nm) and UVB (280-325 nm) are absorbed by the ozone layer, some remaining UVB rays are transmitted to the earth with enough energy to break certain chemical bonds leading to accelerated chemical degradation of polymers [141,143,144]. In the literature, the UV-degradation of polymers such as polyvinyl alcohol, polyurethane, polyvinyl chloride has been reported [141,145–147]. Despite its extensive use in outdoor applications, epoxy is among these polymers that undergoes considerable photo-degradation under the exposure of Ultraviolet (UV) light [145,148,149].

Epoxies exposed to UV radiation undergo discoloration, making them aesthetically unappealing [145]. Longer exposure of epoxy to UV light also results in embrittlement of the polymer starting with the formation of micro-cracks on the surface [145,149]. These are particularly unsuitable for epoxy used in coating or structural composite applications. Thus, epoxy applications in coating are typically limited to underlayers that are not directly exposed to UV radiation. Furthermore, UV degradation deteriorates the mechanical properties of epoxy resins when used as a matrix in structural composites [145]. Such compromise in mechanical properties poses a disadvantage for epoxy by shortening its service life span in critical structural and functional applications such as

in the automotive, construction, and aerospace industries. Hence, most epoxy composites used in structural material applications are coated with UV resistant polymers.

The incorporation of organic and inorganic UV absorbers and other stabilizers to polymeric material formulations has been researched and commercialized. The direct incorporation of inorganic UV stabilizers such as ZnO, TiO_2, and organic stabilizers such as benzotriazoles, benzophenones, benzoic acid and hindered amine light stabilizers (HALS) are extensively studied to reduce UV and other photodegradation [144,148,150]. The use of para-aminobenzoic acid (PABA) as a UVB blocker in sunscreen lotion to prevent skin damage and in extreme cases skin cancer resulting from UV radiation is known due to its UV-blocking properties in the UVB range [151]. While few studies[141,152] investigated the use of PABA as a potential UV absorber in polymers. In both these studies, biopolymers such as lignin or cellulose nanocrystals were functionalized with PABA to be used as a filler for polyvinyl alcohol. Although PABA has been widely accepted as a UV absorber its extensive use in the polymer industry is rather limited. This is attributed to their tendency of migration and decomposition that results in reduced efficiency over an intermediate to longer period of time[150]. Moreover, such small organic molecules (MW 137.14g/mol) can easily leach out of plastics and may pose an environmental hazard [141]. Moreover, such small organic molecules (MW 137.14g/mol) can easily leach out of plastics and may pose an environmental hazard. Particular to epoxy, PABA could not be directly incorporated in the baseline resin. This was becacuse the highly nucleophilic primary amine group of PABA can open and react with the epoxide groups. This can severely limit the crosslinking of epoxy with the typical bifunctional amine crosslinking agent resulting in a less crosslinked network with poor properties.

In this research, the grafting of PABA on the surface of cellulose nanocrystals (CNCs) and its UV absorption efficiency in epoxy nanocomposites was investigated. The covalent bonding of PABA

on the surface of CNCs can circumvent the leaching concern from polymer matrices over the lifetime of the polymer applications and potentially provide a reinforcing effect. Also, CNCs have already obtained substantial interest as a reinforcing filler of polymers, and their use as a multifunctional filler could be of great scientific and industrial interest.

Cellulose nanocrystals (CNC), were selected as a modular nanoparticle due to their substantial interest in the polymer industry associated with their renewability, biodegradability, high strength, and low density. Moreover, CNCs are rich in hydroxyl groups associated with their anhydrous glucose monomer units. These hydroxyl moieties, typically one primary and two secondary, are amenable to several chemical modifications [17,101]. A significant body of research has already been conducted on the use of CNCs as a reinforcing filler of epoxy polymers [153,154]. Investigation of the utilization of nanoparticles and other organic molecules to mitigate UV degradation of polymers is not entirely new either. For instance, Woo et al.[145,149] have studied the photo-degradation and resulting performance of epoxy resins with organoclay as a filler. Nikafsher et al.[144] used organic filler (Tinuvin 1130) to enhance the UV resistance of epoxy. Despite the diversity of modification chemistries and the promising properties already offered by functional agents grafted onto CNCs, the full potential of CNCs has not been utilized, and more applied approaches are in great demand. Furthermore, the use of coupling pathways to attach functional molecules onto CNCs is still relatively rare, most likely due to the lack of facile conjugation agents and methods. CNC modified with PABA can be used as a filler for polymeric matrix to reduce degradation caused by extensive exposure to UV-light. Thus, the goal of this study was to investigate the conjugation of PABA onto CNCs using a coupling agent that has a differentiated reactivity and evaluate their efficiency as functional UV protective nanomaterials in epoxy matrices. To the best of our knowledge such modification of CNC with PABA has not been till now.

3.2. Experimental

3.2.1. Materials

Cellulose nanocrystals were obtained from Innotech Alberta (Edmonton, Canada). The CNC power had a crystalline fraction of 88% and the particle size of the CNC powder was 1–50 μm. CNC obtained from sulfuric acid extraction had a sulfur content and bulk density of 0.87% and 0.7 g/cm3, respectively. Isophorone diisocyanate (IPDI), dimethyl sulphoxide (DMSO), dibutylin dilaurate (DBTDL) were purchased from Sigma Aldrich. Epoxy resin (Araldite 506, epoxide equivalent weight 172–185 Da) and amine curing agent poly(propylene glycol) bis (2-aminopropyl ether) were purchased from Sigma-Aldrich Corporation (Missouri, USA). Para-aminobenzoic acid (PABA) was obtained from Fisher Scientific. All the chemicals used in this research were analytical grade and used as received unless otherwise mentioned.

3.2.2. Preparation of Modified CNCs

The grafting of the PABA to the CNC was conducted in a two-step heterogeneous reaction process. In the first step, 2% (w/v) of dried CNC was dispersed in DMSO via magnetic stirring followed by homogenization (Homogenizer, PowerGen 700) for a total 15 minutes and heated to 60 ^{o}C. Concurrently, an IPDI coupling agent was heated to 60 ^{o}C and 0.8 mol% DBTDL catalyst was added and stirred for 5 minutes in a nitrogen atmosphere. The pre-heated IPDI/DBTDL and CNC dispersion were then mixed at a weight ratio of 1:30 (CNC: IPDI/DBTDL) in a glass reactor equipped with a stirrer and thermostat. The reaction was then carried out at 60 ^{o}C under nitrogen atmosphere for 4 hours. The CNC–IPDI intermediate product was then washed with toluene, which involved dispersion in toluene and centrifugation (4000 rpm for 3 minutes) and repeated 5 times to remove unreacted IPDI. The recovered CNC–IPDI intermediate is referred as iCNC throughout the manuscript. Part of iCNC was oven-dried at 80 ^{o}C overnight for further characterization.

The remaining iCNC was re-dispersed in DMSO and mixed with the UV absorbing molecule, PABA, which was solubilized in DMSO and pre-heated to 60 ^{o}C to produce the final tailored CNC nanoparticles. The weight ratio of CNC to PABA in this reaction was set to 1:3 based on preliminary experimental observations, and the reaction was conducted at 60 ^{o}C overnight. The product was recovered via successive toluene and acetone wash. This involved dispersing the product in excess toluene followed by centrifugation (4000 rpm for 3 minutes) 3 times, and then acetone washing (3 times). The washed final product (CNC–IPDI–PABA) referred to as pCNC throughout this manuscript, was dried overnight at 80^{o}C and used.

3.2.3. Characterization of the Modified CNCs

3.2.3.1.Fourier Transform Infrared Spectroscopy (FTIR)

In order to investigate the modification of CNC, samples were characterized by Fourier Transform Infrared Spectroscopy (FTIR) using model Nicolet 6700, Thermo Scientific unit. Sample pellets were prepared by mixing dried sample powders of native CNC, iCNC, pCNC, PABA and nanocomposites with dried potassium bromide (KBr) salt powder and pressing it into a pellet using a Carver Press. FTIR scans, in transmittance mode, were then collected between 500 and 4000 cm^{-1} frequency range.

3.2.3.2.Elemental Analysis

Elemental analysis was carried out to confirm the coupling of IPDI to cellulose nanocrystals to produce CNC–IPD (iCNC) intermediate product, followed by attachment of PABA to the iCNC to produce CNC–IPDI–PABA (pCNC). CNC, iCNC and pCNC samples were dried overnight at 70 ^{o}C prior to analysis. The elements C, H, and N were quantified using a 4010 elemental analyzer (Costech instruments, Italy) equipped with a Delta Plus XL continuous flow isotope ratio mass

spectrometer (Thermo-Finnigan, Germany). Analysis was conducted on samples from two independent batches.

The coupling efficiency of PABA onto CNC was calculated in accordance with a method reported by Guan *et al.*[155] based on elemental analysis results. The coupling efficiency was calculated as:

$$\mathbf{CE} = \frac{\mathbf{W_m - W_C}}{\mathbf{W_P}} \times \mathbf{100} \quad \textbf{(1)}$$

W_m, W_C, and W_p represent the weight of modified CNC (pCNC), native CNC and PABA, respectively. W_C, and W_p were the weights used to conduct the reaction, W_m was a calculated value as shown below.

$$\boldsymbol{W_m} = \frac{\mathbf{1}}{\mathbf{1-G}} \times \boldsymbol{W_C} \quad \textbf{(2)}$$

$$\mathbf{G} = \frac{\mathbf{137.14}}{\mathbf{1*14}} \times \mathbf{N\%} \quad \textbf{(3)}$$

G was the weight of PABA in the modified CNC, which was calculated based on the percent nitrogen (N%) obtained from elemental analysis. 137.14, 1 and 14 represented the molar mass of PABA, number of nitrogen atoms present in PABA, and molar mass of nitrogen, respectively. Calculated weight of PABA in pCNC (G) was then used to calculate W_m.

3.2.3.3.Proton Nuclear Magnetic Resonance (^{1}H NMR)

The proton NMR spectra of CNC, PABA, iCNC and pCNC were recorded using a Bruker 500 MHz high-resolution NMR spectrophotometer (Bruker-electrospin 500 MHz Ultrashield, Bruker Corporation, MA). Samples were prepared by dispersing 1 mg in deuterated DMSO and the spectra were collected at 500 MHz at room temperature.

3.2.3.4.Thermogravimetric Analysis (TGA)

The thermal stability of CNC, modified CNC, and their nanocomposites was performed using TA instrument (TGA Q500) to study the impact of modification on the thermal behavior of CNC. The thermal degradation behaviour of the samples was recorded from 25 ^{o}C to 550 ^{o}C with a ramp rate of 5 ^{o}C/minute under nitrogen environment. The weight loss was used as an indicator to analyze the thermal stability/degradation behaviour of the samples.

3.2.3.5.Contact Angle Measurement

The impact of attaching PABA on the hydrophilicity of CNC was studied by employing water contact angle (WCA) measurement. In order to test the WCA, 200 mg of CNC and pCNC were pressed into two pellets using Carver Press. The pellets were then dried at 60 ^{o}C for one hour before conducting the contact angle measurement. Using a sessile drop device, a water droplet was dropped onto the pellet, and the instantaneous water contact angle was recorded.

3.2.3.6.UV-Visible (UV-Vis) Spectroscopy

The UV absorbance of native CNCs, modified CNCs, PABA, and nanocomposite samples were analyzed using Cary 100 Bio UV-Visible (UV-Vis) Spectrophotometer. For this, 1 g of CNC and pCNC were dispersed in 10 mL DMSO, and the UV absorbance was collected from 200 to 800 nm wavelength with DMSO as the baseline solvent. Similarly, the effect of UV absorber (grafted onto the CNC) in the epoxy-CNC nanocomposites was analyzed using UV-Vis Spectrophotometer. Neat epoxy polymers that were not exposed to UV irradiation (Neat epoxy_0) were used as the baseline material and other samples with varying CNC and pCNC compositions and UV irradiation treatments were analyzed from 200 nm to 800 nm.

3.2.4. Epoxy-CNC Nanocomposite

3.2.4.1.Preparation

Epoxy matrices for the nanocomposite sheets were prepared by combining 70% (w/w) of epoxy resin and 30% (w/w) of curing agent. For neat epoxy composite, curing agent was added to epoxy at room temperature and stirred with a glass rod. The mixture was further sonicated Ultrasonic Processor (FB120, Fisher Scientific) for 2 minutes. Nanocomposites were prepared by incorporating 5 wt.% and 10 wt.% loading content of native and modified CNC (pCNC). For this, calculated quantities of CNC and pCNC were first dispersed well in the amine based curing agent using a homogenizer (PowerGen 700) and then mixed with the epoxy resin. The mixture was then further sonicated for 2 minutes to obtain an enhanced dispersion of the native and tailored CNCs and degassed to remove air bubbles. Resin mixtures prepared as such were then poured into a silicon mold and cured at 60 ^{o}C for 4 hours followed by room temperature curing overnight to produce the nanocomposite test specimens.

3.2.4.2.UV-Irradiation

Epoxy nanocomposites, which includes neat epoxy baseline, Epoxy-CNC and epoxy-pCNC were subjected to a controlled UV irradiation exposure. For this, a UV lamp obtained from LSE Lighting (120V and 50 W) was placed 25 cm above the samples and allowed to irradiate the samples for 0 (control), 72 and 144 hours, and in selected samples for 250 and 500 hours. For the labelling purposes, three parts system was used, xy_z. The prefix x represents the weight percent of the filler added to epoxy composite. Epoxy composites were prepared with different filler loadings, which was indicated by 5 or 10 wt.%, y is the filler type used (CNC, pCNC and PABA). Finally, z is the number of hours the sample was exposed to UV irradiation (0, 72, 144, 250 or 500 hours). Epoxy without any filler added was denoted as neat epoxy with appropriate irradiation time.

3.2.4.3.Color analysis

Discoloration is one of the indications of photo-degradation. In order to quantify the change in color for UV irradiated epoxy nanocomposites, samples were tested using MiniScan EZ Diffuse SAV color measurement spectrophotometer (HunterLab, VA, USA). Samples were tested at least in triplicate, and the average was used for further calculations. L*a*b* values were measured, which represent the lightening-fading, red-green and yellow-blue coordinates, respectively [156]. A positive ΔL^* value represents lightening of the samples and a negative value represents fading. Similarly, positive Δa^* corresponds with color shift towards red, and negative towards green. In this way, positive Δb^* corresponds with color shift towards yellow, and color shift towards blue is represented by negative Δb^*. The total color change, ΔE, was then computed using the following expression:

$$\Delta E = \sqrt{(\boldsymbol{L_2^* - L_1^*})^2 + (\boldsymbol{a_2^* - a_1^*})^2 + (\boldsymbol{b_2^* - b_1^*})^2} \quad \textbf{(4)}$$

The subscripts 1 and 2 corresponded with values for reference sample and values for samples after exposure, respectively. For each of the epoxy nanocomposite samples before exposure, 0 hours of exposure were taken as a reference sample to study the discoloration effect due to UV exposure.

3.2.4.4.Water Absorption

The moisture absorption of the baseline epoxy, native, and modified CNC based nanocomposites were studied in accordance with ASTM D570-98. Sample specimens were cut into 20 x 20 x 2 mm and dried in a vacuum oven at 60 ^oC for two hours. Weight of each dried sample was recorded as W_1 and then submerged into deionized water at room temperature. After 24 hours samples were removed from water, dried the surface with a blotting paper, and weighed, which was recorded as W_2. The samples were then re-immersed into water and the process was repeated for 7 days with

measurement every 24 hours. The water absorption, which was measured in terms of weight increase was calculated using the following relation:

$$\% \textbf{ Water Absorbance} = \frac{W_2 - W_1}{W_1} \times 100 \quad \textbf{(5)}$$

3.2.4.5.Statistical Analysis

Experimental replicate results were expressed as mean value ± standard deviation. The statistical analyses of the data were conducted using the statistical software package Minitab (Version 18). Single factor analysis of variance (ANOVA) was employed to identify significant differences among mean values with a 95% confidence level ($P < 0.05$) LSD criteria.

3.3.Results and Discussion

3.3.1. Modification of CNC

3.3.1.1.Surface Grafting of PABA on CNC

The surface of cellulose nanocrystals was decorated with PABA, a UV absorbing molecule, using IPDI as the coupling agent. The grafting of PABA onto CNCs was conducted in a two-step process as shown in Scheme 1. IPDI, containing dual isocynate functional groups with differentiated selectivity, was used as a coupling agent between the PABA and the CNC nanoparticles. It has been reported that in the presence of DBTDL as the reaction catalyst, the secondary isocyanate functional group of IPDI has higher reactivity as compared to the primary group [157,158]. In Scheme 1(a) the first step of the reaction has been presented, where the secondary isocyanate group was activated in the presence of DBTDL at a moderate temperature (60°C). The isocyanate -group (-NCO) was then covalently bonded with hydroxyls (-OH) on the surface of CNC as reported by Girouard *et al*. producing the intermediate product CNC–IPDI (iCNC) [158]. The primary amine group of PABA was then allowed to react with the unreacted primary –NCO group of the iCNC

intermediate product as shown in Scheme 1(b) to produce CNC–IPDI–PABA (pCNC). To validate these modifications of CNCs, FTIR, elemental analysis, and ^{1}H NMR analysis were employed and discussed in the next sections.

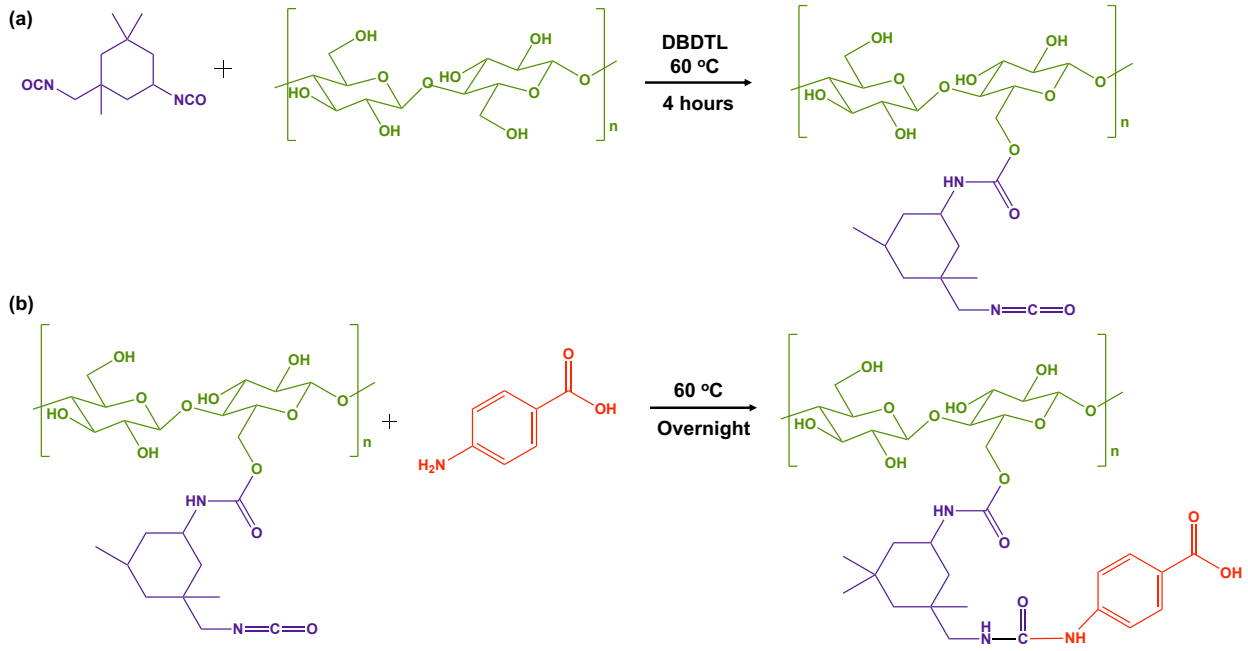

Scheme 1. Reaction scheme for (a) modification of CNC surface using IPDI to produce CNC–IPDI intermediate product (iCNC) (b) attachment of PABA to modified the CNC to produce CNC–IPDI–PABA (pCNC)

Native and modified CNC, iCNC, pCNC and PABA were analyzed using IR to confirm the proposed grafting between the PABA and the CNC. Figure 16 (a) compares the IR spectra for CNC, iCNC and pCNC along with PABA. The broad peak at 3000-3550 cm^{-1} of the CNC was attributed to -OH functional groups. The reduction in the -OH peak (3000-3550 cm^{-1}) and appearance of -NCO peak at 2260 cm^{-1} for iCNC as shown in Figure 16 (a) was indicative of the modification of surface hydroxyls on CNC as illustrated in Scheme 1 (a) to form iCNC [109,158,159]. Furthermore, the emergence of a carbonyl band at 1700 cm^{-1} in iCNC provided further evidence of urethane linkage formed as -NCO reacted with the -OH moieties of CNCs [160,161].

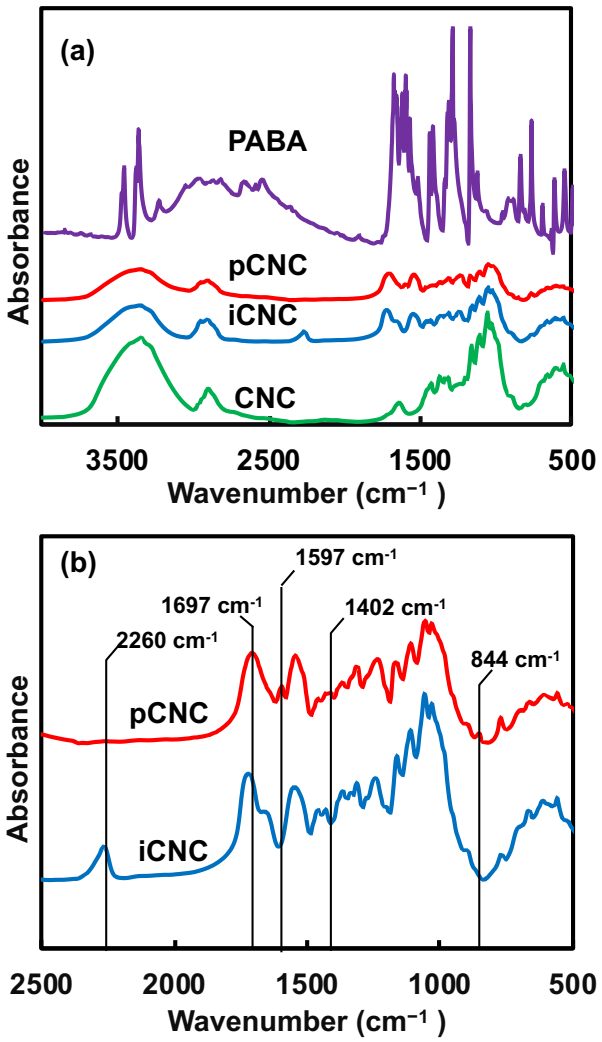

Figure 16. (a) IR spectra of CNC, iCNC, pCNC, and PABA (b) Detailed spectra of intermediate (iCNC) and final reaction product (pCNC).

The reaction between the amine groups of PABA with the unreacted -NCO of the intermediate product as shown in Scheme 1 (b) was observed from the complete consumption of the -NCO in the pCNC as compared to the iCNC (Figure 16 (a)). Close analysis of pCNC (Figure 16 (b)) showed the presence of an absorbance band at 1597 and 1402 cm^{-1}, which were attributed to C=C bond from aromatic ring of PABA[162]. The -C-H bond of the benzene ring, observed at 844 cm^{-1}, was an additional evidence of a conjugated PABA onto the CNCs surface. Moreover, the broadening of carbonyl peak at 1697 cm^{-1} in pCNC as compared to the iCNC was indicative of

further modifications. The carboxyl group from PABA and conjugation of primary and secondary isocyanate group leading to urea and urethane linkages, respectively were detected within the carbonyl peak observed at 1775-1625 cm^{-1} with maxima at 1697 cm^{-1} [162,163].

The tailoring of CNC was further analyzed by ^{1}H NMR. Figure 17 displays the proton signal spectrum of the different samples. The main peaks at δ 2.51 and 3.33 ppm in all the samples correspond to DMSO, the solvent in which the samples were dispersed to obtain ^{1}H NMR spectra. Characteristic signals of –OH from CNC were observed at δ 3.6, 3.9, 4.7 and 5.48 ppm [141]. ^{1}H NMR spectrum for PABA showed the aryl protons at δ 5.94, 6.57 and 7.53 ppm. The protons adjacent to amine ($-NH_2$) on PABA causes the signal at 6.57 ppm to split into a triplet. As the amin group reacts with isocyanate group in pCNC, a doublet was observed instead of a triplet at 6.57 as one of the protons gets was consumed in coupling. Substituents of the aromatic ring from the PABA in pCNC at 5.94, 6.42 and 7.61 provided further confirmation of the covalent grafting of PABA onto CNC.

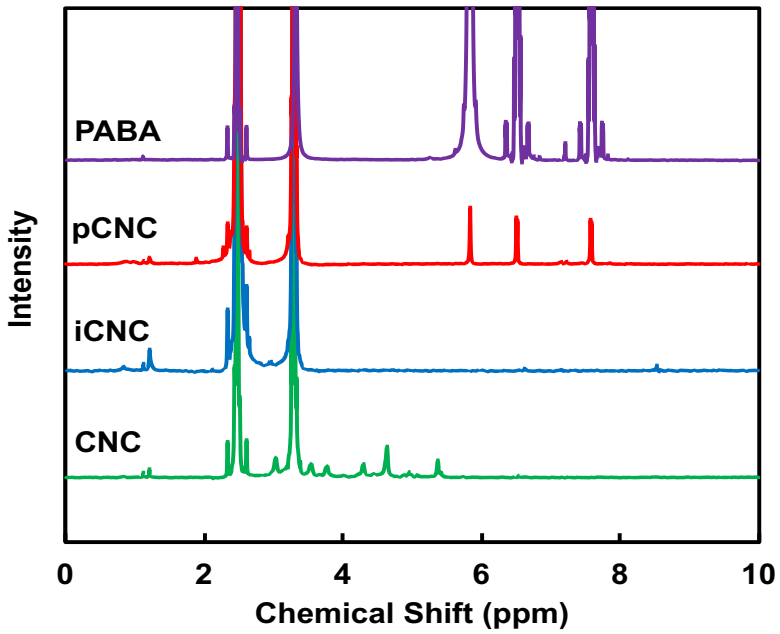

Figure 17. Proton NMR spectra analysis of PABA grafting onto CNCs.

In addition to FTIR and ^{1}H NMR studies, the changes in elemental Carbon and Nitrogen composition between the native (CNC), the reaction intermediate (iCNC) and final product (pCNC) samples were analyzed using elemental analysis. CNC, a polymer of anhydrous glucose units, does not contain any nitrogen atoms. The increase in the nitrogen content for iCNC shown in Table 4 was attributed to the covalent attachment of isocyanate from IPDI. Further increase in nitrogen weight percent (6.4%) in pCNC was associated with the attachment of PABA to the iCNC. Furthermore, nitrogen weight percent from elemental analysis was used to estimate coupling efficiency for modified CNC according to Guan *et al.*[155]. Calculations based on equation (1) provided a remarkable coupling efficiency of 8%. This demonstrated that the use of IPDI as a coupling agent between CNCs and PABA was efficient, and a substantial amount of PABA was grafted onto the CNCs.

Table 4. Elemental Analysis for the modification of CNC

Sample	%C	%N
CNC	42.47 ± 1.08	-
iCNC	48.93 ± 0.92	5.47 ± 1.23
pCNC	49.46 ± 2.75	5.82 ± 1.03

3.3.1.2.Characterization of Modified CNC

The thermal stability of additives and fillers used in polymeric materials is important, because most polymer processing operations such as melt processing, thermal curing, injection or compression molding typically involve high temperatures. To evaluate the impact of grafting PABA onto CNC on the thermal stability, native and modified CNC (pCNC) and PABA were analyzed using TGA, and their thermograms are shown in Figure 18. The native and pCNC showed slight weight loss near 100 ^{o}C which was attributed to evaporation of bound water. Major weight loss of CNC was observed between 295-325 ^{o}C ranges with degradation peak at 319 ^{o}C. The degradation of CNC could be attributed to concurrent dehydration, depolymerisation of the cellulose chain, and decomposition of glycosyl units [164]. As displayed in Figure 18 (b), the peak degradation temperature of PABA was observed at 211^{o}C, which was much lower than that of the native CNC. In comparison to CNC, the degradation of pCNC (CNC–IPDI–PABA) began at a much lower temperature, with a 15% weight loss observed at 265 ^{o}C. This was likely associated with the degradation of the less thermally stable PABA that was attached to the surface of CNCs. Despite the lower thermal degradation initiation of the pCNC, the peak degradation was remarkably higher than CNC (18% increase). The increase in the peak degradation temperature of pCNC beyond that of CNCs' could be pertaining to the reduction in the number of the surface hydroxyls groups, responsible for the thermal dehydration as a result of the grafting of PABA. This clearly indicated that the incorporation of PABA onto CNCs improved the thermal stability

of native CNC. Such improvement in the thermal stability of CNCs is of great importance for use as a functional filler in polymer nanocomposites as this limits the risk of degradation, which could occur during melt processing (in thermoplastics) or curing in thermoset polymers.

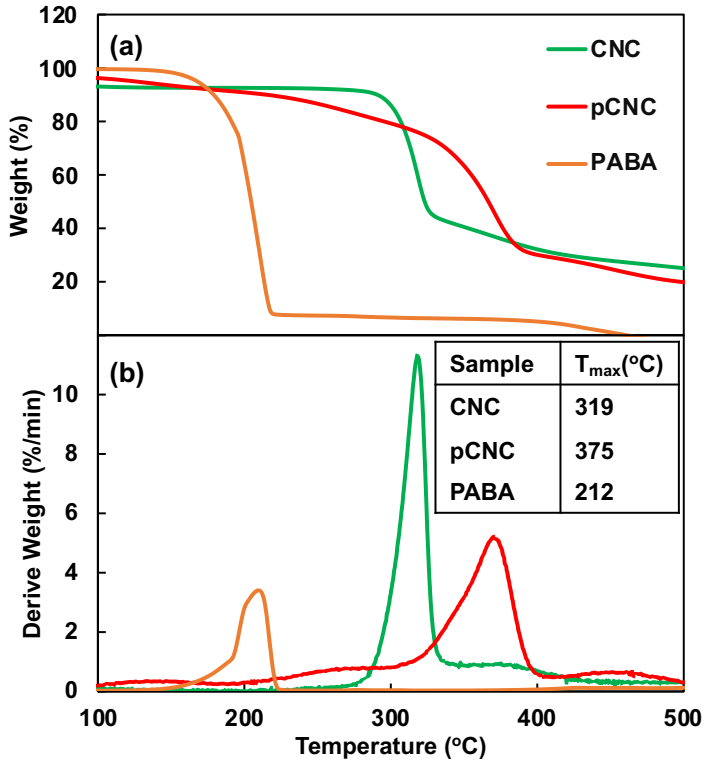

Figure 18. TGA analysis of CNCs, PABA and pCNC: (a) Weight loss curve (b) Weight loss derivative curve.

CNCs display great potential as a sustainable nanomaterial for a range of material applications. Studies have indicated that they show an inherently high hydrophilicity owing to the tendency of their –OH moieties to associate with water via hydrogen bonding with slight variation depending on the source and extraction process of CNCs [153]. The recorded water contact angle (WCA) of native CNCs ranges from 9-30° [57,153,165,166]. This can be an advantage in some cases, for instance, to conduct water-based chemistries and in certain applications that enjoy wettability and water dispersability[167]. However, such high hydrophilicity is detrimental in many polymer

nanocomposite systems, including epoxy mainly because of their lack of dispersability in non-polar polymer systems. Some outstanding properties of epoxy polymer that make it the polymer of choice in several applications can be negatively impacted by water absorption [168–171]. For example, moisture uptake can cause a marked reduction in the modulus, toughness, crack resistance and adhesion strength of epoxy materials [171–173]. Combining the hydrophilic CNCs with epoxy is anticipated to aggravate the overall moisture absorption of the nanocomposites. Figure 19 (a and b) presented WCA for native and modified CNCs. The WCA observed for native

CNC was 32.7°. CNC modified with PABA showed a higher WCA (64.9°), which was a 98% increase from the native CNCs and a marked reduction in hydrophilicity. This was because the grafting of PABA onto CNC consumed the hydroxyl groups responsible for the hydrophilicity of CNCs as shown in Scheme 1 and Figure 16. Thus, the grafting of PABA onto CNC has significantly improved the hydrophobicity of CNC, which is a desired attribute in enhancing its dispersability in mostly non-polar polymers.

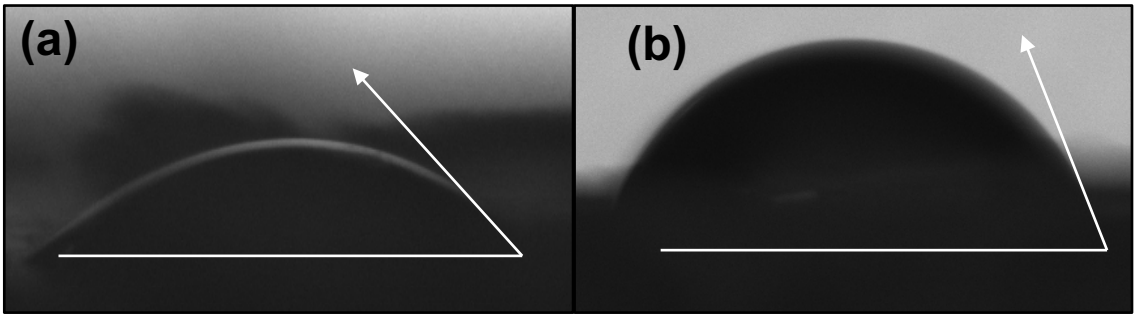

Figure 19. Water contact angle for (a) native CNC b) pCNC (CNC-IPDI-PABA)

3.3.2. UV Absorption

Epoxy resins are among the most common thermosetting polymers with a range of applications due to their marked physical properties, chemical resistance, and processability. However, epoxy-based materials often degrade under direct exposure to UV radiation, which curtails their use in

many applications. For instance, the discoloration, chalking, loss of adhesion, cracking etc. as a result of direct UV exposure limit their use as an external layer coating in the construction and automotive industries [174]. This is because epoxy polymers have an aromatic backbone chain that can absorb UV and undergoes detrimental chemical and physical changes, resulting in poor material performance properties [175]. The incorporation of UV absorbing molecule decorated CNCs into epoxy and the UV absorption properties are investigated using UV Vis Spectrophotometer and results are presented in Figure 20.

It was noted that native CNC absorbed very minimal UV radiation. The PABA on the other hand displayed excellent UV absorption within the UV light range, 250 – 330 nm. The CNC with grafted PABA (pCNC) exhibited UV absorbance within a similar UV range (260 – 320 nm) as that of the PABA. Compared to PABA itself, lower absorbance is observed for pCNC this is due to only 44% of PABA loading CNC. Despite pCNC carrying lower amount of PABA, it still indicated UV absorbance properties, and that it can bring about the desired UV absorption when incorporated in polymer matrices.

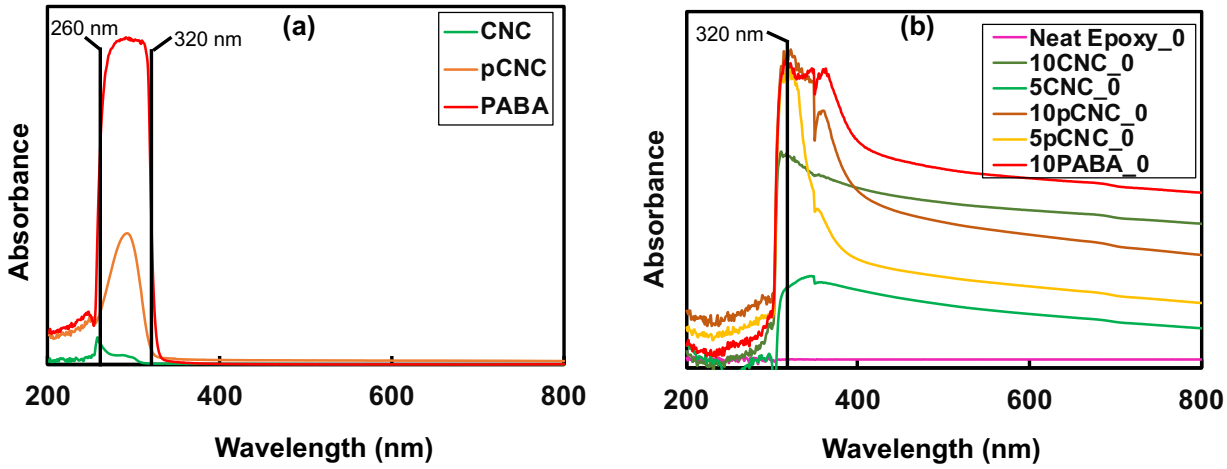

Figure 20. Comparative UV absorbance of (a) CNC, PABA and pCNC; (b) Epoxy nanocomposites prior to UV irradiation.

As presented in Figure 20 (b), the spectra for neat epoxy showed no absorbance in the ultraviolet or visible region. Epoxy-CNC nanocomposites showed slight UV absorbance, when the UV absorbance of 5CNC_0 was compared with 10CNC_0 (Figure 20 (b)) it was evident that an increase in the CNC loading increased the UV absorbance. However, the UV absorbance was enhanced significantly with the use of pCNC. For comparison reasons, 10 wt.% of PABA was directly incorporated in epoxy to produce 10PABA_0 epoxy nanocomposite that displayed the greatest UV absorbance. 10PABA_0 also showed an additional peak at 360 nm (in visible range). Similar peak was observed for the 10 wt.% of pCNC in epoxy. Comparing the direct addition of PABA in epoxy with pCNC, it was observed that the use of pCNC at both 5 and 10% loading displayed excellent UV absorption similar to the direct addition of PABA confirming that the anchored PABA onto CNC maintained its UV absorbance efficiency. As expected, 10pCNC provided an enhanced UV absorbance as compared to 5pCNC. However, when comparing the absorbance spectra for PABA and pCNC in Figure 20 (a) with their incorporation in respective

epoxy matrix, in Figure 20 (b), blue-shift effect can be observed. This can potentially be because of the interaction between the filler and the epoxy matrix. While the native CNC exhibited some UV absorbance, the pCNC displayed a remarkably higher UV absorbance owing to the aromatic benzene with carboxyl and amine functionalities of PABA that are known to provide high UV radiation absorption (290–320 nm in the UVB region)[176].

Baseline epoxy, native CNC and pCNC based epoxy composites were subjected to a controlled UV irradiation for 72 and 144 hours, and the impact of the irradiation on the UV absorption properties and color changes were evaluated. Figure 21 ((a) and (b)) displayed the UV absorption of nanocomposite samples of CNC and pCNC before and after UV-irradiation with 5 wt.% and 10 wt.% loading, respectively. It was observed that nanocomposite samples with pCNC had greater absorbance compared to those that contain CNC even after the UV irradiation. Moreover, as the samples were irradiated for a longer time (144 hours), the absorbance displayed a higher intensity, indicating that a continued UV exposure may not change the UV absorbance properties. Nikafshar *et al.*[144] also reported a similar observation of UV absorbance increase with an increase in the UV irradiation with the use of another UV absorber (Tinuvin 1130) in epoxy materials. A possible explanation for this observation could be that under UV-exposure molecular arrangements of nanocomposite occurred that led to the formation of chromophores, which could absorb specific wavelength resulting in higher absorbance.

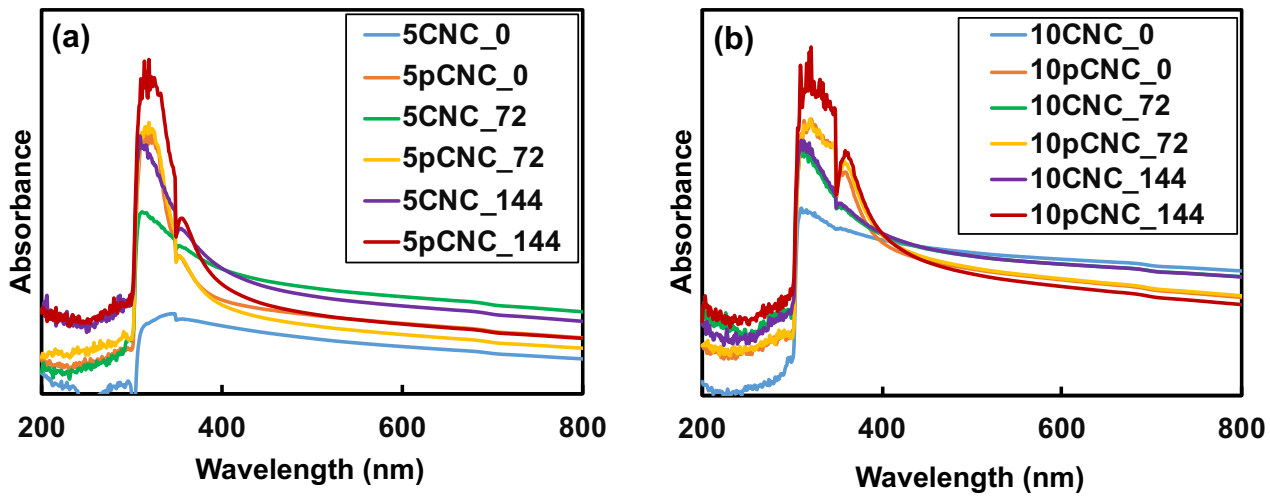

Figure 21. Effect of UV irradiation on the UV absorption of (a) epoxy nanocomposites with 5wt % of CNC and pCNC after UV irradiation for 0, 72, and 144 hours; (b) epoxy nanocomposites with 10wt % of CNC and pCNC after UV irradiation for 0, 72, and 144 hours.

3.3.3. Effect of UV Irradiation on the Chemical Structure of Epoxy Nanocomposites

The changes to chemical structure of epoxy caused by UV irradiation were analyzed by FTIR. As epoxy goes through photo-degradation, mainly hydroxyl and carbonyl groups are formed. Such photo-degradation mechanisms of epoxy have been reported extensively in literature [144,148,177,178]. It has been reported that under extensive UV light, oxidation of the phenoxy part of epoxy leads to the formation of hydroxyl and carbonyl groups [144,148]. Furthermore, photo-reaction of hydroxy-alkyl-ether groups of epoxy forms methyl-end groups [144,179]. In order to study structural change of the nanocomposites, FTIR analysis of samples irradiated for different times was conducted. Figure 22 presents the effect of such UV irradiation on the chemical structure of the epoxy nanocomposites. With an increase in the UV exposure time, all nanocomposites (neat epoxy baseline, 10CNC and 10pCNC) exhibited common changes as noted form the IR spectra. There was an increase in the hydroxyl groups between 3000 and 3650 cm^{-1} of the nanocomposites indicating oxidation of phenoxy part. A remarkable increase in the peak between 2798-2985 and

1445 cm^{-1}, which represents stretching of C-H bond and presence of methyl groups, was noted as well. These increases in peaks can be attributed to the increase in the methyl groups formed as a result of reaction of hydroxy-ether groups. Moreover, an increase in the carbonyl peak at 1610 cm^{-1} was observed for all the nanocomposites. For the neat epoxy baseline sample another peak was observed at 1505 cm^{-1}, which was intensified with an increase in the UV irradiation time. This can be attributed to the formation of chromophores, such as C=C. The formation of C=O and C=C was a result of chain scission or chain crosslinking [149,178]. These were chromophoric chemical species, in which electrons were excited from the ground state upon absorbance of the light when exposed to UV light, leading to the discoloration of epoxy materials [149,178].

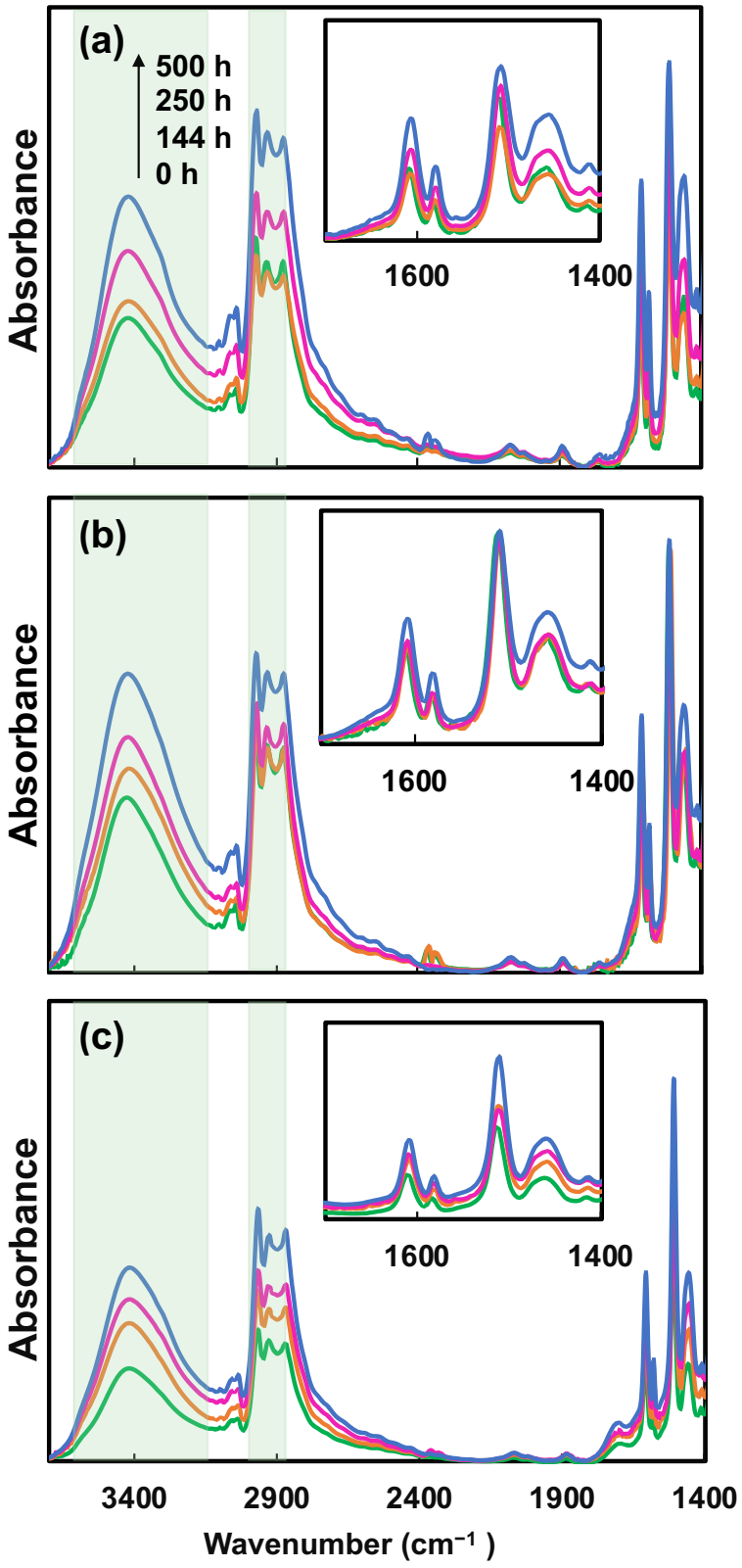

Figure 22. FTIR spectra of (a) Neat epoxy (b) 10CNC and (c) 10pCNC upon UV degradation

3.3.4. Discoloration of Epoxy Nanoomposites

One of the vital indicators of epoxy degradation is its discoloration. As epoxy is exposed to UV-light from the sun, it displays yellowing over a period of time which makes it aesthetically unappealing and weakens certain performance properties. Figure 23 (a) shows the appearance of the cured epoxy nanocomposite samples upon UV exposure. The top row showed the cured samples prior to UV-exposure (t = 0). The second and third row displayed the changes in the color of the nanocomposites as a result of UV exposure for 72 and 144 hours, respectively. The incorporation of the both native and pCNC provided various degrees of off-colors color to the transparent baseline epoxy as noticed from Figure 23 (a) (first row) and 8b. The off-colors produced by pCNC were more pronounced. This was associated with the inherent grey color of the PABA molecule. As observed from Figure 23 (b), these off-colors were produced prior to curing.

The UV irradiation for 72 and 144 hours caused substantial color changes as compared to the samples that were not exposed to UV irradiation. The color changes as a result of the UV irradiation were calculated based on colorimetric measurements and results are shown in Figure 23 (c).

For the calculation, respective samples before UV irradiation were used as references, thus for each sample at 0 hours the calculated change was taken as the baseline. It can be noticed that as the time of irradiation increased, more changes in color were observed in all nanocomposite samples. Neat epoxy was the most impacted as a result of the UV irradiation that led to extensive discoloration of the samples. As seen in Figure 22, UV radiation leads to formation of chromophores, which may absorb visible light leading to discoloration. While the incorporation of native CNCs reduced the discoloration at both 5 wt.% and 10 wt.% loading concentrations, the

10 wt.% provided a more distinct reduction in discoloration compared to the non-filled epoxy baseline (Figure 23 (c)). However, the best results were achieved with the use of 10pCNC.

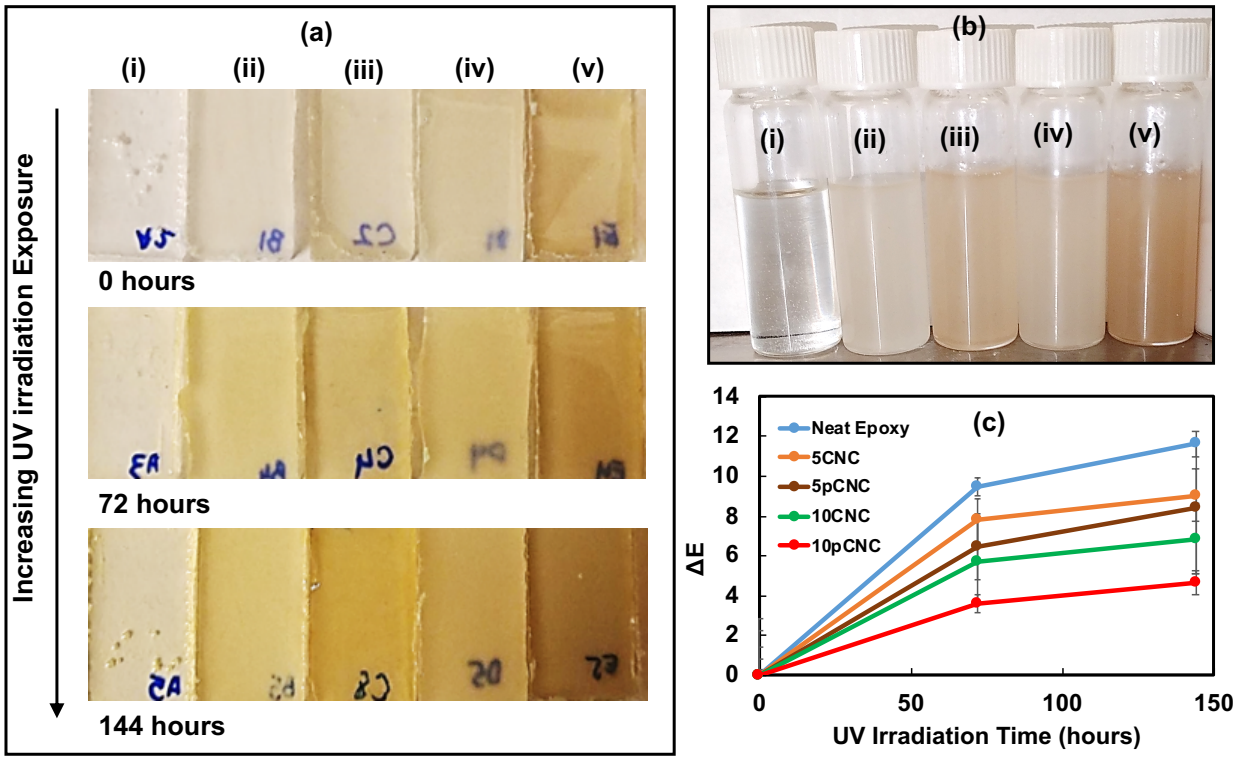

Figure 23. (a) Epoxy nanocomposite cured and UV irradiated for 0, 72 and 144 hours; (b) Epoxy nanocomposite before curing where (i) Neat epoxy, (ii) 5CNC, (iii) 5pCNC, (iv)10CNC and (v) 10pCNC respectively; (c) Color change related of samples

To further investigate the impact of long-term UV exposure on epoxy materials and the UV absorbance of pCNC, selected samples were exposed to UV radiation for extended period of time (250 and 500 hours), and the discoloration was calculated and are presented in Figure 24. The unfilled epoxy continued to discolor further with an increase in the UV irradiation time. In contrast, epoxies filled with 10CNC showed a lower rate of discoloration as compared with the unfilled baseline epoxy. It was interesting to note that the irradiation of the 10CNC based epoxy nanocomposites for 250 and 500 hours did not present a statistically different color change, as shown in Figure 24. The suspected reason for the UV absorption of CNC based nanocomposites

was residual lignins left attached to CNCs during their manufacture, as lignin is a known UV blocker due to its phenolic, ketone and other chemophore functionalities[180,181]. The incorporation of pCNC at 10 wt. % (10pCNC) substantially diminished the impact of UV-irradiation as observed from the lessened discoloration of the nanocomposites as compared to both the unfilled and the 10CNC based nanocomposites. Moreover, the 10pCNC based nanocomposites displayed no color change beyond 144 hours of UV exposure. Hence, the grafting of PABA onto CNC and their use as a UV protective molecule provided a very promising approach to mitigate discoloration and other property deterioration of epoxy as a result of UV degradation.

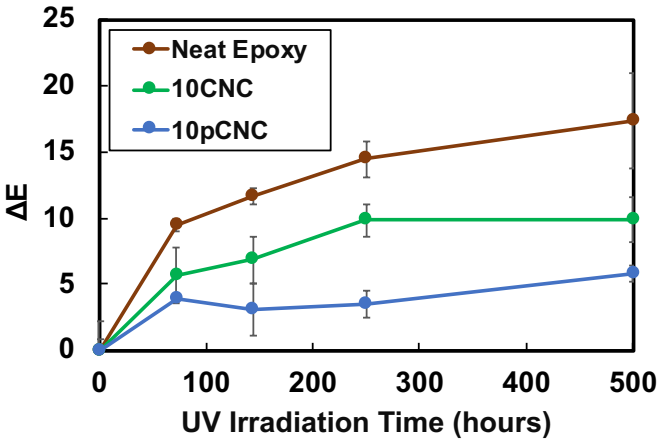

Figure 24. Discoloration of selected samples after exposure to UV irradiation for a prolonged period of time.

3.3.5. Thermal Degradation of Modified CNC and the Nanocomposite

The thermal degradation behaviour of Epoxy-CNC was analyzed to investigate two main effects. The first goal was to analyze the impact of incorporating CNC, pCNC, and PABA on the thermal stability of epoxy matrices. Secondly, to inspect the change in the thermal decomposition behaviour of the epoxy nanocomposites subsequent to subjecting them to UV-irradiation. The TGA thermograms of unfilled epoxy, epoxy nanocomposites with CNC and pCNC at 5 and 10

wt.% loadings are presented in Figure 25. For comparison purpose, the thermal degradation behavior of epoxy filled with PABA via direct addition was included in this study. Table 5 shows the results of onset temperature, defined as temperature at which 95% of original sample mass still remains, and T_{max}, peak degradation temperature. The unfilled epoxy displayed a peak degradation at 302 ^{o}C. Such thermal decomposition of epoxy is mainly attributed to the dehydration caused by the elimination of water from the backbone structure of epoxy [182].

Table 5. Thermal degradation behaviour of epoxy composite

Samples	T_{onset}	T_{max}
Neat Epoxy	269.9	301.8
5 CNC	265.9	301.5
5 PCNC	269.4	301.9
10 CNC	264.1	302.5
10 PCNC	266.9	302.1
10 PABA	189.5	304.7

The addition of CNC and pCNC at both 5 and 10 wt.% loading had negligible impacts on the thermal decomposition of the nanocomposites and the thermal stability was similar to the unfilled epoxy. Some literature reported that the incorporation of fillers such as clay at higher concentrations could result in deterioration of thermal stability of epoxy nanocomposites [183,184]. The observation here with the addition of CNC and pCNC at concentrations as high as10 wt.% did not cause a slump in the thermal stability of epoxy. This indicated that the CNCs (native and pCNC) did not impact the reactivity of epoxy with the amine curing agent and hence the crosslinking was maintained. Moreover, in all the CNC and pCNC nanocomposites, a single degradation peak was observed suggesting that there was good interfacial interactions between the nanofillers and the epoxy. In contrast, the direct addition of PABA to epoxy resulted in a significantly reduced degradation onset temperature as shown in Figure 25 ((a) and (b)). As presented in Figure 18, PABA itself has low onset thermal degradation temperature. Thus, epoxy-

nanocomposites with PABA had also exhibited a lower onset degradation temperature as the PABA decomposes at lower temperature substantiated by the observation of a new derivative degradation peak at a lower temperature (190 °C) than the rest of the epoxy nanocomposites. Thus, the covalent grafting of PABA onto CNC was quite useful to overcome the thermal stability limitation of PABA for their use as a functional UV absorbing additives to epoxy and possibly other polymer systems.

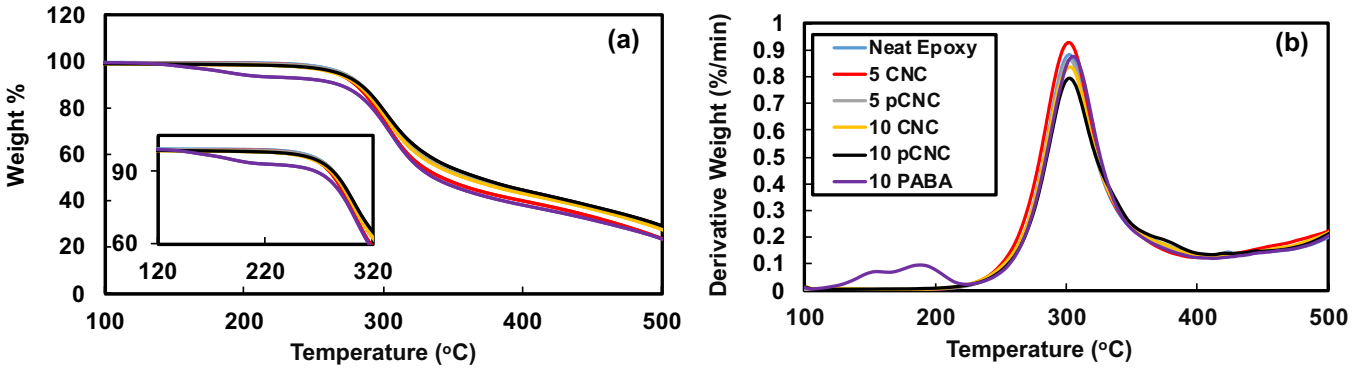

Figure 25. TGA analysis of epoxy nanocomposites with different filler (a) Weight loss curve (b) Weight loss derivative curve.

3.3.6. Water Absorption

Due to the inherent hydrophilicity of CNC associated with its -OH moieties, CNC-polymer nanocomposites typically display higher water absorption [169]. Figure 26 presents the water absorption of the unfilled epoxy and its CNC and pCNC nanocomposites at 5 and 10 wt.% loading. It was observed that as the immersion time increased, the water uptake continued in all samples. The unfilled epoxy displayed a relatively low water uptake. However, the incorporation of CNC led to a dramatic water absorption increase, and the increase was further exacerbated with the increase in the CNC loading from 5 wt.% to 10 wt.%. This was attributed to the hydrophilic nature of CNCs as shown in Figure 19 (a). The grafting of PABA onto CNCs (pCNC) substantially

reduced the water absorption as compared to the native CNC based nanocomposites. This was in line with the enhanced hydrophobicity of pCNC as observed from the WCA studies (Figure 19). The increase in the loading of CNCs (native and pCNC) noticeably increased the water absorption. While a slowing trend in the water absorption kinetics was noticed with the increase in the soaking hours, equilibration was not achieved at the end of the seventh day.

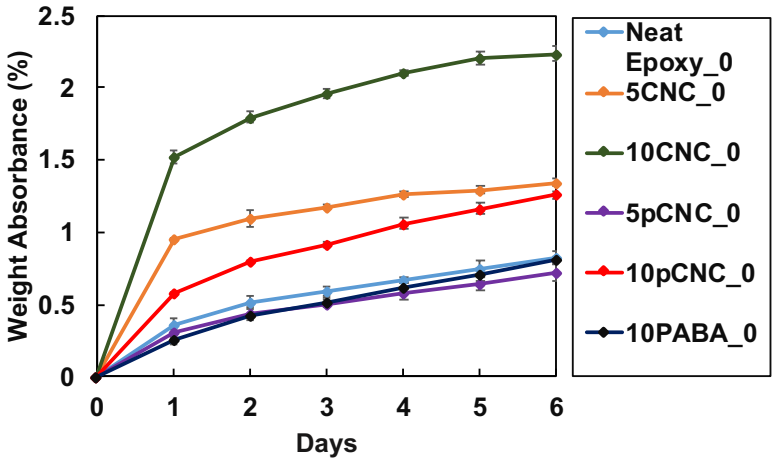

Figure 26. Water Absorbance for samples a) before UV exposure b) with 5wt% c) 10wt% of CNC and pCNC-epoxy nanocomposite before and after UV exposure.

3.4. Conclusions

In this study, tailored CNCs with excellent UV absorption properties were prepared by grafting a known UV filter molecule, para-aminobenzoic acid (PABA) onto CNCs in a two-step heterogeneous reaction using a coupling agent that had differentiated reactivity (IPDI) among its reactive groups. The grafting of the UV filter molecule onto CNCs was confirmed by elemental analysis, FTIR, and proton NMR spectroscopy analysis. The tailored CNCs exhibited enhanced thermal stability, hydrophobicity, and more importantly excellent UV absorption properties. Unfilled epoxies suffered from substantial structural changes and severe discoloration under UV exposure, due mainly to chain secession and chromophores formation. In contrast, epoxy polymers

filled with the modified CNCs as a UV filter functional nanofiller displayed remarkable structural stability and less discoloration over a prolonged UV exposure. Additionally, the incorporation of pCNC maintained the thermal stability and reduced the hydrophilicity of epoxy nanocomposites that are beneficial for a range of material applications. In recent times, a large amount of research has been conducted using CNC as a reinforcing filler to improve mechanical performance. However, CNC has not been fully utilized to its full potential. This research focuses on one such functionalization of CNC, modifying CNC for UV-absorbing properties. The use of CNC-PABA could extend to other polymers that suffer from UV degradation as a general UV protective functional filler. The potential application of modified CNC is mainly in polymeric composite suffering from UV-degradation due to extensive exposure to UV light.

Chapter 4: Lignin Nanoparticles

4.1. Introduction

As environmental concerns increase, many initiatives have been taken globally. One of their primary aims in the material sector is to find an alternatives to fossil fuel-derived polymers that are eco-friendly (e.g. biodegradable, compostable) and sustainable sources for polymer-based materials to limit environmental impacts. The use of other natural resources such as protein, lipids, CNCs, lignin, starch, and chitosan to develop sustainable or functional materials for tailored applications have been explored [17,82,188].

Lignin found in terrestrial plants, is a large component biomass. Over the past decade, many reviews have been published on the utilization of lignin for value-added applications [20,22,138]. Over 70 million tons of lignin have been produced as a by-product from pulp industries and biorefineries [124,125]. Most of the lignin recovered from such operations is typically used as a fuel or an energy source. This, however, decreases the value of the recovered lignin [185,186]. The utilization of lignin in value-added and speciality chemical products is still limited. A few factors that contribute to these challenges are the complex structure of lignin, the inherent variability in lignin composition, and further differences imposed by lignin extraction and purification methods [138]. Depending on the source and separation process, the structure of lignin may vary. This discrepancy leads to difficulty in predicting the accurate properties of lignin.

The majority of the biomass used in the pulp industry is delignified using the Kraft process. Other delignification processes include soda pulping, sulfite pulping leading to the production of technical lignin such as Kraft lignin, Soda lignin, Lignosulfonates, and Ionic liquid lignin [130,187].

Lignin has a 3-D, polydispersed, branched structure. It is naturally produced via enzymatic radical coupling polymerization of monolignols: p-coumaryl alcohol, coniferyl alcohol, and sinapyl alcohol [20,125]. The monomeric units are polymerized into p-hydroxyphenyl, guaiacyl, and syringyl from p-coumaryl, coniferyl, and sinapyl alcohol units respectively [125]. Lignin is a complex, phenolic polymer which is known for its antioxidant, antimicrobial, and UV absorbing properties [20]. Thus lignin can be an attractive biorenewable polymer in material applications, which can provide such additional functionaly on top of biodegradability.

Lignin particles have the aforementioned appealing properties, and forming lignin nanoparticles can increase surface area leading to enhancement of these properties when added to a composite[131]. Nanoparticles have gained popularity in material applications. They can be used as a filler or as a reinforcing agent of polymers. Nanoparticles from chitosan and modified nanocellulose are widely studied and they can produce functional nano-composite for value-added applications [17,82,188]. Thus, the focus of this chapter is to evaluate the use of various processes to produce lignin nanoparticles (LNP), which can be further utilized. Experiments were conducted to prepare LNPs through a top-down approach, using ultra-sonication energy as a means to form nanoparticles. In literature, LNPs prepared through the bottom-up approach where an pH-shift method was employed in ethylene glycol has been well-studied and reported[23,189]. However, for the first time, this method was extended to a different solvent, glycerol. In this work, on top of LNP prepared through ultrasonication method, LNP prepared through pH-shift method in water, glycerol and ethylene glycol are compared. Several characterization methods were employed to analyze the particle size, chemical structure and other desirable properties of produced LNPs, which were formed through top-downa and bottom-up approach.

4.2. Experimental

4.2.1. Materials

Dealkaline lignin (L0045) was purchased from TCI Chemicals. Potassium hydroxide (KOH, 85 %) in a pellet form and hydrochloric acid (37%) was purchased from Sigma Aldrich, USA. Ethylene glycol (99%) and glycerol (99.5%) were purchased from VWR and Fisher Scientific respectively.

4.2.2. Lignin Nanoparticles Synthesis

4.2.2.1.Lignin Nanoparticles Synthesis through Sonication

To prepare an alkali lignin solution, KOH pellets were added to DI water to obtain a pH of 12. Lignin was then added to alkali water to prepare 5 wt.% of lignin solution. The solution was bath-sonicated for 4 hours using ultrasonication. The solution was then centrifuged at 4000 rpm for 10 minutes. The supernatant was recovered and further sonicated for 2 more hours. The solution containing lignin nanoparticles was used for further characterization. Lignin nanoparticles were dried at 60 °C overnight and ground into a powder for further analysis. For further analysis, lignin nanoparticles prepared through bath sonication method is referred to as LNPS.

4.2.2.2.Lignin Nanoparticles Synthesis through Acid Shift Method

5 g of lignin was dissolved in 50 mL of glycerol at alkaline pH using KOH as the base. The solution was heated at 50 °C under nitrogen environment. 20 mL of 0.5M HCl was added to the lignin solution at a rate of 3 drops per minute. The solution was stirred under a nitrogen environment for 3 hours. Lignin nanoparticles were then dialyzed against DI water for 72 hours. The solution containing lignin nanoparticles was used for further characterization. Lignin nanoparticles were dried at 60 °C overnight and ground into a powder form for further analysis. A similar process was used with different solvent: ethylene glycol and water. For further analysis, lignin nanoparticles

prepared in glycerol, ethylene glycol, and water were referred to as LNPG, LNPEG, and LNPW, respectively.

4.2.3. LNP Characterization

4.2.3.1.Particle Size

The particle size of the lignin nanoparticles retained in dispersion form after synthesis was measured using a Brookhaven instrument (New York, USA). Lignin nanoparticles, LNPS, LNPG< LNPEG and LNPG were diluted to 0.15 wt.%. Particle size was measured from two independent synthesized batches with 5 measurements each. Average particle size was reported.

4.2.3.2.Zeta Potential

10 mg of lignin and lignin nanoparticles prepared through four different methods LNPS, LNPW, LNPG, and LNPEG were dispersed in 10 mL water. The samples were sonicated for 30 minutes in bath-sonicator and allowed to settle for 30 minutes. Zeta potential of the solution was measured using a Zetasizer nano series, DTS 1061. Three measurements with a hundred runs each were taken at 25 ^{o}C.

4.2.3.3.Dispersity Test

The dispersibility of lignin and different LNPs were analyzed in different organic solvents. To analyze the interaction of lignin and LNP in a solvent, solvents with different polarity were chosen. In the order of decreasing polarity, the solvents chosen were water, ethylene glycol, ethanol, dimethyl sulfoxide (DMSO), chloroform, tetrahydrofuran (THF) and toluene. 10 mg of sample was added to 10 mL of solvent. The samples were then sonicated for 5 minutes and after 60 minutes of settlement, photographs were taken.

4.2.3.4.UV-Visible Spectroscopy (UV-Vis)

0.1 mg/mL of samples dispersed in water and ethylene glycol were sonicated for 5 minutes using samples dispersed in 10 mL of water. A probe sonicator (sonic dismembrator model 120, Fisher Scientific Inc) was used for 3 minutes to achieve a better dispersion. The UV absorbance of lignin and lignin nanoparticles was analyzed using a Cary 100 Bio UV-visible (UV-vis) spectrophotometer.

4.2.3.5.Fourier Transform Infrared Spectroscopy (FTIR)

FTIR spectra of native lignin and LNP were analyzed to investigate the change in chemical structure as a result of the LNP preparation process. To prepare IR samples, sample pellets (5 mg) were mixed with KBr (200 mg) using a mortar and pestle. The mixture was then pressed into a pellet using Carver Press. FTIR scans were collected in transmission mode in the frequency range of 500 to 4000 cm^{-1}, using the Nicolet 6700 model.

4.2.3.6.X-ray Photoelectron Spectroscopy (XPS)

An XPS analysis of lignin and LNP was conducted to analyze the structural and chemical composition of each sample. The samples were analyzed using a Thermo-VG Scientific ESCA Lab 250 microprobe (Thermo Fisher Scientific) instrument with monochromatic Al-Kα radiations (1486.6 eV). The step size of the survey spectra was 0.5 eV with a pass energy of 50 eV. The high-resolution spectra were conducted with a step size of 0.1 eV and pass energy of 30 eV. The spectra were analyzed using CasaXPS software.

4.2.3.7.Water Contact Angle (WCA)

For water contact angle measurement, samples were diluted to a concentration of 0.15 wt.%. The samples were prepared on a Petri dish. Using a transfer pipette, a single droplet was placed on a

petri dish and allowed to dry at 80 ºC. Another droplet was placed and subsequently dried, layering 4 droplets. The samples were allowed to air-dry and then placed in a vacuum oven at 35 ºC for 30 minutes. The water contact angle of lignin and LNP samples were then measured using a sessile drop device.

4.3. Results

4.3.1. Lignin Nanoparticles

Lignin, a natural polymer, has an abundance of useful properties that can be exploited for value-added applications. Therefore, when synthesising lignin nanoparticles, it is important to analyze the particle size as well as the structure of the lignin. Lignin nanoparticles were prepared using two methods as shown in Figure 27. To produce LNP from native lignin mechanical treatment of lignin using homogenization[127] and sonication[190] have been reported. Gilca *et al.*[190] conducted a sonication of 0.7 wt.% of aqueous lignin reporting average particle diameter between 100-500 nm. For an economically feasible process, it is important to use more concentrated lignin. In this work, 10 wt.% of the lignin solution was subjected to sonication to produce LNP which resulted in nanoparticles with an average volumetric diameter of 152.6 nm.

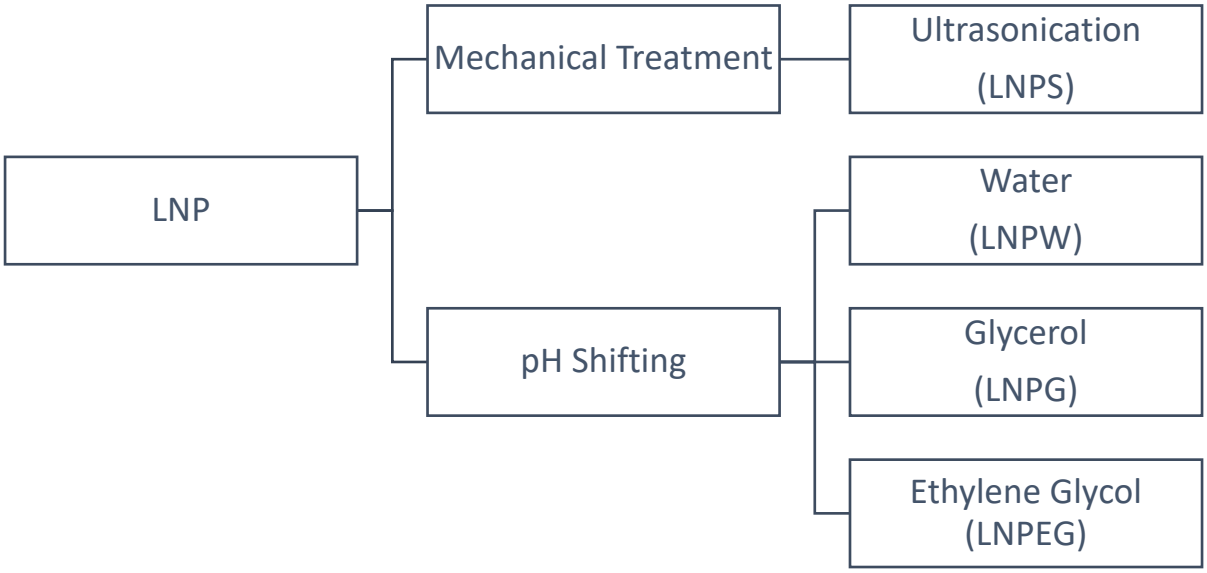

Figure 27. LNP Synthesis

Another commonly accepted method for the production of lignin nanoparticles is the pH shifting method. Frangville *et al.*[23] widely investigated the growth and control of LNP through pH shifting in ethylene glycol. Using the findings and optimal conditions from this study, Rahman *et al.*[189] synthesized LNP in ethylene glycol, water, and castor oil. In this work, the nanoparticles were synthesized in ethylene glycol and water with the addition of glycerol as the solvent. The precipitation approach followed in this work involved a pH change. Dealkaline lignin with measured particle size of 2027 nm ($\pm$ 190) was added to water, glycerol, and ethylene glycol, respectively. Since dealkaline lignin dissolves well in alkaline solution, solvents were made alkaline with the addition of a base. The solubility was then slowly changed by the addition of acid. As the solvent quality worsens, particles precipitate. At the initial stage of acid addition, supersaturation of lignin occurs, leading to variation in local concentration. As a result, nuclei form and grow due to aggregation. The particle size was controlled with slow addition of acid. Nanoparticles formed in water and glycerol have statistically similar particle sizes, with an average volumetric mean diameter of 90.0 and 96.9 nm each. Nanoparticles in ethylene glycol had a

slightly higher diameter of 104.5 nm. Rahman *et al.*[189] reported particle size of larger than 100 nm measured through DLS method for LNP prepared in water and ethylene glycol.

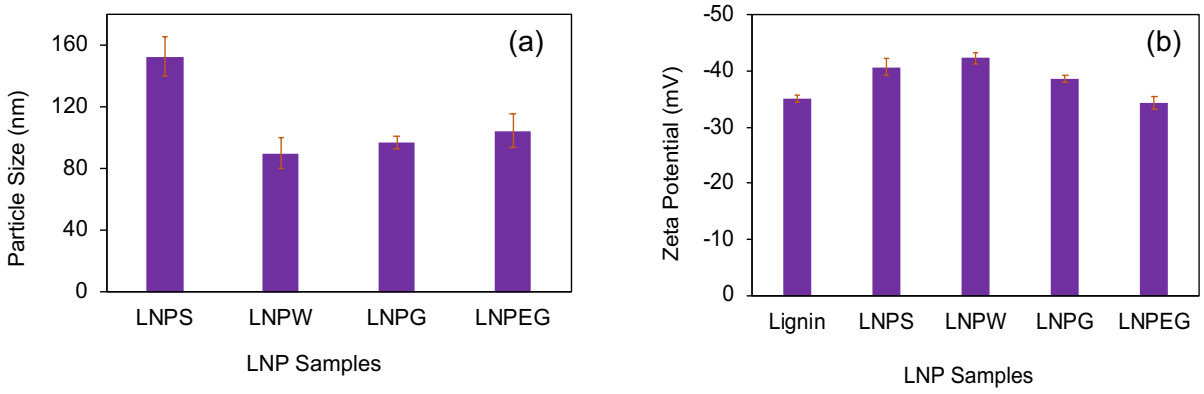

Figure 28. (a) Particle size and (b) Zeta potential of samples

The stability of nanoparticles was analyzed by zeta potential. Lignin and LNP possess a negative charge incurred from phenolic groups and other functional moieties, such as sulfate groups, emerging on the surface due to the extraction process [23]. The zeta potential of dealkaline lignin was measured to be -35.1 mV. It has been reported that as the pH increases, the surface charge of lignin becomes more negative [191]. Dealkaline lignin has a pH of 3, and therefore the surface charge of lignin is relatively low compared to other LNP. LNP prepared through pH-shift method were precipitated in acidic condition, and dialized further to bring pH above 5. These samples showed slightly more negative surface than compared to lignin. LNPS was prepared in alkaline solution (pH above 10) had more negative surface charge compared to lignin. Therefore, a correlation between pH and zeta-potential can be predicted, samples with higher pH would display more negative zeta potential.

On the other side, the particle size can also has an effect on the surface charge. Comparing the size of LNPW, LNPG, and LNPEG with zeta potential, it can be observed that, with increasing particle

size, the surface charge becomes more positive. The observation shows that the LNP prepared through the acid shift method has a smaller particle size and negative zeta potential, which may help maintain its stability in polar solvents.

4.3.2. Dispersity Test

Lignin is an excellent source of renewable biopolymer. To further utilize it for material applications, it is important to investigate its compatibility with other organic solvents. Figure 29 shows the dispersibility of lignin in solvents in order of decreasing relative polarity. Dealkaline lignin has limited dispersibility in water as shown in as shown in Figure 29. It is visibly dispersible in ethylene glycol and DMSO. Table 6 shows relative polarity and δ_h of the solvents used. After water, ethylene glycol and DMSO have the next highest polarity and hydrogen bonding capability. Lignin dispersion in these two solvents show that, dispersibility is improved in slightly polar solvents. As the solvents become non-polar, lignin becomes insoluble and settles at the bottom. Minimal or insignificant dispersibility of lignin in chloroform, THF, and toluene can be attributed to their low hydrogen bonding capability, δ_h.

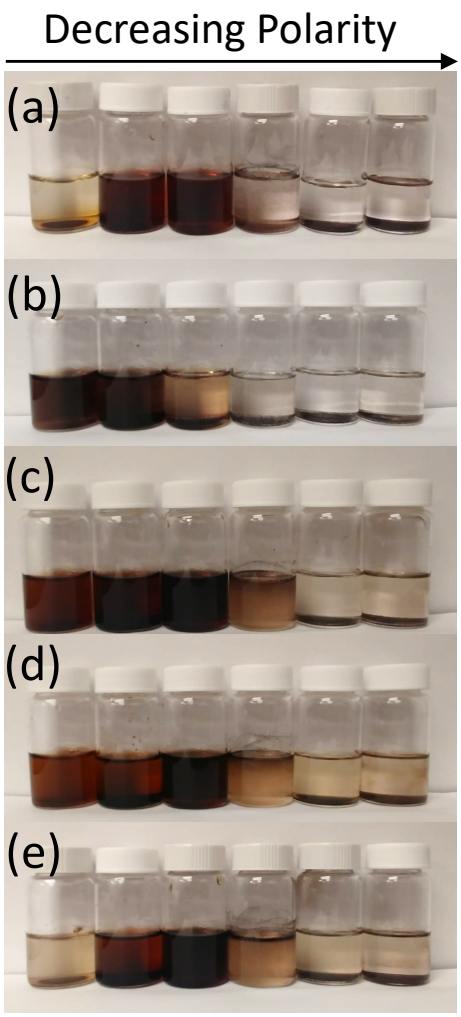

Figure 29. Dispersibility of (a) Lignin (b) LNPS (c)LNPW (d)LNPG and (e)LNPEG in solvents arranged in decreasing polarity water, ethylene glycol, DMSO, chloroform, THF and toluene

LNPEG displayed the same dispersibility as native lignin, while other samples showed slight variation. LNPS, LNPW, and LNPG had better dispersibility in water than dealkaline lignin. LNPS was well-dispersed in EG followed by DMSO. Dispersibility of LNP prepared through pH-shifting method had lower dispersibility in non-polar solvents (chloroform, THF and toluene), similar to lignin and LNPS. However, there was a relatively better dispersion in chloroform compared to native lignin. Overall, LNP maintained similar structure as lignin and therefore, there were only a few differences in the dispersibility.

Table 6. Properties of solvents: relative polarities and hydrogen bonding parameter (δ_h)[192] from Hansen Theory

Solvent	Relative Polarity	δ_h ((Cal/Cm^3)$^{1/2}$)
Water	1.0	16.7
Ethylene Glycol	0.790	12.7
Dimethyl Sulfoxide	0.444	5.0
Chloroform	0.259	2.8
Tetrahydrofuran	0.207	3.9
Toluene	0.099	1.0

4.3.3. UV-Visible Spectroscopy

Due to the aromatic structure of lignin, it is expected to have a good UV-absorbing properties. Figure 30 shows UV spectra for lignin and LNP dispersed in two solvents. In general, lignin has a characteristic absorbance peak at 280 nm [193,194]. Figure 30 (a) shows UV-visible spectra for lignin and LNP dispersed in water. A correlation can be made with dispersibility results and UV-absorbance peak. As shown in Figure 29, lignin and LNPEG have significantly lower dispersibility in water. Thus, the UV-absorbance of those two samples is low. LNPS, LNPW, and LNPG, samples that were well-dispersed in water, have a significant absorbance peak at 280 nm and a shoulder can be observed at 340 nm.

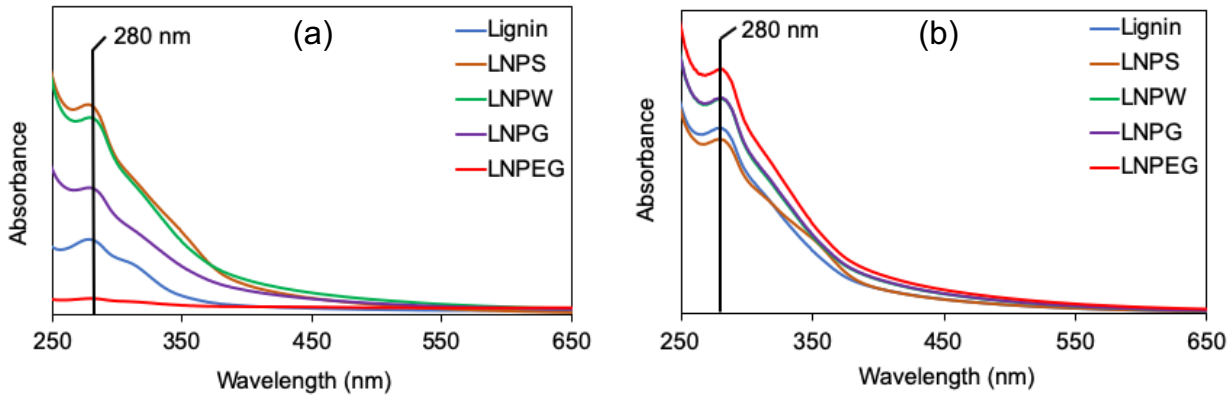

Figure 30. UV-Visible spectroscopy for lignin and lignin nanoparticles dispersed in (a) Water and (b) Ethylene Glycol

All samples were well-dispersed in ethylene glycol. Therefore UV-visible spectra of sample dispersed in ethylene glycol were recorded (as shown in Figure 30 (b)). Lignin and LNP show a typical absorbance peak of benzene chromophore at 280 nm. As the wavelength increases towards the visible region, the absorbance decreases. The dispersion of lignin gives a dark-brownish colour to the solution and, as a result, some absorbance can be seen in the visible range.

4.3.4. Fourier Transform Infrared Spectroscopy (FTIR)

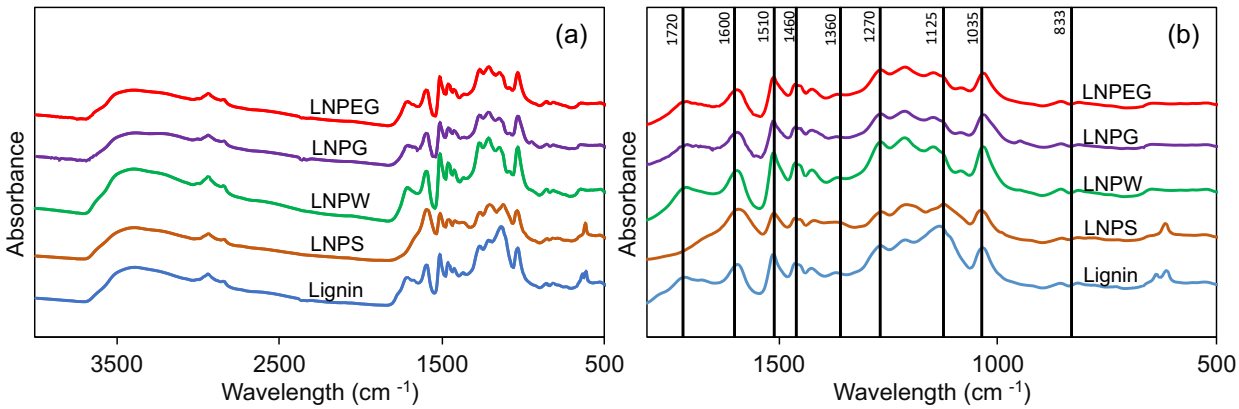

Figure 31. (a) IR spectra for lignin and nanoparticles (b) Detailed spectra from 1800-400 cm^{-1}

Lignin has a complex structure with an abundance of aromatic groups. Figure 31 shows the IR absorbance of lignin and LNP synthesised through different methods. Lignin shows a broad absorbance band at 3415 cm $^{-1}$, which is typical for hydroxyl groups from a phenolic and aliphatic structure. C-H peak can be observed at 2920 and 2855 cm^{-1} arising from C-H stretching of methoxyl and hydroxymethyl group.

The characteristic peaks of the phenolic structure are identified in Figure 31 (b). The band at 1700 cm^{-1} is a characteristic for C=O, the carbonyl groups, of lignin. Characteristic peaks of lignin are evident in lignin and LNP at 1600, 1510, 1460, 1360, 1270, and 833 cm^{-1}, indicating the presence of an aromatic structure. Table 7 lists the detailed assignment of each absorption peak. The structure of lignin was maintained in LNP, formed through different methods except for the disappearance of the 1700 cm^{-1} peak for LNPS. LNPS were produced by applying mechanical energy through an ultrasonication process.

Table 7. FTIR absorption assignment for Lignin

Characteristic Absorption (cm^{-1})	**Functional Group Assignment**
3415	O-H groups from the aliphatic and aromatic structure
2920	C-H stretching from methoxyl group
2855	C-H stretching from hydroxymethyl group
1720	C=O carbonyl stretch
1600	C=C aromatic skeletal vibration
1510	C-C aromatic skeletal vibration
1460	C-H aromatic stretch
1360	C-O syringyl units
1270	C-O guaiacyl units
1125	C-O secondary alcohol
1035	C-O primary alcohol
833	C-H aromatic vibration

4.3.5. X-ray Photoelectron Spectroscopy (XPS)

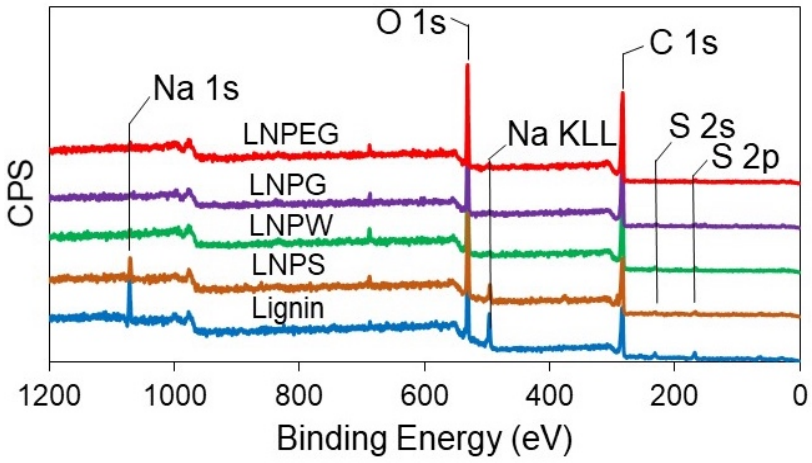

Figure 32. XPS survey for lignin and nanoparticles

An XPS analysis of lignin and LNP surface was conducted in a sensitive environment to obtain their chemical composition. Figure 32 shows typical spectra for lignin and nanoparticles obtained through different methods. Dealkaline lignin has a typical O 1s and C 1s peak. Moreover, the presence of Na and S can be seen. Dealkaline lignin was prepared from sodium lignosulfonate and, thus, the distinct peak for each can be observed. LNPS also shows some traces of sodium and sulfur. However, for LNP prepared through the acid shift process, the sodium peak is negligible, indicating that, during the dialysis process, such impurities were removed.

Table 8. Elemental composition of samples obtained from XPS

	C%	O%	S%	C/O
Lignin	65.87	29.73	4.4	2.22
LNPS	69.87	27.8	2.33	2.51
LNPW	77.22	21.3	1.49	3.63
LNPG	76.91	22.15	0.94	3.47
LNPEG	78.16	21.01	0.83	3.72

Quantitative analysis of lignin nanoparticles prepared through different processes was conducted using XPS. Table 8 shows the elemental composition of lignin and LNPs. Dealkaline lignin contains 65.87, 29.73, and 4.4% of C, O, and S, respectively. It has a C/O ratio of 2.22, which is slightly lower than the values reported in literature [21,195]. Each commercial lignin is extracted through a different process and the lower C/O ratio can be a result of oxidation of lignin during the extraction process [195]. Table 8 also lists change in the C/O for the different LNP produced. For the LNP produced through sonication and the pH shift method, sulfur content decreases while increasing the C/O ratio, which is in correlation with the results obtained by Yang *et al.*[21]. During the lignin dissolution process, possible side reactions between solvent and lignin may lead to a decrease in the C/O ratio as suggested by Gupta *et al.*[196]. In acidic conditions, hydrolysis of lignin may also lower the C/O ratio. LNP produced through pH-shift method showed a reduction in Oxygen content. Acidic conditions can result in possible hydrolysis of lignin and fragment the hydroxyl groups, which can reduce the oxygen leading to an increase in C/O ratio.

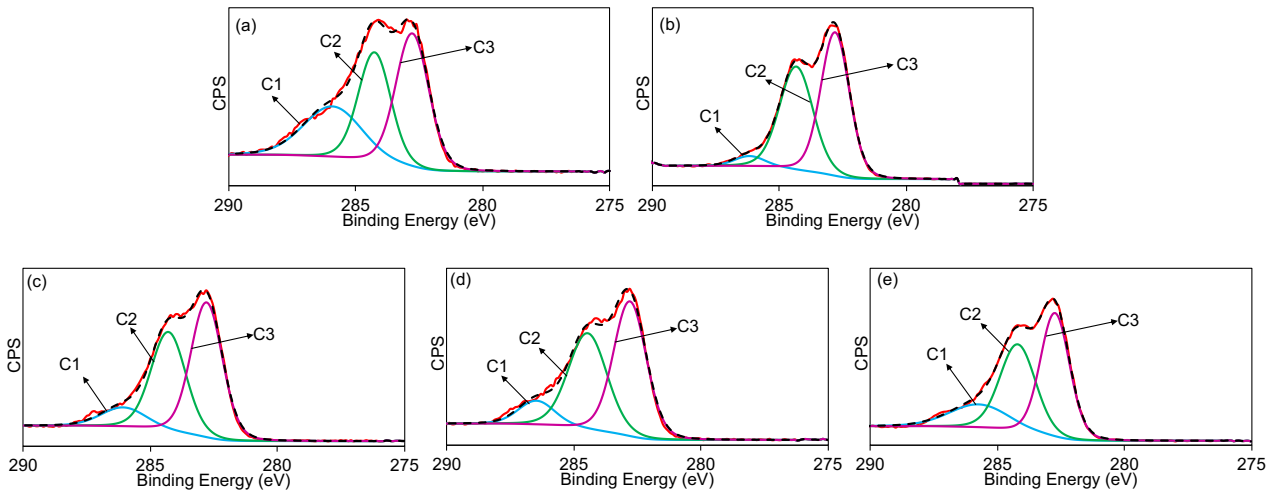

Figure 33. XPS C 1s spectra for (a) Lignin (b) LNPS (c) LNPW (d) LNPG (e) LNPEG

C 1s spectra for the samples were further analyzed, with the corresponding data shown in Figure 33 and Table 9. C1 positioned at approximately 286 eV corresponds to C=O including carboxyl,

ester, and aromatic carbon double-bonded with oxygen. C2 represents C-O associated with alcohol and ether groups. C3 corresponds to aliphatic carbon (C-C, C=C, C-H). As shown in Table 9., lignin contains an abundance of carbonyl, carboxyl, ester, ether, and hydroxyl groups. There is a significant reduction in the C1 peak for LNPS compared to dealkaline lignin. During the sonication process, the carbonyl functional groups were lost as analyzed in FT-IR and XPS. LNPW and LNPG showed a slight reduction in the C1 peak while increasing the C3 peak. Lignin-solvent interaction may reduce some carbonyl groups while maintaining the backbone structure leading to a reduction in C1 peak. Compared to other LNPs, LNPEG had the most similar composition to as lignin. The dispersibility observation of LNPEG and lignin in Figure 29 also display the same trend.

Table 9. Quantified analysis of C 1s and O 1s spectra

	C1		**C2**		**C3**		**O1**		**O2**	
	Position	%Area	Position	%Area	Position	%Area	Position	%Area	Position	%Area
Lignin	285.9	26.9	284.25	32.48	282.77	40.62	531.51	10.86	530.86	89.14
LNPS	286.16	3.88	284.32	43.83	282.8	52.3	531.48	9.14	530.52	90.86
LNPW	286.06	9.99	284.28	39.99	282.78	50.02	531.4	9.61	530.9	90.39
LNPG	286.47	9.64	284.45	41.11	282.79	49.25	531.54	9.43	530.85	90.57
LNPEG	285.72	16.99	284.2	38.13	282.73	44.88	531.42	10.78	530.95	89.22

Figure 34 illustrates the O 1s spectra with a different composition fitted. O1 in Figure 34 represents the O=C bond corresponding to carbonyl, carboxyl, ester, ether, and O bonded to aromatic groups. O2 represents O-C, which is approximately 9 times higher in concentration than O1. Compared to lignin, the LNPS, LNPW, and LNPG showed a slight reduction in O=C. This observation was agreeable to the results obtained from the C 1s spectra. Moreover, although LNPEG had the most similar composition to lignin. XPS is a sensitive analysis dictating small differences in structure. XPS showed that the nanoparticles obtained through sonication had some slight structural changes.

LNPW and LNPG were similar in composition, slightly deviating from the lignin structure. LNPEG maintained the structure of lignin to the largest extent.

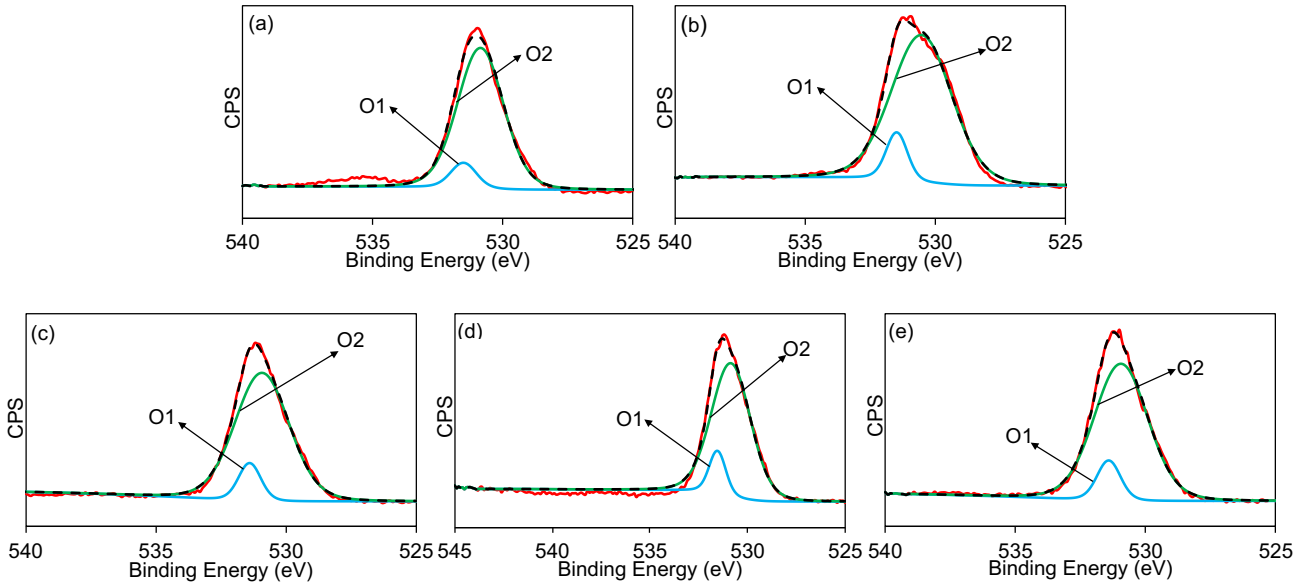

Figure 34. XPS O 1s spectra for (a) Lignin (b) LNPS (c) LNPW (d) LNPG (e) LNPEG

4.3.6. Water Contact Angle (WCA)

Lignin is a complex material with an abundance of phenolic groups. To valorize lignin and lignin nanoparticles in material applications, it is important to analyze their surface energy. Figure 35 shows the water contact analysis of lignin and LNP at 0 seconds and after 60 seconds. The aromatic structure of lignin makes it hydrophobic. However, the presence of polar groups negatively impacts the hydrophobicity of lignin. Thus, lignin has a WCA of 35.5^{o} and decreases to 18.2^{o} within 60 seconds. One limitation that can potentially affect the WCA analysis of lignin sample is the porosity of the sample prepared. Lignin, larger molecule in size, also can have pores in larger dimension. It is possible that the water molecule, also in comparable size, can be absorbed by the lignin surface. Thus the rapid deacrease in WCA for lignin can be attributed to some level of absorbance as well. This challenge is overcome when samples of samller particle size, LNPs, are

analyzed. A lignin nanoparticle prepared through mechanical energy has substantially low WCA as shown in Figure 35 and Table 10. These results could correspond to the decrease in the carbonyl peak as shown in the FTIR (Figure 31) and an increase in the C-O peak as observed from the XPS result (Figure 32-34). When mechanical energy is applied to lignin for a significant time, the carbonyl linkages of lignin were broken, potentially exposing more higher energy on the surface. As a result of an increase in surface energy, LNPS displays a lower water contact angle.

Table 10. The water contact angle of lignin samples at 0 and 60 seconds

	0 Seconds	**60 Seconds**
Lignin	35.3 ± 4.5	18.2 ± 3.2
LNPS	23.7 ± 0.2	14.6 ± 0.1
LNPW	68.0 ± 4.5	39.2 ± 1.6
LNPG	65.3 ± 0.3	25.9 ± 2.1
LNPEG	65.6 ± 2.1	35.8 ± 5.3

Lignin nanoparticles prepared through the acid shift method demonstrated a significant increase in the water contact angle. The lignin-solvent interaction potentially changed the structure of lignin, making it more hydrophobic. Moreover, the XPS analysis shows an increase in the C/O ratio and the aliphatic carbon made LNP more hydrophobic. LNPW, LNPG, and LNPEG with a higher WCA makes it more suitable nanoparticle for further application where hydrophobic surfaces are required.

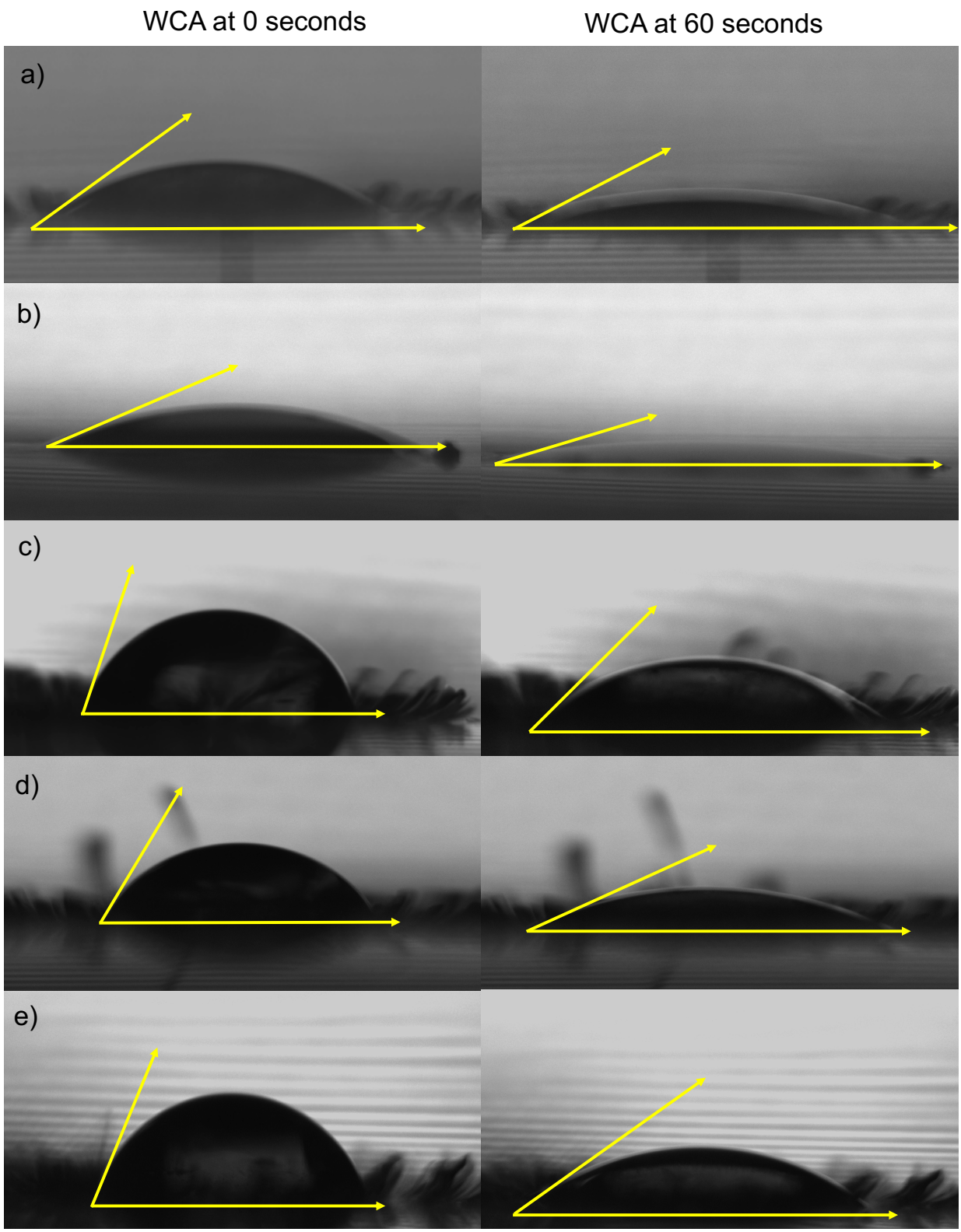

Figure 35. Water contact angle of (a) lignin (b) LNPS (c) LNPW (d) LNPG (e) LNPEG

4.4. Conclusion

Lignin is the second most abundant biopolymer found on the biosphere. It is known for its aromatic structure, providing it with UV-absorbing properties. Lignin can be further processed to make nanoparticles which can be used for many other functional applications. LNPs were made through two main methods, the ultra-sonication and pH-shifting method. From the analysis, it was observed that nanoparticles obtained through LNPS underwent a slight structural change. FTIR and XPS showed a relatively small change in the chemical composition for LNPS. While the WCA of LNPS was significantly lower than lignin, the other lignin nanoparticles (LNPW, LNPG, and LNPEG) displayed higher WCA. LNPW, LNPG, and LNPEG had a smaller particle size while maintaining negative zeta potential. All the LNPs prepared through various methods were dispersible in polar solvents and demonstrated UV-absorbing properties when dispersed in ethylene glycol. Overall, LNP prepared through acid precipitation method using different solvents demonstrated promising attributes, that warrant further investigations for a range of material applications (e.g. UV barrier for coating applications, polymer fillers). Moreover, because of their nanostructure with sufficient functional moieties, they can further be modified or decorated with other functionalities (e.g. antimicrobial agents, corrosion inhibitors) for material applications.

Chapter 5: Concluding Remarks

The need for sustainable and biodegradable materials is at its peak, not only due to the depleting fossil fuel resources but also to reduce the negative environmental impacts of such fossil fuel-derived materials. Lignocellulose is the most abundant, sustainable source of carbon and bio-renewable polymer on earth. Thus, this thesis has focused on the valorization of components of lignocellulose, cellulose and lignin, for functional material applications.

CNC, the crystalline part extracted from cellulose, has high crystallinity, high rigidity, low density along with high hydrophilicity. It has gained popularity as a reinforcing agent as it increases the mechanical strength of many polymetric matrices. As a result of its high surface energy and strong hydrogen bonding capabilities, CNC also has a high tendency to aggregate, making it incompatible with many matrices. However, CNC can be modified to induce compatibility, which can then be easily dispersed in a range of matrices. CNC has an abundant number of hydroxyl groups, amenable for chemical modification and transformation.

CNC, with such excellent properties, has the potential to be used in functional material applications. Chemical modification of hydroxyl groups on CNC surface with functional agents can open doors to many advanced applications. One such application of CNC is to tailor its surface for producing UV-absorbing composite materials.

In this research, CNC was modified with a UV-absorbing molecule, PABA, using IPDI as the coupling agent. Characterization of the modified CNC validated the modification also displaying UV-absorbing capabilities. Modified CNC incorporated in epoxy reduced the discolouration owing to the UV-irradiation of the composite. Due to the relatively lower thermal degradation temperature and incompatibility of PABA in epoxy, the direct addition of PABA in epoxy was not suitable. Thus, CNC was used as the modular polymer to carry the UV-absorber, which also avoids

the potential risk of UV-absorber leaching out of the matrix. Epoxy is a great adhesive used in coating industries; however, it is known for its poor UV stability limiting its use as an exterior layer. Therefore, an epoxy-modified CNC composite can avoid the need for an extra layer of UV protective polymer, such as polyurethane. In this research, epoxy containing 10 wt.% of modified CNC showed the least amount of discoloration due to UV irradiation.

Aromatic, biopolymer lignin also has many advantageous properties but due to complexity in its structure and heterogeneity arising from source and extraction of it, its use has been limited. To obtain more uniform lignin with functional attributes in material applications, the fabrication of lignin nanoparticles can be of interest. LNPs can even further enhance the attractive inherent properties of lignin. Thus, in this research, LNPs were produced via different processing approaches and their properties are compared. LNP produced through a top-down approach, the ultrasonication method, showed a slight structural change compared to native lignin. LNPs synthesized through the pH-shift method in water, glycerol and ethylene glycol maintained similar structures to the baseline lignin and displayed enhanced water contact angles. These LNPs produced through all the methods also displayed UV-absorbing properties. LNPs produced through pH shift method showed the most promosing structure. The LNPs can find applications in nanocomposites, biomedical, biotechnology, drug delivery system and other advanced applications. LNP can also be used in other specialty products, such as personal care products, increasing the utilization of lignin for value-added applications.

References

1. Geyer, R., Jambeck, J. R. & Law, K. L. Production, use, and fate of all plastics ever made. *Sci. Adv.* **3**, 25–29 (2017).
2. Mohanty, A. K., Misra, M. & Hinrichsen, G. Biofibres, biodegradable polymers and biocomposites: An overview. *Macromol. Mater. Eng.* **276**–**277**, 1–24 (2000).
3. Pérez, J., Muñoz-Dorado, J., de la Rubia, T. & Martínez, J. Biodegradation and biological treatments of cellulose, hemicellulose and lignin: an overview. *Int. Microbiol.* **5**, 53–63 (2002).
4. Thakur, V. K. & Thakur, M. K. Recent advances in green hydrogels from lignin: a review. *Int. J. Biol. Macromol.* **72**, 834–847 (2015).
5. Lu, P. & Hsieh, Y.-L. Preparation and properties of cellulose nanocrystals: Rods, spheres, and network. *Carbohydr. Polym.* **82**, 329–336 (2010).
6. Eyley, S. & Thielemans, W. Surface modification of cellulose nanocrystals. *Nanoscale* **6**, 7764–7779 (2014).
7. Wang, B., Sain, M. & Oksman, K. Study of structural morphology of hemp fiber from the micro to the nanoscale. *Appl. Compos. Mater.* **14**, 89–103 (2007).
8. Kim, J.-H. *et al.* Review of nanocellulose for sustainable future materials. *Int. J. Precis. Eng. Manuf. Technol.* **2**, 197–213 (2015).
9. Kan, K. H. M., Li, J., Wijesekera, K. & Cranston, E. D. Polymer-grafted cellulose nanocrystals as pH-responsive reversible flocculants. *Biomacromolecules* **14**, 3130–3139 (2013).
10. Jonoobi, M. *et al.* Different preparation methods and properties of nanostructured cellulose from various natural resources and residues: a review. *Cellulose* **22**, 935–969 (2015).
11. Shojaeiarani, J., Bajwa, D. S. & Stark, N. M. Green esterification: A new approach to improve thermal and mechanical properties of poly(lactic acid) composites reinforced by cellulose nanocrystals. *J. Appl. Polym. Sci.* **135**, 46468 (2018).
12. Inai, N. H., Lewandowska, A. E., Ghita, O. R. & Eichhorn, S. J. Interfaces in polyethylene oxide modified cellulose nanocrystal - polyethylene matrix composites. *Compos. Sci. Technol.* **154**, 128–135 (2018).
13. Zhang, W. *et al.* High performance poly (vinyl alcohol)/cellulose nanocrystals nanocomposites manufactured by injection molding. *Cellulose* **21**, 485–494 (2014).
14. Rahimi, S. K. & Otaigbe, J. U. The effects of the interface on microstructure and rheo-mechanical properties of polyamide 6/cellulose nanocrystal nanocomposites prepared by in-situ ring-opening polymerization and subsequent melt extrusion. *Polymer.* **127**, 269–285 (2017).
15. Lam, E., Male, K. B., Chong, J. H., Leung, A. C. W. & Luong, J. H. T. Applications of functionalized and nanoparticle-modified nanocrystalline cellulose. *Trends Biotechnol.* **30**, 283–290 (2012).
16. Akhlaghi, S. P., Berry, R. C. & Tam, K. C. Surface modification of cellulose nanocrystal with chitosan oligosaccharide for drug delivery applications. *Cellulose* **20**, 1747–1764 (2013).
17. Panchal, P., Ogunsona, E. & Mekonnen, T. Trends in Advanced Functional Material Applications of Nanocellulose. *Processes* **7**, 10 (2018).
18. Kobayashi, H. & Fukuoka, A. Synthesis and utilisation of sugar compounds derived from

lignocellulosic biomass. *Green Chem.* **15**, 1740–1763 (2013).
19. Gosselink, R. J. A. *et al.* Characterisation and application of NovaFiber lignin. *Ind. Crops Prod.* **20**, 191–203 (2004).
20. Ganewatta, M. S. *et al.* Lignin Biopolymers in the Age of Controlled Polymerization. *Polymers (Basel).* **11**, 1176 (2019).
21. Yang, W. *et al.* Valorization of Acid Isolated High Yield Lignin Nanoparticles as Innovative Antioxidant/Antimicrobial Organic Materials. *ACS Sustain. Chem. Eng.* **6**, 3502–3514 (2018).
22. Zhao, W., Simmons, B., Singh, S., Ragauskas, A. & Cheng, G. From lignin association to nano-/micro-particle preparation: extracting higher value of lignin. *Green Chem.* **18**, 5693–5700 (2016).
23. Frangville, C. *et al.* Fabrication of environmentally biodegradable lignin nanoparticles. *ChemPhysChem* **13**, 4235–4243 (2012).
24. Habibi, Y., Lucia, L. A. & Rojas, O. J. Cellulose Nanocrystals: Chemistry, Self-Assembly, and Applications. *Chem. Rev.* **110**, 3479–3500 (2010).
25. Bettaieb, F., Khiari, R., Dufresne, A., Mhenni, M. F. & Belgacem, M. N. Mechanical and thermal properties of Posidonia oceanica cellulose nanocrystal reinforced polymer. *Carbohydr. Polym.* **123**, 99–104 (2015).
26. Ogunsona, E. O., Misra, M. & Mohanty, A. K. Accelerated hydrothermal aging of biocarbon reinforced nylon biocomposites. *Polym. Degrad. Stab.* **139**, 76–88 (2017).
27. Ogunsona, E. O., Misra, M. & Mohanty, A. K. Sustainable biocomposites from biobased polyamide 6,10 and biocarbon from pyrolyzed miscanthus fibers. *J. Appl. Polym. Sci.* **134**, 44221 (2017).
28. Ogunsona, E. O., Misra, M. & Mohanty, A. K. Influence of epoxidized natural rubber on the phase structure and toughening behavior of biocarbon reinforced nylon 6 biocomposites. *RSC Adv.* **7**, 8727–8739 (2017).
29. Ogunsona, E. O., Misra, M. & Mohanty, A. K. Effects of Accelerated Aging on the Flammability of Polypropylene Based Biocomposites. in *ANTEC Conference Proceedings* (Society of Plastics Engineers, 2015).
30. Ogunsona, E. O., Codou, A., Misra, M. & Mohanty, A. K. Thermally Stable Pyrolytic Biocarbon as an Effective and Sustainable Reinforcing Filler for Polyamide Bio-composites Fabrication. *J. Polym. Environ.* (2018). doi:10.1007/s10924-018-1232-5
31. Ogunsona, E. O., Misra, M. & Mohanty, A. K. Impact of interfacial adhesion on the microstructure and property variations of biocarbons reinforced nylon 6 biocomposites. *Compos. Part A Appl. Sci. Manuf.* **98**, 32–44 (2017).
32. Ilyas, R. A., Sapuan, S. M., Sanyang, M. L., Ishak, M. R. & Zainudin, E. S. Nanocrystalline Cellulose as Reinforcement for Polymeric Matrix Nanocomposites and its Potential Applications: A Review. *Curr. Anal. Chem.* **14**, 203–225 (2018).
33. Sobolčiak, P. *et al.* The preparation, properties and applications of electrospun co-polyamide 6,12 membranes modified by cellulose nanocrystals. *Mater. Des.* **132**, 314–323 (2017).
34. Orts, W. J. *et al.* Application of Cellulose Microfibrils in Polymer Nanocomposites. *J. Polym. Environ.* **13**, 301–306 (2005).
35. Moon, R. J., Martini, A., Nairn, J., Simonsen, J. & Youngblood, J. Cellulose nanomaterials review: structure, properties and nanocomposites. *Chem. Soc. Rev.* **40**, 3941 (2011).

36. Lee, K.-Y., Aitomäki, Y., Berglund, L. A., Oksman, K. & Bismarck, A. On the use of nanocellulose as reinforcement in polymer matrix composites. *Compos. Sci. Technol.* **105**, 15–27 (2014).
37. Xu, X. *et al.* Cellulose Nanocrystals vs. Cellulose Nanofibrils: A Comparative Study on Their Microstructures and Effects as Polymer Reinforcing Agents. *ACS Appl. Mater. Interfaces* **5**, 2999–3009 (2013).
38. Ojogbo, E., Blanchard, R. & Mekonnen, T. Hydrophobic and Melt Processable Starch-Laurate Esters: Synthesis, Structure-Property Correlations. *J. Polym. Sci. Part A Polym. Chem.* **56**, 2611–2622 (2018).
39. Ogunsona, E., Ojogbo, E. & Mekonnen, T. Advanced material applications of starch and its derivatives. *Eur. Polym. J.* **108**, 570–581 (2018).
40. Brown, A. J. XIX.—The chemical action of pure cultivations of bacterium aceti. *J. Chem. Soc., Trans.* **49**, 172–187 (1886).
41. Kim, N. & Retsina, T. Innovative nanocellulose process breaks the cost barrier. *TAPPI J.* **13**, 19–23 (2014).
42. Peng, B. L., Dhar, N., Liu, H. L. & Tam, K. C. Chemistry and applications of nanocrystalline cellulose and its derivatives: A nanotechnology perspective. *Can. J. Chem. Eng.* **89**, 1191–1206 (2011).
43. Chen, L. *et al.* Tailoring the yield and characteristics of wood cellulose nanocrystals (CNC) using concentrated acid hydrolysis. *Cellulose* **22**, 1753–1762 (2015).
44. Silvério, H. A., Flauzino Neto, W. P., Dantas, N. O. & Pasquini, D. Extraction and characterization of cellulose nanocrystals from corncob for application as reinforcing agent in nanocomposites. *Ind. Crops Prod.* **44**, 427–436 (2013).
45. Kalashnikova, I., Bizot, H., Bertoncini, P., Cathala, B. & Capron, I. Cellulosic nanorods of various aspect ratios for oil in water Pickering emulsions. *Soft Matter* **9**, 952–959 (2013).
46. Cao, X., Dong, H. & Li, C. M. New nanocomposite materials reinforced with flax cellulose nanocrystals in waterborne polyurethane. *Biomacromolecules* **8**, 899–904 (2007).
47. Habibi, Y., Foulon, L., Aguié-Béghin, V., Molinari, M. & Douillard, R. Langmuir–Blodgett films of cellulose nanocrystals: Preparation and characterization. *J. Colloid Interface Sci.* **316**, 388–397 (2007).
48. Garcia de Rodriguez, N. L., Thielemans, W. & Dufresne, A. Sisal cellulose whiskers reinforced polyvinyl acetate nanocomposites. *Cellulose* **13**, 261–270 (2006).
49. Kaboorani, A. & Riedl, B. Surface modification of cellulose nanocrystals (CNC) by a cationic surfactant. *Ind. Crops Prod.* **65**, 45–55 (2015).
50. Bravo, J., Zhai, L., Wu, Z., Cohen, R. E. & Rubner, M. F. Transparent superhydrophobic films based on silica nanoparticles. *Langmuir* **23**, 7293–7298 (2007).
51. Song, J. & Rojas, O. J. Approaching super-hydrophobicity from cellulosic materials: A Review. *Pap. Chem. Nord. Pulp Pap. Res. J.* **28**, (2100).
52. Li, S., Xie, H., Zhang, S. & Wang, X. Facile transformation of hydrophilic cellulose into superhydrophobic cellulose. *Chem. Commun.* 4857–4859 (2007). doi:10.1039/b712056g
53. Teisala, H., Tuominen, M. & Kuusipalo, J. Superhydrophobic Coatings on Cellulose-Based Materials: Fabrication, Properties, and Applications. *Adv. Mater. Interfaces* **1**, 1300026 (2014).
54. Manca, M. *et al.* Durable superhydrophobic and antireflective surfaces by trimethylsilanized silica nanoparticles-based sol-gel processing. *Langmuir* **25**, 6357–6362

(2009).
55. Salam, A., Lucia, L. A. & Jameel, H. Fluorine-based surface decorated cellulose nanocrystals as potential hydrophobic and oleophobic materials. *Cellulose* **22**, 397–406 (2015).
56. Shang, W. *et al.* Hydrophobic modification of cellulose nanocrystal via covalently grafting of castor oil. *Cellulose* **20**, 179–190 (2013).
57. Salajková, M., Berglund, L. A. & Zhou, Q. Hydrophobic cellulose nanocrystals modified with quaternary ammonium salts. *J. Mater. Chem.* **22**, 19798 (2012).
58. Yu, M., Gu, G., Meng, W.-D. & Qing, F.-L. Superhydrophobic cotton fabric coating based on a complex layer of silica nanoparticles and perfluorooctylated quaternary ammonium silane coupling agent. *Appl. Surf. Sci.* **253**, 3669–3673 (2007).
59. Ogihara, H., Xie, J., Okagaki, J. & Saji, T. Simple Method for Preparing Superhydrophobic Paper: Spray-Deposited Hydrophobic Silica Nanoparticle Coatings Exhibit High Water-Repellency and Transparency. *Langmuir* **28**, 4605–4608 (2012).
60. Samyn, P. Wetting and hydrophobic modification of cellulose surfaces for paper applications. *J. Mater. Sci.* **48**, 6455–6498 (2013).
61. Bae, G. Y. *et al.* Superhydrophobicity of cotton fabrics treated with silica nanoparticles and water-repellent agent. *J. Colloid Interface Sci.* **337**, 170–175 (2009).
62. Xue, C.-H., Jia, S.-T., Zhang, J. & Ma, J.-Z. Large-area fabrication of superhydrophobic surfaces for practical applications: an overview. *Sci. Technol. Adv. Mater.* **11**, 033002 (2010).
63. Zhou, S. *et al.* Sustainable, Reusable, and Superhydrophobic Aerogels from Microfibrillated Cellulose for Highly Effective Oil/Water Separation. *ACS Sustain. Chem. Eng.* **4**, 6409–6416 (2016).
64. Cheng, Q.-Y., Guan, C.-S., Wang, M., Li, Y.-D. & Zeng, J.-B. Cellulose nanocrystal coated cotton fabric with superhydrophobicity for efficient oil/water separation. *Carbohydr. Polym.* **199**, 390–396 (2018).
65. Huang, J., Wang, S., Lyu, S. & Fu, F. Preparation of a robust cellulose nanocrystal superhydrophobic coating for self-cleaning and oil-water separation only by spraying. *Ind. Crops Prod.* **122**, 438–447 (2018).
66. Guo, J. *et al.* Superhydrophobic and Slippery Lubricant-Infused Flexible Transparent Nanocellulose Films by Photoinduced Thiol–Ene Functionalization. *ACS Appl. Mater. Interfaces* **8**, 34115–34122 (2016).
67. Fan, T., Qian, Q., Hou, Z., Liu, Y. & Lu, M. Preparation of smart and reversible wettability cellulose fabrics for oil/water separation using a facile and economical method. *Carbohydr. Polym.* **200**, 63–71 (2018).
68. Varesano, A., Vineis, C., Aluigi, A. & Rombaldoni, F. Antimicrobial polymers for textile products. *Sci. against Microb. ...* 99–110 (2011).
69. Mauriello, G., De Luca, E., La Storia, A., Villani, F. & Ercolini, D. Antimicrobial activity of a nisin-activated plastic film for food packaging. *Lett. Appl. Microbiol.* **41**, 464–469 (2005).
70. Kodjak, A. FDA Bans 19 Chemicals Used in Antibacterial. *Your Health* (2016).
71. Laxminarayan, R. *et al.* Antibiotic resistance—the need for global solutions. *Lancet Infect. Dis.* **13**, 1057–1098 (2013).
72. Roy, D., Knapp, J. S., Guthrie, J. T. & Perrier, S. Antibacterial Cellulose Fiber via RAFT Surface Graft Polymerization. *Biomacromolecules* **9**, 91–99 (2008).

73. Wang, L., Hu, C. & Shao, L. The antimicrobial activity of nanoparticles: present situation and prospects for the future. *Int. J. Nanomedicine* **12**, 1227–1249 (2017).
74. Appendini, P. & Hotchkiss, J. H. Review of antimicrobial food packaging. *Innov. Food Sci. Emerg. Technol.* **3**, 113–126 (2002).
75. Huang, K.-S. *et al.* Recent Advances in Antimicrobial Polymers: A Mini-Review. *Int. J. Mol. Sci.* **17**, (2016).
76. Fortunati, E. *et al.* Nano-biocomposite films with modified cellulose nanocrystals and synthesized silver nanoparticles. *Carbohydr. Polym.* **101**, 1122–1133 (2014).
77. Drogat, N. *et al.* Antimicrobial silver nanoparticles generated on cellulose nanocrystals. *J. Nanoparticle Res.* **13**, 1557–1562 (2011).
78. Lala, N. L. *et al.* Fabrication of nanofibers with antimicrobial functionality used as filters: protection against bacterial contaminants. *Biotechnol. Bioeng.* **97**, 1357–1365 (2007).
79. Ramos, A. I. *et al.* Analysis of the microcrystalline inclusion compounds of triclosan with β-cyclodextrin and its tris-O-methylated derivative. *J. Pharm. Biomed. Anal.* **80**, 34–43 (2013).
80. Suller, M. T. E. & Russell, A. D. Triclosan and antibiotic resistance in Staphylococcus aureus. *J. Antimicrob. Chemother.* **46**, 11–18 (2000).
81. Helander, I. M., Nurmiaho-Lassila, E.-L., Ahvenainen, R., Rhoades, J. & Roller, S. Chitosan disrupts the barrier properties of the outer membrane of Gram-negative bacteria. *Int. J. Food Microbiol.* **71**, 235–244 (2001).
82. Rabea, E. I., Badawy, M. E. T., Stevens, C. V., Smagghe, G. & Steurbaut, W. Chitosan as antimicrobial agent: Applications and mode of action. *Biomacromolecules* **4**, 1457–1465 (2003).
83. El-tahlawy, K. F., El-bendary, M. A., Elhendawy, A. G. & Hudson, S. M. The antimicrobial activity of cotton fabrics treated with different crosslinking agents and chitosan. *Carbohydr. Polym.* **60**, 421–430 (2005).
84. CHA, D. S. & CHINNAN, M. S. Biopolymer-Based Antimicrobial Packaging: A Review. *Crit. Rev. Food Sci. Nutr.* **44**, 223–237 (2004).
85. Salmieri, S. *et al.* Antimicrobial nanocomposite films made of poly(lactic acid)-cellulose nanocrystals (PLA-CNC) in food applications: Part A-effect of nisin release on the inactivation of Listeria monocytogenes in ham. *Cellulose* **21**, 1837–1850 (2014).
86. Weishaupt, R. *et al.* Enhanced Antimicrobial Activity and Structural Transitions of a Nanofibrillated Cellulose–Nisin Biocomposite Suspension. *ACS Appl. Mater. Interfaces* **10**, 20170–20181 (2018).
87. Lee, C. H., Park, H. J. & Lee, D. S. Influence of antimicrobial packaging on kinetics of spoilage microbial growth in milk and orange juice. *J. Food Eng.* **65**, 527–531 (2004).
88. Tang, J., Song, Y., Berry, R. M. & Tam, K. C. Polyrhodanine coated cellulose nanocrystals as optical pH indicators. *RSC Adv.* **4**, 60249–60252 (2014).
89. Fortunati, E. *et al.* Multifunctional bionanocomposite films of poly(lactic acid), cellulose nanocrystals and silver nanoparticles. *Carbohydr. Polym.* **87**, 1596–1605 (2012).
90. Tang, J. *et al.* Polyrhodanine Coated Cellulose Nanocrystals: A Sustainable Antimicrobial Agent. *ACS Sustain. Chem. Eng.* **3**, 1801–1809 (2015).
91. Unnithan, A. R., Gnanasekaran, G., Sathishkumar, Y., Lee, Y. S. & Kim, C. S. Electrospun antibacterial polyurethane–cellulose acetate–zein composite mats for wound dressing. *Carbohydr. Polym.* **102**, 884–892 (2014).
92. Zhang, H., Chen, H., She, Y., Zheng, X. & Pu, J. Anti-yellowing property of polyurethane

improved by the use of surface-modified nanocrystalline cellulose. *BioResources* **9**, 673–684 (2014).
93. Wonnie Ma, I. A. *et al.* Anticorrosion Properties of Epoxy/Nanocellulose Nanocomposite Coating. *BioResources* **12**, 2912–2929 (2017).
94. Panda, S. S., Katz, H. E. & Tovar, J. D. Solid-state electrical applications of protein and peptide based nanomaterials. *Chem. Soc. Rev.* **47**, 3640–3658 (2018).
95. Csoka, L. *et al.* Piezoelectric Effect of Cellulose Nanocrystals Thin Films. *ACS Macro Lett.* **1**, 867–870 (2012).
96. Csoka, L., Hoeger, I. C., Peralta, P., Peszlen, I. & Rojas, O. J. Dielectrophoresis of cellulose nanocrystals and alignment in ultrathin films by electric field-assisted shear assembly. *J. Colloid Interface Sci.* **363**, 206–212 (2011).
97. Le Bras, D., Strømme, M. & Mihranyan, A. Characterization of Dielectric Properties of Nanocellulose from Wood and Algae for Electrical Insulator Applications. *J. Phys. Chem. B* **119**, 5911–5917 (2015).
98. Kocherbitov, V., Ulvenlund, S., Kober, M., Jarring, K. & Arnebrant, T. Hydration of Microcrystalline Cellulose and Milled Cellulose Studied by Sorption Calorimetry. *J. Phys. Chem. B* **112**, 3728–3734 (2008).
99. Mihranyan, A., Llagostera, A. P., Karmhag, R., Strømme, M. & Ek, R. Moisture sorption by cellulose powders of varying crystallinity. *Int. J. Pharm.* **269**, 433–442 (2004).
100. Gaspar, D. *et al.* Nanocrystalline cellulose applied simultaneously as the gate dielectric and the substrate in flexible field effect transistors. *Nanotechnology* **25**, 094008 (2014).
101. Xu, S., Girouard, N., Schueneman, G., Shofner, M. L. & Meredith, J. C. Mechanical and thermal properties of waterborne epoxy composites containing cellulose nanocrystals. *Polymer (Guildf).* **54**, 6589–6598 (2013).
102. Bras, J. *et al.* Mechanical, barrier, and biodegradability properties of bagasse cellulose whiskers reinforced natural rubber nanocomposites. *Ind. Crops Prod.* **32**, 627–633 (2010).
103. Cao, Y., Zavaterri, P., Youngblood, J., Moon, R. & Weiss, J. The influence of cellulose nanocrystal additions on the performance of cement paste. *Cem. Concr. Compos.* **56**, 73–83 (2015).
104. Jorfi, M. & Foster, E. J. Recent advances in nanocellulose for biomedical applications. *J. Appl. Polym. Sci.* **132**, n/a-n/a (2015).
105. Dong, S. & Roman, M. Fluorescently Labeled Cellulose Nanocrystal for Bioimaging. *J. AM. CHEM. SOC* **129**, 3 (2007).
106. Armentano, I., Dottori, M., Fortunati, E., Mattioli, S. & Kenny, J. M. Biodegradable polymer matrix nanocomposites for tissue engineering: A review. *Polym. Degrad. Stab.* **95**, 2126–2146 (2010).
107. Domingues, R. M. A., Gomes, M. E. & Reis, R. L. The Potential of Cellulose Nanocrystals in Tissue Engineering Strategies. (2014). doi:10.1039/c0cs00108b
108. Yang, X. & Cranston, E. D. Chemically cross-linked cellulose nanocrystal aerogels with shape recovery and superabsorbent properties. *Chem. Mater.* **26**, 6016–6025 (2014).
109. Lin, N., Bruzzese, C. & Dufresne, A. TEMPO-oxidized nanocellulose participating as crosslinking aid for alginate-based sponges. *ACS Appl. Mater. Interfaces* **4**, 4948–4959 (2012).
110. Zhou, Y. *et al.* Recyclable organic solar cells on cellulose nanocrystal substrates. *Sci. Rep.* **3**, 1536 (2013).
111. Qiu, X. & Hu, S. 'Smart' materials based on cellulose: A review of the preparations,

properties, and applications. *Materials (Basel).* **6**, 738–781 (2013).
112. Way, A. E., Hsu, L., Shanmuganathan, K., Weder, C. & Rowan, S. J. PH-responsive cellulose nanocrystal gels and nanocomposites. *ACS Macro Lett.* **1**, 1001–1006 (2012).
113. Kafy, A. *et al.* Cellulose nanocrystal/graphene oxide composite film as humidity sensor. *Sensors Actuators A Phys.* **247**, 221–226 (2016).
114. Zhang, L., Li, Q., Zhou, J. & Zhang, L. Synthesis and Photophysical Behavior of Pyrene-Bearing Cellulose Nanocrystals for Fe^{3+} Sensing. *Macromol. Chem. Phys.* **213**, 1612–1617 (2012).
115. Sadasivuni, K. K. *et al.* Transparent and Flexible Cellulose Nanocrystal/Reduced Graphene Oxide Film for Proximity Sensing. *Small* **11**, 994–1002 (2015).
116. Wang, S., Zhang, X., Wu, X. & Lu, C. Tailoring percolating conductive networks of natural rubber composites for flexible strain sensors via a cellulose nanocrystal templated assembly. *Soft Matter* **12**, 845–852 (2016).
117. Annamalai, P. K. *et al.* Water-responsive mechanically adaptive nanocomposites based on styrene-butadiene rubber and cellulose nanocrystals - Processing matters. *ACS Appl. Mater. Interfaces* **6**, 967–976 (2014).
118. Mendez, J. *et al.* Bioinspired mechanically adaptive polymer nanocomposites with water-activated shape-memory effect. *Macromolecules* **44**, 6827–6835 (2011).
119. Zoppe, J. O. *et al.* Poly(*N* -isopropylacrylamide) Brushes Grafted from Cellulose Nanocrystals via Surface-Initiated Single-Electron Transfer Living Radical Polymerization. *Biomacromolecules* **11**, 2683–2691 (2010).
120. Zoppe, J. O., Österberg, M., Venditti, R. A., Laine, J. & Rojas, O. J. Surface Interaction Forces of Cellulose Nanocrystals Grafted with Thermoresponsive Polymer Brushes. *Biomacromolecules* **12**, 2788–2796 (2011).
121. Zoppe, J. O., Venditti, R. A. & Rojas, O. J. Pickering emulsions stabilized by cellulose nanocrystals grafted with thermo-responsive polymer brushes. *J. Colloid Interface Sci.* **369**, 202–209 (2012).
122. Lin, N. & Dufresne, A. Nanocellulose in biomedicine: Current status and future prospect. *Eur. Polym. J.* **59**, 302–325 (2014).
123. Bawa, P., Pillay, V., Choonara, Y. E. & du Toit, L. C. Stimuli-responsive polymers and their applications in drug delivery. *Biomed. Mater.* **4**, 022001 (2009).
124. Lievonen, M. *et al.* A simple process for lignin nanoparticle preparation. *Green Chem.* **18**, 1416–1422 (2016).
125. Kai, D. *et al.* Towards lignin-based functional materials in a sustainable world. *Green Chem.* **18**, 1175–1200 (2016).
126. Khan, A., Nair, V., Colmenares, J. C. & Gläser, R. Lignin-Based Composite Materials for Photocatalysis and Photovoltaics. *Top. Curr. Chem.* **376**, 20 (2018).
127. Nair, S. S. *et al.* High Shear Homogenization of Lignin to Nanolignin and Thermal Stability of Nanolignin-Polyvinyl Alcohol Blends. *ChemSusChem* **7**, 3513–3520 (2014).
128. Lu, Q. *et al.* Comparative antioxidant activity of nanoscale lignin prepared by a supercritical antisolvent (SAS) process with non-nanoscale lignin. *Food Chem.* **135**, 63–67 (2012).
129. Satheesh Kumar, M. N., Mohanty, A. K., Erickson, L. & Misra, M. Lignin and Its Applications with Polymers. *J. Biobased Mater. Bioenergy* **3**, 1–24 (2009).
130. Vishtal, A. & Kraslawski, A. Challenges in industrial applications of technical lignins. *BioResources* **6**, 3547–3568 (2011).

131. Beisl, S., Miltner, A. & Friedl, A. Lignin from Micro- to Nanosize: Production Methods. *Int. J. Mol. Sci.* **18**, 1244 (2017).
132. Qian, Y., Qiu, X. & Zhu, S. Lignin: a nature-inspired sun blocker for broad-spectrum sunscreens. *Green Chem.* **17**, 320–324 (2015).
133. Baurhoo, B., Ruiz-Feria, C. A. & Zhao, X. Purified lignin: Nutritional and health impacts on farm animals—A review. *Anim. Feed Sci. Technol.* **144**, 175–184 (2008).
134. Shafaghat, H. *et al.* In-situ catalytic pyrolysis of lignin in a bench-scale fixed bed pyrolyzer. *J. Ind. Eng. Chem.* **54**, 447–453 (2017).
135. Laurichesse, S. & Avérous, L. Chemical modification of lignins: Towards biobased polymers. *Prog. Polym. Sci.* **39**, 1266–1290 (2014).
136. McClelland, D. J. *et al.* Functionality and molecular weight distribution of red oak lignin before and after pyrolysis and hydrogenation. *Green Chem.* **19**, 1378–1389 (2017).
137. Brebu, M. & Vasile, C. *Thermal Degradation of Lignin-A Review*. *Cellulose Chemistry And Technology Cellulose Chem. Technol* **44**, (2010).
138. Grossman, A. & Vermerris, W. Lignin-based polymers and nanomaterials. *Curr. Opin. Biotechnol.* **56**, 112–120 (2019).
139. Cao, Y., Zavattieri, P., Youngblood, J., Moon, R. & Weiss, J. The relationship between cellulose nanocrystal dispersion and strength. *Constr. Build. Mater.* **119**, 71–79 (2016).
140. Jin, F.-L., Li, X. & Park, S.-J. Synthesis and application of epoxy resins: A review. *J. Ind. Eng. Chem.* **29**, 1–11 (2015).
141. Sirviö, J. A., Visanko, M., Heiskanen, J. P. & Liimatainen, H. UV-absorbing cellulose nanocrystals as functional reinforcing fillers in polymer nanocomposite films. *J. Mater. Chem. A* **4**, 6368–6375 (2016).
142. Andrady, A. L., Harnid, S. H., Hu ', X. & Torikai, A. *Effects of increased solar ultraviolet radiation on materials*. *Journal of Photochemistry and Photobiology B: Biology* **46**, (1998).
143. Gijsman, P., Meijers, G. & Vitarelli, G. Comparison of the UV-degradation chemistry of polypropylene, polyethylene, polyamide 6 and polybutylene terephthalate. *Polym. Degrad. Stab.* **65**, 433–441 (1999).
144. Nikafshar, S. *et al.* The Effects of UV Light on the Chemical and Mechanical Properties of a Transparent Epoxy-Diamine System in the Presence of an Organic UV Absorber. *Materials (Basel).* **10**, 180 (2017).
145. Woo, R. S. C., Zhu, H., Leung, C. K. Y. & Kim, J.-K. Environmental degradation of epoxy-organoclay nanocomposites due to UV exposure: Part II residual mechanical properties. *Compos. Sci. Technol.* **68**, 2149–2155 (2008).
146. Zhang, Z., Sèbe, G., Wang, X. & Tam, K. C. UV-Absorbing Cellulose Nanocrystals as Functional Reinforcing Fillers in Poly(vinyl chloride) Films. *ACS Appl. Nano Mater.* **1**, 632–641 (2018).
147. Rosu, D., Rosu, L. & Cascaval, C. N. IR-change and yellowing of polyurethane as a result of UV irradiation. *Polym. Degrad. Stab.* **94**, 591–596 (2009).
148. Mailhot, B., Morlat-Thérias, S., Ouahioune, M. & Gardette, J.-L. Study of the Degradation of an Epoxy/Amine Resin, 1 Photo- and Thermo-Chemical Mechanisms. *Macromol. Chem. Phys.* **206**, 575–584 (2005).
149. Woo, R. S. C. *et al.* Environmental degradation of epoxy–organoclay nanocomposites due to UV exposure. Part I: Photo-degradation. *Compos. Sci. Technol.* **67**, 3448–3456 (2007).
150. Allen, N. S. *et al.* Degradation and stabilisation of polymers and coatings: nano versus

pigmentary titania particles. *Polym. Degrad. Stab.* **85**, 927–946 (2004).
151. Hu, M.-L., Chen, Y.-K., Chen, L.-C. & Sane, M. Para-aminobenzoic acid scavenges reactive oxygen species and protects DNA against UV and free radical damage. *Nutr. Biochem.* 504–508 (1995).
152. Fernandes, D. M., Winkler Hechenleitner, A. A., Job, A. E., Radovanocic, E. & Gómez Pineda, E. A. Thermal and photochemical stability of poly(vinyl alcohol)/modified lignin blends. *Polym. Degrad. Stab.* **91**, 1192–1201 (2006).
153. Trinh, B. M. & Mekonnen, T. Hydrophobic esterification of cellulose nanocrystals for epoxy reinforcement. *Polymer (Guildf).* **155**, 64–74 (2018).
154. Abraham, E. *et al.* Highly Modified Cellulose Nanocrystals and Formation of Epoxy-Nanocrystalline Cellulose (CNC) Nanocomposites. *ACS Appl. Mater. Interfaces* **8**, 28086–28095 (2016).
155. Guan, Y., Qian, L., Xiao, H. & Zheng, A. Preparation of novel antimicrobial-modified starch and its adsorption on cellulose fibers: Part I. Optimization of synthetic conditions and antimicrobial activities. *Cellulose* **15**, 609–618 (2008).
156. Forsthuber, B., Schaller, C. & Grüll, G. Evaluation of the photo stabilising efficiency of clear coatings comprising organic UV absorbers and mineral UV screeners on wood surfaces. *Wood Sci. Technol.* **47**, 281–297 (2013).
157. Ono, H.-K., Jones, F. N. & Pappas, S. P. Relative reactivity of isocyanate groups of isophorone diisocyanate. Unexpected high reactivity of the secondary isocyanate group. *J. Polym. Sci. Polym. Lett. Ed.* **23**, 509–515 (1985).
158. Girouard, N. M., Xu, S., Schueneman, G. T., Shofner, M. L. & Meredith, J. C. Site-Selective Modification of Cellulose Nanocrystals with Isophorone Diisocyanate and Formation of Polyurethane-CNC Composites. *ACS Appl. Mater. Interfaces* **8**, 1458–1467 (2016).
159. Schyrr, B. *et al.* Biosensors based on porous cellulose nanocrystal-poly(vinyl alcohol) scaffolds. *ACS Appl. Mater. Interfaces* **6**, 12674–12683 (2014).
160. Rueda, L. *et al.* Isocyanate-rich cellulose nanocrystals and their selective insertion in elastomeric polyurethane. *Compos. Sci. Technol.* **71**, 1953–1960 (2011).
161. Mekonnen, T. H., Mussone, P. G., Choi, P. & Bressler, D. C. Adhesives from Waste Protein Biomass for Oriented Strand Board Composites: Development and Performance. *Macromol. Mater. Eng.* **299**, 1003–1012 (2014).
162. Roik, N. V. & Belyakova, L. A. Thermodynamic, IR spectral and X-ray diffraction studies of the "β-cyclodextrin-para-aminobenzoic acid" inclusion complex. *J. Incl. Phenom. Macrocycl. Chem.* **69**, 315–319 (2011).
163. Teo, L.-S., Chen, C.-Y. & Kuo, J.-F. Fourier Transform Infrared Spectroscopy Study on Effects of Temperature on Hydrogen Bonding in Amine-Containing Polyurethanes and Poly(urethane-urea)s. *Macromolecules* 1793–1799 (1997).
164. Roman, M. & Winter, W. T. Effect of sulfate groups from sulfuric acid hydrolysis on the thermal degradation behavior of bacterial cellulose. *Biomacromolecules* **5**, 1671 (2004).
165. Lin, N. & Dufresne, A. Physical and/or chemical compatibilization of extruded cellulose nanocrystal reinforced polystyrene nanocomposites. *Macromolecules* **46**, 5570–5583 (2013).
166. Dankovich, T. A. & Gray, D. G. Contact Angle Measurements on Smooth Nanocrystalline Cellulose (I) Thin Films. *J. Adhes. Sci. Technol.* **25**, 699–708 (2011).
167. Cao, J., Zhang, X., Wu, X., Wang, S. & Lu, C. Cellulose nanocrystals mediated assembly

of graphene in rubber composites for chemical sensing applications. *Carbohydr. Polym.* **140**, 88–95 (2016).
168. Chow, W. S. Water absorption of epoxy/glass fiber/organo-montmorillonite nanocomposites. *Express Polym. Lett.* **1**, 104–108 (2007).
169. Alamri, H. & Low, I. M. Mechanical properties and water absorption behaviour of recycled cellulose fibre reinforced epoxy composites. *Polym. Test.* **31**, 620–628 (2012).
170. Takeshita, Y., Becker, E., Sakata, S., Miwa, T. & Sawada, T. States of water absorbed in water-borne urethane/epoxy coatings. *Polymer (Guildf).* **55**, 2505–2513 (2014).
171. Jelinski, L. W., Dumais, J. J., Cholli, A. L., Ellis, T. S. & Karasz, F. E. Nature of the water-epoxy interaction. *Macromolecules* **18**, 1091–1095 (1985).
172. Blanco, I., Cicala, G., Costa, M. & Recca, A. Development of an epoxy system characterized by low water absorption and high thermomechanical performances. *J. Appl. Polym. Sci.* **100**, 4880–4887 (2006).
173. Li, L. *et al.* Water Transportation in Epoxy Resin. *Chem. Mater.* **17**, 839–845 (2005).
174. El Saeed, A. M., Fattah, M. A. E.- & Dardir, M. M. Synthesis and characterization of titanium oxide nanotubes and its performance in epoxy nanocomposite coating. *Prog. Org. Coatings* **78**, 83–89 (2015).
175. Ghasemi-Kahrizsangi, A., Neshati, J., Shariatpanahi, H. & Akbarinezhad, E. Improving the UV degradation resistance of epoxy coatings using modified carbon black nanoparticles. *Prog. Org. Coatings* **85**, 199–207 (2015).
176. Doub, L. & Vandenbelt, J. M. The Ultraviolet Absorption Spectra of Simple Unsaturated Compounds. I. Mono- and p-Disubstituted Benzene Derivatives. *J. Am. Chem. Soc.* **69**, 2714–2723 (1947).
177. Mailhot, B., Morlat-Thérias, S., Bussière, P.-O. & Gardette, J.-L. Study of the Degradation of an Epoxy/Amine Resin, 2. *Macromol. Chem. Phys.* **206**, 585–591 (2005).
178. Kumar, BG., Singh, RP., Nakamura, T. Degradation of Carbon Fiber-reinforced. *J. Compos. Mater.* **36**, 2713–2733 (2002).
179. Gesner, B. D. & Kelleher, P. G. Oxidation of bisphenol a polymers. *J. Appl. Polym. Sci.* **13**, 2183–2191 (1969).
180. Barsberg, S., Elder, T. & Felby, C. Lignin−Quinone Interactions: Implications for Optical Properties of Lignin. *Chem. Mater.* **15**, 649–655 (2003).
181. Parit, M., Saha, P., Davis, V. A. & Jiang, Z. Transparent and Homogenous Cellulose Nanocrystal/Lignin UV-Protection Films. *ACS Omega* **3**, 10679–10691 (2018).
182. Macan, J., Brnardić, I., Orlić, S., Ivanković, H. & Ivanković, M. Thermal degradation of epoxy–silica organic–inorganic hybrid materials. *Polym. Degrad. Stab.* **91**, 122–127 (2006).
183. Gu, A. & Liang, G. Thermal degradation behaviour and kinetic analysis of epoxy/montmorillonite nanocomposites. *Polym. Degrad. Stab.* **80**, 383–391 (2003).
184. Uhl, F. M., Webster, D. C., Davuluri, S. P. & Wong, S. C. UV curable epoxy acrylate-clay nanocomposites. *Eur. Polym. J.* **42**, 2596–2605 (2006).
185. Thielemans, W., Can, E., Morye, S. S. & Wool, R. P. Novel applications of lignin in composite materials. *J. Appl. Polym. Sci.* **83**, 323–331 (2002).
186. Lora, J. H. & Glasser, W. G. *Recent Industrial Applications of Lignin: A Sustainable Alternative to Nonrenewable Materials*. *Journal of Polymers and the Environment* **10**, (2002).
187. Obst, B. J. R. & Kirk, T. K. ISOLATION OF LIGNIN. in *Methods in Enzymology* **161**,

1985 (1985).
188. Song, J. *et al.* Antibacterial effects of electrospun chitosan/poly(ethylene oxide) nanofibrous membranes loaded with chlorhexidine and silver. *Nanomedicine Nanotechnology, Biol. Med.* **12**, 1357–1364 (2016).
189. Rahman, O. ur *et al.* Lignin nanoparticles: synthesis, characterization and corrosion protection performance. *New J. Chem.* **42**, 3415–3425 (2018).
190. Gilca, I. A., Popa, V. I. & Crestini, C. Obtaining lignin nanoparticles by sonication. *Ultrason. Sonochem.* **23**, 369–375 (2015).
191. Wu, Y., Zhang, S., Guo, X. & Huang, H. Adsorption of chromium(III) on lignin. *Bioresour. Technol.* **99**, 7709–7715 (2008).
192. Hansen, C. M. The Universality of the Solubility Parameter. *Ind. Eng. Chem. Prod. Res. Dev.* **8**, 2–11 (1969).
193. Örså, F., Holmbom, B. & Thornton, J. Dissolution and dispersion of spruce wood components into hot water. *Wood Sci. Technol.* **31**, 279–290 (1997).
194. Sameni, J., Krigstin, S. & Sain, M. Solubility of Lignin and Acetylated Lignin in Organic Solvents. *BioResources* **12**, 1548–1565 (2017).
195. Tian, Z. *et al.* Recovery and characterization of lignin from alkaline straw pulping black liquor: As feedstock for bio-oil research. *J. Appl. Polym. Sci.* **132**, (2015).
196. Gupta, A. K., Mohanty, S. & Nayak, S. K. Synthesis, Characterization and Application of Lignin Nanoparticles (LNPs). *Mater. Focus* **3**, 444–454 (2015).